U.PORTO

MESTRADO
TOXICOLOGIA E CONTAMINAÇÃO AMBIENTAIS

# ANTICANCER ACTIVITY OF SEAWEED COMPOUNDS, ALONE AND IN COMBINATION WITH CHEMOTHERAPY DRUGS, IN BREAST CANCER CELL LINES USING 2D AND 3D CELL CULTURE MODELS

ANA CATARINA REBELO DE MACEDO

M
2019

U.PORTO

ANA CATARINA MACEDO. **ANTICANCER ACTIVITY OF SEAWEED COMPOUNDS, ALONE AND IN COMBINATION WITH CHEMOTHERAPY DRUGS, IN BREAST CANCER CELL LINES USING 2D AND 3D CELL CULTURE MODELS**

**M**.ICBAS **2019**

**ANTICANCER ACTIVITY OF SEAWEED COMPOUNDS, ALONE AND IN COMBINATION WITH CHEMOTHERAPY DRUGS, IN BREAST CANCER CELL LINES USING 2D AND 3D CELL CULTURE MODELS**

ANA CATARINA REBELO DE MACEDO

INSTITUTO DE CIÊNCIAS BIOMÉDICAS ABEL SALAZAR

ANA CATARINA F. P. REBELO DE MACEDO

# ANTICANCER ACTIVITY OF SEAWEED COMPOUNDS, ALONE AND IN COMBINATION WITH CHEMOTHERAPY DRUGS, IN BREAST CANCER CELL LINES USING 2D AND 3D CELL CULTURE MODELS

Dissertation for the Master's degree in
Environmental Contamination and Toxicology, presented to
Institute of Biomedical Sciences Abel Salazar
of the University of Porto

Supervisor – Alice Fernanda Abreu Ramos
Category – Invited Assistant Professor
Affiliation – Institute of Biomedical Sciences Abel Salazar,
University of Porto

Co-supervisor – Eduardo Jorge Sousa da Rocha
Category – Full Professor
Affiliation – Institute of Biomedical Sciences Abel Salazar,
University of Porto

## ACKNOWLEDGEMENTS

I would like to express my sincere gratitude and appreciation to the following people, who one way or another, contributed for the realization of this dissertation:

To my supervisor, Professor Doctor Alice Ramos, for all the guidance, unconditional support, friendship, advices, dedication, availability, and for all always giving me strength and motivation to continue. The academic and emotional support that you provided me was crucial for this accomplishment and I am grateful that I had the pleasure to work with you.

To my co-supervisor, Professor Doctor Eduardo Rocha, for accepting me in his research group and providing me the opportunity of work with this project, as well as for the help provided in the solution of problems occurred throughout the course of this work.

To Dr. Fernanda Malhão, for all the dedication, patient, availability, suggestions, friendship, dynamism, and especially, for the time and tireless efforts spent to help me, either with the experimental procedures or with the writing of this dissertation.

To Dr. Célia for the support and help provided during the realization of experiments.

To the research team of Professor João Paulo Teixeira, namely Doctor Carla Costa and Dr. Ana Inês Silva of the Department of Environmental Health of National Institute of Health Dr. Ricardo Jorge (INSA) for receiving me and allowing the performance of experimental procedures related with the comet assay.

To all my laboratory colleagues and friends, Inês Pereira, Inês Dias, Annette Veiga and Paula Teixeira for all for companionship, strength and support provided during difficult times.

To my family, especially my parents, for their affection, unconditional support and encouragement to overcome obstacles and moments of discouragement.

To all my friends for their comprehension and for always being there for me, even when I did not have time to spend with them.

This work was financially supported by the ICBAS of the University of Porto, namely via its Laboratory of Histology and Embryology and Master Program in Environmental Contamination and Toxicology, and also by the Strategic Funding UID/Multi/04423/2019 through national funds provided by FCT and ERDF, in the framework of the program PT2020.

## ABSTRACT

Breast cancer (BC) accounts for the most cancer-related deaths amongst women worldwide. The therapeutic approaches applied for BC patients depends upon the tumor molecular subtypes and may include chemotherapy. However, the development of multidrug resistance and cytotoxicity in normal cells constitute two of the main drawbacks adjacent to the use of conventional chemotherapeutic drugs, such as doxorubicin (Dox) and cisplatin (Cis). Strategies to overcome these limitations may include the search for new anticancer drugs as well as the administration of conventional anticancer drugs in combination with natural products. Several marine organisms have been explored in the last decades and among them, brown algae constitute a rich source of bioactive compounds [e.g. fucoxanthin (Fx), fucosterol (Fct) and fucoidan (Fc)] with several health-promoting properties, namely anticancer activity. Therefore, studying their antitumor activity as isolated compounds or adjuvant agents might be important for the development of potential anticancer drugs. However, the development of new anticancer drugs is associated with high attrition rates, essentially due to the use of limited in vitro drug screening methodologies. As an attempt to improve this process, three-dimensional (3D) cell cultures have emerged, bridging the gap between two-dimensional (2D) cell cultures and in vivo studies.

The aim of the present study was to evaluate the anticancer effects of the natural compounds Fx, Fct and Fc alone and in combination with the standard anticancer drugs Dox and Cis on a panel of three BC cell lines (MCF-7, MDA-MB-231 and SKBR3), representatives of distinct BC molecular subtypes, and in a non-tumorigenic cell lines (MCF-12A) using 2D and 3D cell cultures. The results from the 2D cultures showed that Cis and Dox caused cytotoxicity on all the cell lines tested, involving mechanisms of cell death induction (all the cell lines treated with Cis and MCF-12A cells treated with Dox) and genotoxicity (MDA-MB-231 cells treated with Dox). Fx alone was the only natural compound tested that induced cytotoxic effects on BC cell lines, however, no cell death or genotoxic mechanisms seemed to be associated with the observed cytotoxicity. In combination, all three compounds (Fx, Fct and Fc) increased Dox cytotoxic activity in MDA-MB-231 cells without effects on DNA damage and cell death induction. Thus, based on the data obtained from the 2D cultures, Dox and Fx were selected to be tested on 3D models.

Before exposure, generation and characterization of the 3D multicellular aggregates (MCAs) were conducted by testing several cell densities and formation times. Thus, the analysis of MCAs morphology by stereomicroscopy, optical and electron microscopy, and immunocytochemistry for caspase-3 and Ki67 were performed. The results showed that shorter formation periods (3 days) and higher cell seeding densities [40 x $10^4$ cells/ml and

20 x $10^4$ cells/ml (MCF-12A)] were the most suitable conditions for MCAs formation. Under those optimal conditions, compact aggregates were formed from the MDA-MB-231 and MCF-7 cell lines, while SKBR3 and MCF-12A cell lines originated loose aggregates.

The exposure of the MCAs to Dox and Fx, alone, showed that cells were less responsive to the anticancer effects of these compounds, compared to 2D cultures. Antiproliferative effects were noted in SKBR3 MCAs exposed to Dox and Fx, and in MCF-12A MCAs exposed to Dox.

In conclusion, Fx alone and the co-incubation of the natural compounds Fx, Fct and Fc with Dox appear as promising treatment conditions with anticancer activity in BC. However, they need to be further investigated to elucidate the underlying mechanism of its associated cytotoxicity. Future studies exploring the best approaches for the formation of 3D culture models also need to be conducted.

**Key words:** Breast cancer; anticancer drugs; seaweed compounds; 2D and 3D cell culture.

## RESUMO

O cancro da mama é o cancro com maior número de mortes entre as mulheres de todo o mundo. As abordagens terapêuticas utilizadas em doentes com cancro da mama dependem dos subtipos moleculares do tumor, podendo incluir quimioterapia. No entanto, o desenvolvimento de resistências a diversos fármacos e a citotoxicidade em células saudáveis constituem duas das principais desvantagens adjacentes ao uso dos medicamentos quimioterapêuticos convencionais, como a doxorrubicina (Dox) e a cisplatina (Cis). Estratégias para combater estas limitações incluem a procura de novos fármacos anticancerígenos, assim como a administração de fármacos convencionais combinados com produtos naturais. Durante as últimas décadas, alguns organismos marinhos têm sido investigados, entre eles as algas castanhas, uma fonte rica em compostos bioactivos [ex: a fucoxantina (Fx), o fucosterol (Fct) e o fucoidan (Fc)] que apresentam propriedades benéficas para a saúde, como a atividade anticancerígena. Deste modo, o estudo da atividade antitumoral destes compostos isolados ou como agentes coadjuvantes, pode ser importante para o desenvolvimento de potenciais medicamentos anticancerígenos. No entanto, o desenvolvimento de novos fármacos antineoplásicos está associado a uma elevada taxa de insucesso, principalmente devido ao uso de métodos limitados de triagem in vitro. Na tentativa de melhorar este processo, surgiram as culturas celulares tridimensionais (3D) que permitiram fazer a ponte entre as culturas bidimensionais (2D) e os estudos in vivo.

O objetivo do presente estudo foi avaliar os efeitos anticancerígenos dos compostos naturais Fx, Fct e Fc isolados e em combinação com os fármacos convencionais Dox e Cis, utilizando três linhas celulares de cancro da mama, representativas de diferentes subtipos moleculares (MCF-7, MDA-MB-231, SKBR3) e uma linha de células não tumorais (MCF-12A) cultivadas sob condições de cultura 2D e 3D. Os resultados referentes às culturas 2D mostraram que a Cis e a Dox causaram citotoxicidade em todas as linhas celulares testadas, envolvendo mecanismos de indução de morte celular (em todas as células que foram tratadas com Cis, e nas células MCF-12A tratadas com Dox) e genotoxicidade (nas células MDA-MB-231 tratadas com Dox). A Fx foi o único composto natural testado individualmente que induziu efeitos citotóxicos nas linhas celulares de cancro da mama, no entanto, a citotoxicidade observada não pareceu estar associada a mecanismos de morte celular ou de genotoxicidade. Em combinação, os três compostos (Fx, Fct e Fc) potenciaram a atividade citotóxica da Dox em células MDA-MB-231 sem provocar danos

no DNA nem induzir morte celular. Assim, com base nos dados obtidos das culturas 2D, a Dox e a Fx foram selecionadas para serem testadas em modelos 3D.

Antes da exposição, foi necessário proceder-se à formação e caracterização dos agregados multicelulares 3D (MCAs) testando diversas densidades celulares e tempos de formação. Deste modo, realizou-se a análise da morfologia dos MCAs através de técnicas de estereomicroscopia, microscopia ótica e eletrónica, e ainda análise imunocitoquímica para caspase-3 e Ki67. Os resultados mostraram que períodos mais curtos de formação (correspondentes a 3 dias) e elevadas densidades celulares [$40x10^4$ células/ml e $20x10^4$ células/ml (MCF-12A)] foram as condições mais adequadas para a formação de MCAs. Sob essas condições foram formados agregados compactos pelas linhas celulares MDA-MB-231 e MCF-7, enquanto as linhas celulares SKBR3 e MCF-12A formaram agregados laxos.

A exposição de MCAs à Dox e à Fx isoladas, mostrou que as células apresentavam uma menor resposta aos efeitos anticancerígenos destes compostos, comparativamente às culturas 2D. Foram observados efeitos antiproliferativos nos MCAs da linha SKBR3 expostos à Dox e à Fx, e nos MCAs da linha MCF-12A exposta à Dox.

Em conclusão, a Fx isolada e a co-incubação dos compostos naturais Fx, Fct e Fc com a Dox parecem ser promissoras, relativamente à sua possível atividade anti-cancerígena no cancro da mama. Porém, estes compostos precisam de ser investigados em maior pormenor de forma a elucidar os mecanismos associados à sua citotoxicidade. Estudos futuros que explorem as melhores abordagens para a formação de modelos de cultura 3D necessitam igualmente de serem realizados.

**Palavras-chave:** cancro da mama; fármacos anticancerígenos; compostos de algas marinhas; cultura celular em 2D e 3D.

**TABLE OF CONTENTS**

Acknowledgements ..... iii
Abstract ..... v
Resumo ..... vii
Index ..... ix
List of Figures and Tables ..... xii
Abbreviations ..... xviii

CHAPTER I – General Introduction ..... 1
1. Cancer ..... 3
2. Breast Cancer ..... 4
    2.1. Molecular Intrinsic Subtypes ..... 5
        2.1.1. Luminal-like Subtype ..... 6
        2.1.2. Her-2 Enriched Subtype ..... 7
        2.1.3. Basal-like/Triple Negative Subtype ..... 7
        2.1.4. Normal Breast-like Subtype ..... 8
    2.2. Breast Cancer Therapies ..... 8
        2.2.1. Chemotherapy ..... 9
            2.2.1.1. Alkylating Agents (Platinum-based agents) ..... 9
            2.2.1.2. Anthracycline Antibiotics ..... 11
3. Marine Natural Compounds ..... 13
    3.1. Seaweed as a Source of Bioactive Compounds ..... 14
        3.1.1 Carotenoids- Fucoxanthin ..... 14
        3.1.2 Polysaccharides- Fucoidan ..... 16
        3.1.3 Phytosterols- Fucosterol ..... 18
4. Two-Dimensional (2D) and Three-Dimensional (3D) in vitro Cell Culture Models in Drug Discovery ..... 19

CHAPTER II – Objectives ..... 23

CHAPTER III- Material and Methods ..... 27
1. Chemicals and Cell Culture Reagents ..... 29
2. Cell Cultures ..... 29
    2.1. Thawing of Frozen Cell Lines ..... 30
    2.2. Subculture of Adherent Cells ..... 30

2.3. Cell Quantification by Trypan Blue Exclusion Method ..... 30
3. 2D Cultures ..... 31
3.1. Determination of Cell Viability by MTT Reduction Assay ..... 31
3.2. Cell Death Assessment by Nuclear Condensation Assay ..... 32
3.3. Genotoxicity Assessment by Comet assay ..... 33
4. 3D cultures ..... 34
4.1. Generation and Characterization of 3D MCAs Cultures ..... 34
4.2. Exposure ..... 35
4.3. Image Analysis ..... 35
4.4. Determination of Cell Viability by MTT Reduction Assay ..... 35
4.5. Determination of Cell Viability by LDH Assay ..... 36
4.6. Cell Proliferation Assessment by BrdU Assay ..... 36
4.7. Histological Analysis ..... 37
4.8. Transmission Electron Microscopy (TEM) ..... 38
4.9. Immunocytochemistry ..... 39
5. Statistical Analysis ..... 40

CHAPTER IV-Results ..... 41
1. Effects in 2D Cultures ..... 43
1.1. Assessment of Cytotoxic Effects – 72 h Exposure ..... 43
1.2. Assessment of Cell Death Induction ..... 51
1.3. Assessment of Cytotoxic Effects – 24 h Exposure ..... 53
1.4. Assessment of Genotoxic Effects ..... 54
2. 3D Multicellular Aggregates (MCAs) ..... 56
2.1. MCAs Generation and Characterization ..... 56
2.1.1 Image Analysis ..... 57
2.1.2 Histological Analysis ..... 62
2.1.3 Immunocytochemical Analysis ..... 65
2.1.4 Transmission Electron Microscopy Analysis ..... 66
3. Effects in 3D Cultures ..... 70
3.1. Assessment of Cytotoxic Effects ..... 71
3.2. Assessment of Antiproliferative Effects ..... 72
3.3. Image Analysis ..... 73
3.4. Histological Analysis ..... 75
3.5. Immunocytochemical Analysis. ..... 77

CHAPTER V- Discussion ..... 81
1. Anticancer Effects of Fx, Fct and Fc Alone and in Combination with Dox or Cis on 2D Cultures ..... 83
2. MCAs Generation and Characterization ..... 88
3. Anticancer Effects of Fx and Dox on 3D Cultures ..... 92

CHAPTER VI- Conclusion and Future Perspectives ..... 95

CHAPTER VII- References ..... 101

## LIST OF FIGURES AND TABLES

### CHAPTER I

**Figure 1-** Number of new cancer cases (A) and cancer mortality (B) in 2018 for both sexes in all ages (GLOBOCAN 2018, 2018b, 2018c). Data source: GLOBOCAN 2018. Graph Production: Global Cancer Observatory.....4
**Figure 2-** Global heatmap representing the estimated age-standardized incidence rates (World) in 2018, breast cancer in females of all ages (GLOBOCAN 2018, 2018a). Data source: GLOBOCAN 2018. Graph Production: International Agency for Research on Cancer (IARC). .....5
**Figure 3-** Chemical structure of 2 anticancer drugs: Cisplatin (A) and Doxorubicin (B)....10
**Figure 4-** Schematic representation of the typical three-layer structure of a spheroid.....22

### CHAPTER III

**Table 1-** Experimental concentrations of Dox, Cis, Fx, Fct and Fc tested on each breast cell line**.**.....31

### CHAPTER IV

**Figure 5-** Effect of Fx alone or co-incubated with Dox or Cis on cell viability, after 72 h of incubation, in MCF-7(a and b), SKBR3 (c and d), MDA-MB-231 (e and f) and MCF12A (g and h) cell lines assessed by MTT assay. Untreated cells (C) (cells in culture medium) were included as a negative control. Results are expressed as mean ± (SD) of five independent experiments. Significant differences (* P<0.05; ** P<0.01; *** P<0.001; **** P<0.0001), when compared to the control, were tested by one-way ANOVA, followed by post-hoc Holm-Sidak's multiple comparison test. Additionally, a Student's t-test was selectively used to access significant differences in MDA-MB-231 (Fx 10 + Dox 1 versus Dox1 and Fx 10 + Dox 1 versus Fx 10), and SKBR3 (Dox 0.1 versus C and Cis 10 versus C). ..... 45
**Figure 6-** Effect of Fct alone or co-incubated with Dox or Cis on cell viability, after 72 h of incubation, in MCF-7 (a and b), SKBR3 (c and d), MDA-MB-231(e and f) and MCF12A (g and h) cell lines assessed by MTT assay. Untreated cells (C) (cells in culture medium) were included as a negative control. Results are expressed as mean ± SD of five independent experiments. Significant differences (* P<0.05; ** P<0.01; *** P<0.001; **** P<0.0001), when compared to the control, were tested by one-way ANOVA, followed by post-hoc Holm-Sidak's multiple comparison test. Additionally, a Student's t-test was selectively used to access significant differences in MCF-7 (Fct 5 + Cis 10 versus C)..... 46

**Figure 7-** Effect of Fc alone or co-incubated with Dox or Cis on cell viability, after 72 h of incubation, in MCF-7 (a and b), SKBR3 (c and d), MDA-MB-231 (e and f) and MCF12A (g and h) cell lines assessed by MTT assay. Untreated cells (C) (cells in culture medium) were included as a negative control. Results are expressed as mean ± SD of five independent experiments. Significant differences (* P<0.05; ** P<0.01; *** P<0.001; **** P<0.0001), when compared to the control, were tested by one-way ANOVA, followed by post-hoc Holm-Sidak's multiple comparison test. ..... 47
**Figure 8-** Representative images of the morphological changes in MCF-7, SKBR3, MDA-MB-231 and MCF-12A monolayer cell cultures exposed to Cis, Dox and Fx for 72h. The * indicates that exposure concentrations differed between cell lines. Cis was administrated at 10 µM (in MCF-12A), 20 µM (in MCF-7 and SKBR3) and 50 µM (in MDA-MB-231). Dox was applied at 0.1 µM (in MCF-7, SKBR3 and MCF-12A) and at 1 µM (in MDA-MB-231). Fx was tested at 10 µM in all the cell lines. Untreated cells (cells in culture medium) were included as a negative control (C). In Fx exposure conditions, it is visible some orange precipitates. Scale bar: 100 µm. ..... 50
**Figure 9-** Effect of Fx (10 µM), Fct (5 µM) and Fc (10 and 50 µg/ml) alone and in combination with Dox (0.1 and 1 µM) or Cis (10, 20 and 50 µM) on induction of cell death in 2D cultures. MCF-7 (a), SKBR3 (b), MDA-MB-231 (c, d, e) and MCF-12A (f) cells were incubated for 72 h and induction of cell death assessed by nuclear condensation assay. Untreated cells (cells in culture medium) were included as a negative control (C). Data are expressed as the percentage of condensed nuclei, relative to the negative control, and are presented as mean ± SD of at least three independent experiments. Significant differences (* P < 0.05, ** P < 0.01; *** P < 0.001; **** P < 0.0001), when compared with the negative control, were determined by one-way ANOVA, followed by a Holm-Sidak's multiple comparisons test. Additionally, a Student's t-test was selectively used to access significant differences in SKBR3 (Cis 10 versus C), MDA-MB-231 (Fx 10 + Dox 1 versus Fx 10; Fc 50 + Dox 1 versus Fc 50) and MCF-12A (Cis 10 versus C)..... 52
**Figure 10-** Effect of Fx (10 µM), Fct (5 µM) and Fc (10 and 50 µg/ml), alone and in combination with Dox (0.1 and 1 µM) or Cis (10, 20 and 50 µM) on cell viability in 2D cultures. MCF-7 (a), SKBR3 (b), MDA-MB-231 (c, d, e) and MCF-12A (f) cells were incubated for 24 h and viability was assessed by the MTT assay. Untreated cells (cells in culture medium) were included as a negative control (C). Data are expressed as the percentage of cell viability, relative to the negative control, and are presented as mean ± SD of at least three independent experiments. Significant differences (** P < 0.01), when compared with the negative control, were determined by one-way ANOVA, followed by a Holm-Sidak's multiple comparisons test..... 53

**Figure 11-** Genotoxic effect of Fx (10 µM) and Fc (50 µg/ml), alone and in combination with Dox (1 µM) or Cis (10 and 50 µM) on DNA damage in MCF-7 (a), SKBR3 (b), MDA-MB-231(c and d,) and MCF-12A (e) cells after 2 h of exposure evaluated by the Comet assay. Untreated cells (cells in culture medium) were included as a negative control (C). Data are expressed as the percentage of tail intensity, relative to the negative control, and are presented as mean ± SD of at three independent experiments. Significant differences (* P < 0.05, ** P < 0.01; *** P < 0.001; **** P < 0.0001) were determined by one-way ANOVA, followed by a Holm-Sidak's multiple comparisons test. .....55
**Figure 12-** Representative images of the comet assay in MDA-MB-231 cells treated with A) Culture medium (Negative Control), B) Dox (1 µM), C) Fx (10 µM) and D) Fx (10 µM) + Dox (1 µM). Samples were analysed by the Comet Assay IV software. In the presence of low level of DNA damages, DNA occurs as a nucleoid with no or a small tail (A and C). Cells with DNA strand breaks resembles a comet structure with a head and a damaged DNA streak representing the tail (B and D). The blue line indicates the start of the comet head, the green line represents the middle of the comet head and the purple line limits the end of the comet tail. The fluorescence intensity of the comet tail, in relation the head, is directly proportional to the extent of DNA breaks occurred. Untreated cells (A) as well as cells exposed to Fx (C) present a low level of DNA damage, while cells incubated with Dox alone (B) and in combination with Fx (D) showed higher induction of DNA damages. Original magnification: 250x. .....56
**Figure 13-** Representative morphology images of the 3D MCAs at different incubation periods. SKBR3 and MCF12-A cell lines were seeded in ULA plates at 5 x $10^4$ cells/ml (D1) and 10 x $10^4$ cells/ml (D2) while MDA-MB-231 cell line was seeded at 10 x $10^4$ cells/ml (D1) and 20 x $10^4$ cells/ml (D2). Photographs were taken in a stereomicroscope at 4 days (96 h), 7 days (168 h), 10 days (240 h) and 12 days (288 h) of incubation. Scale bar: 500 µm. ..58
**Figure 14-** Representative morphology images, photographed in a stereomicroscope with a dark field, of the 3D MCAs at different cell densities after 3 days (72 h) of incubation in culture medium. MCF-7 and SKBR3 cells were seeded at 10 x $10^4$ cells/ml (D1), 20 x $10^4$ cells/ml (D2) and 40 x $10^4$cells/ml (D3). MDA-MB-231 cells were seeded at 20 x $10^4$ cells/ml (D1), 40 x $10^4$ cells/ml (D2) and 50 x $10^4$ cells/ml (D3). MCF-12A cells were seeded at 5 x $10^4$ cells/ml (D1), 10 x $10^4$ cells/ml (D2), and 20 x $10^4$ cells /ml (D3). Scale bar: 500µm..59
**Figure 15-** Representative morphology images, photographed in a stereomicroscope with a dark field, of the 3D MCAs at the selected cell densities at day 3 (72 h of MCAs formation) and day 7 (4 days or 96 h of MCAs incubation in culture medium, simulating the exposure period). Each two images correspond to the same MCA. MCF-7, SKBR3 and MDA-MB-231 cells were seeded at 40 x $10^4$ cells/ml. MCF-12A cells were seeded at 20 x $10^4$ cells/ml. Scale bar: 500 µm.....60

**Figure 16-** Area measurements of the 3D MCAs at day 1 (24 h), day 2 (48 h), day 3 (72 h), day 4 (96 h), day 5 (120 h), day 6 (144 h) and day 7 (168 h) of incubation. (a) SKBR3, (b) MCF-7, (c) MDA-MB-231 and (d) MCF12A cells were seeded at the previously optimized cell densities. Culture medium was completely changed after 3 days of incubation in order to simulate the exposure process. Results are presented as mean ± SD of at least twelve MCAs from one single experiment. .....61
**Figure 17-** Representative images of the MCF-7 MCAs 3 µm-thick sections stained with HE after 3 days (72 h) and 7 days (168 h) in culture. Total cell culture medium changes were performed on day 3 to simulate the exposure procedure. Each pair of images of different magnifications correspond to the same MCA. The arrowheads indicate the lumen-like structures. Scale bar: 20, 50 and 100 µm. .....62
**Figure 18-** Representative images of the SKBR3 MCAs 3 µm-thick sections stained with HE after 3 days (72 h) and 7 days (168 h) in culture. Total cell culture medium changes were performed on day 3 to simulate the exposure procedure. Each pair of images of different magnifications correspond to the same MCA. Scale bar: 50 and 500 µm.....63
**Figure 19-** Representative images of the MDA-MB-231 MCAs 3 µm-thick sections stained with HE after 3 days (72 h) and 7 days (168 h) in culture. Total cell culture medium changes were performed on day 3 to simulate the exposure procedure. Each pair of images of different magnifications correspond to the same MCA. Scale bar: 50 and 100 µm.....64
**Figure 20-** Representative images of the MCF-12A MCAs 3 µm-thick sections stained with HE after 3 days (72 h) and 7 days (168 h) in culture. Total cell culture medium changes were performed on day 3 to simulate the exposure procedure. The arrowheads indicate the lumen-like structures Each pair of images of different magnifications correspond to the same MCA. Scale bar: 50, 100 and 200 µm.....65
**Figure 21-** Representative images of the 3D MCAs 3 µm-thick sections immunostained against caspase-3 and Ki67 (brown staining) after 3 and 7 days of incubation. Scale bar: 50, 100 and 200 µm.....66
**Figure 22-** Representative images of TEM analysis of MCF-7 MCAs after 3 days of culture. Arrows: apoptotic cells; Arrowheads: secretory vesicles; Asterisks: microvilli; ExS: external surface; Gly: glycogen; Lm: lumen; Mi: Mitochondria; Nu: Nucleus; Ncl: nucleolus; RER: rough endoplasmic reticulum. Scale bar: 2 µm. .....67
**Figure 23-** Representative images of TEM analysis of SKBR3 MCAs after 3 days of culture. Asterisks: microvilli; White arrowheads: membranes blebs; Gly: glycogen; Mi: Mitochondria; Nu: Nucleus; Ncl: nucleolus. Scale bar: 2 µm. .....68
**Figure 24-** Representative images of TEM analysis of MDA-MB-231 MCAs after 3 days of culture. White arrowheads: membranes blebs; Db: dense bodies; Ld: Lipid droplets; Lu: lumen; Mi: Mitochondria; Nu: Nucleus; Ncl: nucleolus; Vc: vacuoles. Scale bar: 2 µm. ....69

**Figure 25-** Representative images of TEM analysis of MCF-12A MCAs after 3 days of culture. Black arrows: intercellular spaces with membrane blebs; White arrows: bundles of cytoplasmic filaments; ExS: external surface; Ld: Lipid droplets; Lm: lumen; Mi: Mitochondria; Nu: Nucleus; Ncl: nucleolus, Stars: desmosomes. Scale bar: 0.5 (C- inserted image), 1 (B, C, D) and 2 µm (A). .....70
**Figure 26-** Effect of Fx at 10 µM (Fx 10) and Dox at 1 µM (Dox 1) on the viability of MCF-7 (a), SKBR3 (b), MDA-MB-231(c) and MCF-12A (d) MCAs, assessed after 4 days of exposure by the MTT assay. Cells treated with 0.1% DMSO (SC) were included as a negative control. Results are expressed as the percentage of cell viability at 570 nm and presented as mean ± SD of four independent experiments. .....71
**Figure 27-** Effect of Fx at 10 µM (Fx 10) and Dox at 1 µM (Dox 1) on cell viability of MCF-7 (a), SKBR3 (b), MDA-MB-231 (c) and MCF-12A (d) MCAs, assessed after 4 days of exposure by the LDH assay. Cells treated with 0.1% DMSO (SC) and lysed with Lysis Buffer (10x) from the Pierce LDH Cytotoxicity Assay Kit (C+) were included as negative and positive controls, respectively. The percentage of LDH release was calculated in relation to the C+. Results are expressed as mean ± SD of four independent experiments. Significant differences (*** $P < 0.001$ and **** $P < 0.0001$), when compared to the negative control (SC), were determined by one-way ANOVA, followed by a Holm-Sidak's multiple comparisons test.....72
**Figure 28-** Effect of Fx at 10 µM (Fx 10) and Dox at 1 µM (Dox 1) on cell proliferation of MCF-7 (a), SKBR3 (b), MDA-MB-231 (c) and MCF-12A (d) MCAs, assessed after 4 days of exposure by the BrdU assay. Cells treated with 0.1% DMSO (SC) were included as a negative control. Results are expressed as the percentage of cell proliferation at 370 nm-492 nm and presented as mean ± SD of four independent experiments. Significant differences (* $P < 0.05$ and ** $P < 0.01$), when compared to the control, were determined by one-way ANOVA, followed by a Holm-Sidak's multiple comparisons test. An additional unpaired Student's t-test was performed to assess significant differences (* $P < 0.05$), between the condition Dox (1 µM) versus control in MCF-12A cells. .....73
**Figure 29-** Representative morphology images, photographed in a stereomicroscope with a dark field, of the 3D multicellular aggregates (MCAs) after 4 days (96 h) of incubation with Dox at 1 µM and Fx at 10 µM. MCF-7, SKBR3 and MDA-MB-231 cells were seeded at 40 x $10^4$ cells/ml. MCF-12A cells were seeded at 20 x $10^4$ cells/ml. Cells treated with 0.1% DMSO (SC) were included as a negative control. Fx was responsible for the yellowish colour observed in the Fx-treated MCAs. Scale bar: 500 µm. .....74
**Figure 30-** Area measurements ($\mu m^2$) of MCF-7 (a), SKBR3 (b), MDA-MB-231 (c) and MCF-12A (d) MCAs before exposure (day 0; grey bars) and after 4 days of exposure (day 4; black bars) at Fx at 10 µM and Dox at 1 µM. As a negative control, cells were treated

with 0.1% DMSO (SC). Results are expressed as mean ± SD of four independent experiments. Significant differences (* P < 0.05; ** P < 0.01 and **** P < 0.0001), when compared to the MCAs area before exposure (at day 0), were determined by one-way ANOVA, followed by a Holm-Sidak's multiple comparisons test. ..... 75
**Figure 31-** Representative images of 3 µm-thick sections of the MCAs stained with HE, after 4 days of exposure to Dox at 1 µM and Fx at 10 µM. Cells treated with 0.1% DMSO (SC) were included as a negative control. Scale bar: 50, 100 and 200 µm..... 76
**Figure 32-** Representative images of 3 µm-thick sections of the MCAs immunostained against caspase-3, after 4 days of exposure to Dox at 1 µM and Fx at 10 µM. Cells treated with 0.1% DMSO (SC) were included as a negative control. Scale bar: 50, 100 and 200 µm..... ..... 78
**Figure 33-** Representative images of 3 µm-thick sections of the MCAs immunostained against Ki67, after 4 days of exposure to Fx at 10 µM and Dox at 1 µM. Cells treated with 0.1% DMSO (SC) were included as a negative control. Scale bar: 50, 100 and 200 µm. 79

**Table 2-** Heatmap of the qualitative evaluation of the effects induced by the tested compounds (Dox, Cis, Fx and Fc) on different morphological parameters at 72 h of exposure. Comparisons were made relatively to the negative control (untreated cells). The yellow color indicates no changes in relation to the control. The red and green colours indicate a decrease or an increase, respectively, of the measured parameter relative to the control. ..... 49
**Table 3 -** Summary of the conditions that induced statistically significant cytotoxic effects on the different cell lines, in comparison with the negative control or the isolated compounds, after 72 h of exposure. ..... 51

## ABBREVIATIONS

AIS- Apoptosis-inducing Factor
ATCC- American Tissue Culture Collection
BC- Breast Cancer
BrdU- 5′-bromo-2′-deoxyuridine
BSA- Bovine Serum Albumin
Cis- Cisplatin
CK- Cytokeratin
DAPI-4',6-diamidino-2-phenylindole
DMEM- Dulbecco's Modified Eagle's Medium
DMEM/F-12- Dulbecco's Modified Eagle's Medium/Ham's Nutrient Mixture F12
DMSO- Dimethyl Sulfoxide
Dox- Doxorubicin
ECACC- European Collection of Authenticated Cell Cultures
ECM- Extracellular Matrix
EDTA- Ethylenediamine Tetraacetic Acid
EGFR- Epidermal Growth Factor Receptor
EPI- Epirubicin
ER- Estrogen receptor
FBS- Fetal Bovine Serum
Fc- Fucoidan
Fct- Fucosterol
FDA- Food and Drug Admnistration
Fx- Fucoxanthin
GSH- Glutathione
HE- Hematoxylin-Eosin
HER2- Human Epidermal Growth Factor
IARC- International Agency for Research on Cancer
LDH- Lactate Dehydrogenase
MCAs- Multicellular aggregates
MTT- 3-(4,5-Dimethyl-2-thiazolyl)-2,5-diphenyl-2H-tetrazolium bromide
NF-kB- Nuclear Factor Kappa B
PARP- Poly(ADP-Ribose) Polymerase
PBS- Phosphate Buffer Saline
PR- Progesterone receptor
ROS- Reactive Oxygen Species

SCGE- Single Cell Electrophoresis

SD- Standard Deviation

TBS- Tris-Buffered Saline

TE- Tris-EDTA

TEM- Transmission Electron Microscopy

TNBC- Triple Negative Breast Cancer

TP53- Tumor Protein 53

ULA- Ultra-Low Attachment

VEGF-C – Vascular Endothelial Growth Factor C

WHO- World Health Organization

# – CHAPTER I –
General Introduction

# General Introduction

## 1. Cancer

Cancer incidence and associated lethality rates have increased dramatically over the last decades. This malignancy has become the second leading cause of death in the world following cardiovascular diseases (Nagai & Kim, 2017). Researchers listed several factors as responsible for the current increase, including the aging and growth of the population, and increased exposure to carcinogenic environmental factors (Torre et al., 2016; Yu, 2005). Environmental agents (including tobacco, alcohol consumption, diet, radiation, infections, environmental pollution and others) are in the origin of approximately 90-95% of all cancers while genetic factors account for around 5-10% of the cases (Anand et al., 2008). In high-income countries, inadequate lifestyle habits, such as smoking, alcohol intake, unhealthy diet and sedentary behaviours, represent the main causes of cancer onset, whereas in poorly developed countries infection-related cancers are prevalent (Nagai & Kim, 2017). Reports indicate that minimizing exposure to the abovementioned lifestyle and environmental risk factors can prevent the incidence of up to 40% of new cancer cases (Bray et al., 2018).

The GLOBOCAN 2018 project estimations of cancer incidence and mortality demonstrated that the Asian continent accounted for the majority of the cancer cases and related deaths worldwide in that year. In Europe the total cancer cases and deaths represented 23.4% and 20.3%, respectively, while in America there was 21% of cancer incidence and 14.4% of mortality (Bray et al., 2018). According to forecasts, it is expected that by 2020 world population has risen to 7.5 billion, among which 15 million will account for new cancer cases and 12 million for cancer-related deaths (Anand et al., 2008). According to GLOBOCAN data from 2018, breast, lung, colorectal, prostate, skin and stomach cancers are considered the most incident. Lung and breast cancers are leading the list, each one, with around 2 million cases diagnosed (Fig. 1A). However, regarding cancer-related deaths, breast cancer (BC) accounts for about 627 000 deaths, less than in lung (around 1761000 deaths) (Fig. 1B) (GLOBOCAN 2018, 2018b, 2018c).

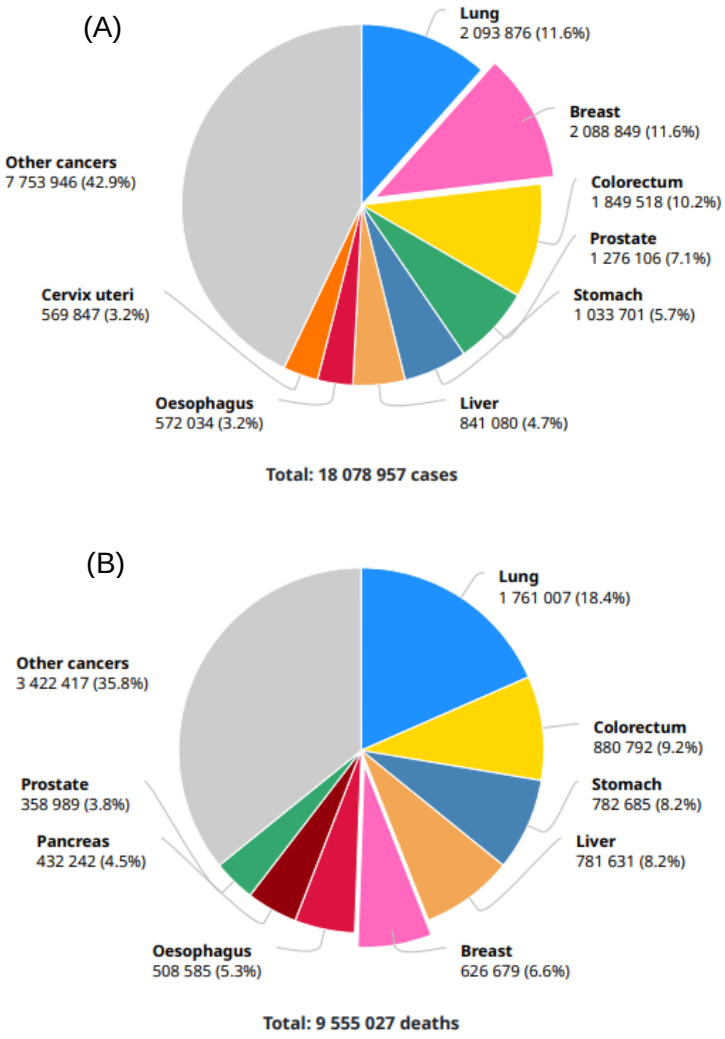



**Figure 1-** Number of new cancer cases (A) and cancer mortality (B) in 2018 for both sexes in all ages (GLOBOCAN 2018, 2018b, 2018c). Data source: GLOBOCAN 2018. Graph Production: Global Cancer Observatory.

## 2. Breast Cancer

BC, also referred as breast carcinoma, is a malignant neoplasm originated in the breast epithelial tissue (Cardoso, 2017). Among women worldwide, BC is the most prevalent type of cancer (23% incidence) and the leading cause of cancer-related deaths (Cardoso, 2017; DeSantis et al., 2015). Men are also susceptible to BC although it is much rare, being the incidence rate of only 1% (Sanguinetti et al., 2016).

BC spatial epidemiology differs among countries (Fig. 2), with the United States of America, Canada and Northern Europe presenting higher incidence rates than Asia and Africa (GLOBOCAN 2018, 2018a). In the United States of America, the chances of having BC during lifetime are 12% (Ataollahi et al., 2015). Data obtained by the American Cancer Society showed that the number of estimated new cases of BC among women in 2019 was

268,600 with 41760 cancer-death cases registered (Siegel et al., 2019). In Europe the number of new cases and deaths are over, respectively, 370000 and 130000 per year in women with their age between 35 and 64 years old (Santilli et al., 2011).

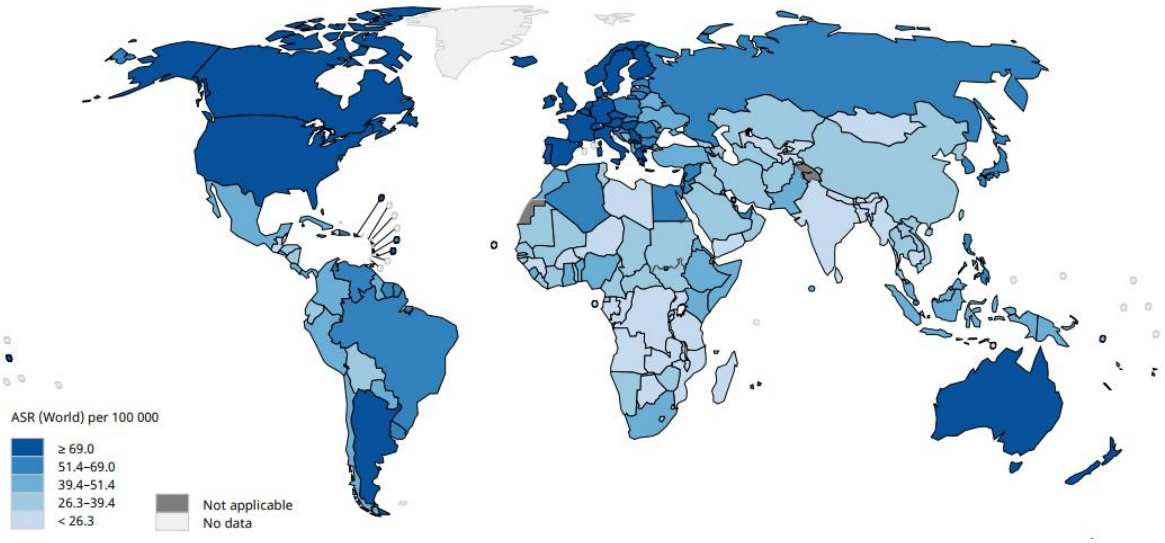



**Figure 2-** Global heatmap representing the estimated age-standardized incidence rates (World) in 2018, breast cancer in females of all ages (GLOBOCAN 2018, 2018a). Data source: GLOBOCAN 2018. Graph Production: International Agency for Research on Cancer (IARC).

In Portugal, BC incidence trends are rising. In 2012 there were reported 6088 new cases and 1570 deaths relative to 30% of all cancer cases in Portugal and 10% of cancer-related mortality (Forjaz de Lacerda et al., 2018).

Just as the majority of epithelial tumors, BC incidence tends to increase with age, especially until menopause age (Bombardieri et al., 2008). There is an assemblage of risk factors that can be associated with the onset and development of BC, such as age and sex, familial and personal history of the disease, reproductive factors, exogenous hormones, environmental factors, diet, physical activity and several others (American Cancer Society, 2015). The actual rising incidence patterns occurring in some low and middle-income countries evince the embracement of a Westerner lifestyle, reflecting modifications in reproduction, nutritional and physical activity trends (DeSantis et al., 2015; Lin & Tripuraneni, 2011).

### 2.1. Molecular Intrinsic Subtypes

In order to stratify patients by risk and treatment strategies and to predict their prognosis, it is necessary to investigate the molecular characteristics of the tumor. In the beginning of the present century conducted studies based on DNA microarrays technology and immunohistochemistry indicated that there is heterogeneity in BC gene and protein expression patterns (Cardoso, 2017; Hon et al., 2016). Therefore, a molecular classification

emerged from the presence or absence of a variety of biomarkers, including estrogen receptor (ER), progesterone receptor (PR), human epidermal growth factor receptor 2 (HER2 or c-erbB2) and antigen Ki67 (Holliday & Speirs, 2011; Yersal & Barutca, 2014).

A molecular-based classification favoured the application of more patient-tailored treatments, allowing the previous prediction of the clinical outcomes (Yersal & Barutca, 2014). According to the literature, the classification of the molecular intrinsic subtypes is divergent, probably due to the analysis of different gene clusters (Pusztai et al., 2006; Yersal & Barutca, 2014). However, physicians assume that BC can be differentiated among at least 5 distinct molecular subtypes: Luminal A, luminal B, HER2-enriched, basal-like and normal-like BC as described in more detail below (Cardoso, 2017; Holliday & Speirs, 2011).

### 2.1.1. Luminal-like Subtype

Luminal-like tumors are the most common subtype accounting for nearly 75% of BC cases (Yersal & Barutca, 2014). This group comprises tumors that express ER, PR, ER responsive genes and other typical genes normally expressed in the mammary luminal epithelial tissue, such as ER1, genes related to ER activation (LIV1, CCND1, FOXA1, GATA3, BCL2) and the luminal cytokeratins (CKs) 8 and 18 (Dai et al., 2015; Yersal & Barutca, 2014) In comparison with non-luminal groups this class have lower tumor grade and more encouraging outcomes (Pusztai et al., 2006). There are two luminal-like subclasses: Luminal A and Luminal B (Dai et al., 2015).

Luminal A tumors represent the $ER^+$ and/or $PR^+$, $HER2^-$, $Ki67^-$ subclass characterized by the hormonal receptor genes overexpression and proliferative genes subexpression (Dai et al., 2015). This type of tumors presents the lowest recurrence rates and the best prognosis amongst all the BC molecular subtypes (Alluri & Newman, 2014; Shim et al., 2014). They tend to have low mitotic activity and nuclear pleomorphism, and are normally associated with specific BC histological groups, including invasive cribiform mucinous, tubular and lobular (Yersal & Barutca, 2014).

Luminal B tumors are generally ER and/or PR positives and characterised by the presence of increased Ki67 and/or HER2 levels which confers them a highly proliferative potential. These carcinomas are less incident (10%) than luminal A cases plus tend to have lower expression of hormone receptor genes, higher histological grade, more aggressive behaviour and consequently poorer prognosis (American Cancer Society, 2015; Ignatiadis & Sotiriou, 2013). Nonetheless not all luminal B tumors are ER/PR and HER2 positives, since up to 6% do not have these receptors (Yersal & Barutca, 2014).

In a clinical context, luminal A cancers are normally treated with hormonal therapy, since they present poorer outcomes when treated with traditional chemotherapy drugs,

however luminal B tumors, which have a higher proliferative index, may benefit from the combination of both chemo- and hormonal treatment approaches (Dai et al., 2015).

### 2.1.2. HER2- Enriched Subtype

HER2-enriched tumors constitute 15-20% of BC and are known for being hormone-receptor negative and HER2 positive ($ER^-$ and/or $PR^-$, $HER2^+$) (Yersal & Barutca, 2014). HER2 and HER2 related genes' overexpression correlates with a higher aggressiveness and proliferative behaviour that constitutes the differentiating factor of this subtype (American Cancer Society, 2015). Therefore, it is mostly linked with high histological grade (mostly grade 3) and the presence of p53 mutations (Dai et al., 2015; Prat et al., 2015). Poor outcomes are expected in patients treated with traditional cytotoxic chemotherapy, since HER2-positive breast carcinomas are often associated with the onset of resistance to conventional drugs. However, survival rates rise when HER2 directed therapies are applied, such as trastuzumab emtansine and pertuzumab (American Cancer Society, 2015; Trendowski, 2015).

### 2.1.3. Basal-like / Triple-negative Subtype

Basal-like cancers account for 10 to 25% of BC classes and are typically defined by the lack of hormone and HER2 receptors (Ho-Yen et al., 2012). Tumors belonging to this subtype present high expression of basal epithelial markers, including laminin, cytokeratins 5, 6 14 and 17, P-cadherin and epidermal growth factor receptor (EGFR) (Dai et al., 2015; Yersal & Barutca, 2014), and low expression of luminal genes (Alluri & Newman, 2014). The majority of basal-like cancers are invasive ductal carcinomas of no special type and have high histological grade, high necrotic cells content in central regions, increased proliferative activity and pushing (non-infiltrative) borders (Badve et al., 2011). The basal-like subtype is often mistaken by the triple-negative subgroup, albeit they are not synonymous. Triple-negative breast cancers (TNBCs) designate tumors that lack all three receptors (ER, PR and HER2). However not all TNBCs express basal markers characteristic of the basal phenotype, as well as not all basal-like cancers lack the hormone and HER2 receptors (triple-negative phenotype) (Rakha et al., 2008). A study performed by Bertucci et al. demonstrated, by gene expression analysis, that only 71% of TNBCs were basal-like tumors and that only 77% of basal-like tumors were triple-negative (Bertucci et al., 2008).

The vast majority of patients with basal-like and TNBCs usually present mutations in tumor suppressor genes such as tumor protein 53 (TP53) gene (up to 85%), BRCA1 gene (over 75%), and alterations in tumor suppressor proteins, including pRB and p16, which are involved in cell-cycle regulation (Alluri & Newman, 2014; Badve et al., 2011; Lanz et al.,

2017; Prat et al., 2015). Racial background seems to be correlated with the development of these types of tumors since they are more prevalent in premenopausal women from Africa and America, especially of a young age (Badve et al., 2011; Carey et al., 2006; Kurian et al., 2010). Among the BC molecular subtypes, both triple-negative and basal-like cancers exhibit the poorest clinical outcomes as a result of their aggressive metastatic behaviour and due to the lack of targeted therapies, since they usually do not express the relevant receptors (Dubois et al., 2017; Garrido-Castro et al., 2019). Novel therapies aiming the blockage of EGFR by antibodies anti-EGFR and tyrosine kinase inhibitors or the inhibition of Poly-ADP-Ribose-Polymerase1 enzyme are in development and waiting to be standardized (Dubois et al., 2017). Currently, traditional chemotherapy still represents the single treatment option (American Cancer Society, 2015; Ho-Yen et al., 2012).

### 2.1.4. Normal Breast-like Subtype

The available information regarding the normal breast-like subtype is highly limited and controversial. Some researchers defend that normal breast-like tumors arise from cross-contamination from normal breast tissue samples during microarrays analysis and hence it should not be classified as a molecular subtype (Tang & Tse, 2016; Weigelt et al., 2010). According to the existent statistics, these tumors represent 5 to 10% of all BC and have similar gene expression patterns to adipose cells. These carcinomas can easily be mistaken by basal-like and triple-negative cancers since they lack the expression of ER, PR and HER2 receptors, however they differentiate from the basal phenotype for the absent expression of CK5 and EGFR (Hon et al., 2016; Yersal & Barutca, 2014).

## 2.2. Breast Cancer Therapies

With the advancement of technology and increasing knowledge about BC biology, improvements in treatments and diagnostic techniques have been made (Ades et al., 2017). Currently treatments strategies are patients-tailored, since they are established according to their personal preferences and characteristics (e.g. age, health condition, menopausal status), and biological features of the tumor at the time of discovery and diagnosis (e.g. stage, grade, size, molecular biomarkers and lymph nodal involvement) (Aydiner et al., 2019; Gianni et al., 2011; Nounou et al., 2015; Schnitt, 2010; Shah et al., 2014). Furthermore, individual risks and benefits need to be evaluated prior to the application of any therapy (McArthur & Hudis, 2007). Generally, the first-line treatment for patients with early-stage BC is based on surgical resection of the tumor and related lymph nodes (Smith et al., 2007). Sometimes patients can choose between having breast-conserving surgery, which includes the removal of the tumor along with a margin of normal tissue, or mastectomy, where the whole breast is removed (American Cancer Society, 2015).

Additionally, surgery is usually followed by the application of adjuvant therapies, including chemotherapy, radiotherapy, endocrine therapy and/or targeted therapy to eliminate the remaining cancer cells and further reduce the risk of recurrence or metastization (American Cancer Society, 2015; Shah et al., 2014). Women with advanced BC normally undergo systemic treatments involving chemotherapy, hormonal therapy and/or targeted therapy (American Cancer Society, 2015).

### 2.2.1. Chemotherapy

Chemotherapy comprises the oral or intravenous administration of chemical drugs with anticancer properties and represents one of the main clinical tools applied to BC patients (American Cancer Society, 2015). These drugs act by targeting cancerous cells located anywhere in the body, destroying them and preventing their spreading through disruption of the cell division process (Caley & Jones, 2012). However as chemotherapeutic agents selectively target mitotically active cells, both tumoral and healthy cells are susceptible to their cytotoxic effects (Chakraborty & Rahman, 2012).

Like other systemic therapies (or radiotherapy), chemotherapy can be applied before the main treatment, normally surgery, to shrink the primary tumor and facilitate the subsequent medical procedures (designated as neoadjuvant chemotherapy) or after to avoid the risk of micrometastatic disease (designated as adjuvant chemotherapy). Clinical trials demonstrated that adjuvant chemotherapy application decreases BC mortality risk by 30 to 40% (Masood, 2016; Zhan et al., 2017). Normally, this approach represents the best option for patients that have large, high grade, ER-negative tumors with positive lymph nodes or to patients that poorly respond to hormone therapies (Burger et al., 2003; Zhan et al., 2017)

Chemotherapy is used in 60% of all cases of early-stage BC and even though BC is one of the most chemosensitive solid tumors, there is still a large number of patients who do not benefit from its therapeutic effects (Burger et al., 2003; Colombo et al., 2011; Florea & Büsselberg, 2013). Several clinical studies demonstrated that greater effectiveness is achieved when BC patients are treated simultaneously with a combination of therapeutic drugs rather than single agents (Bayat Mokhtari et al., 2017).

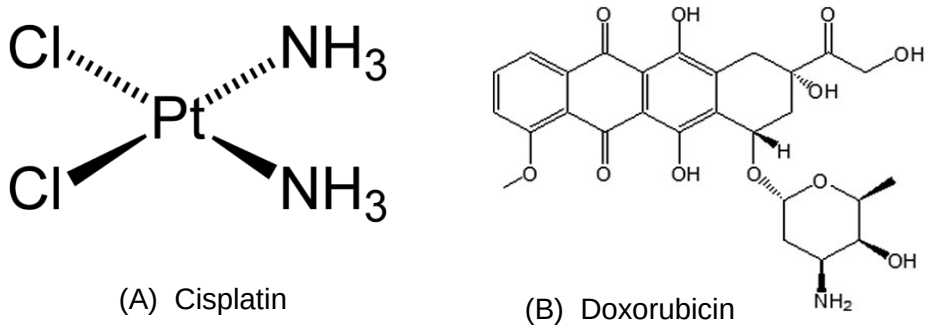
Chemotherapy drugs can be divided into several distinct classes (e.g Alkylating agents, antimetabolites, antitumor antibiotics and plant alkaloids) (Thirumaran et al., 2007), however in the present work, only the classes of alkylating agents and anthracycline antibiotics will be focused.

#### 2.2.1.1. Alkylating Agents (Platinum-based Agents)

Alkylating agents were the first known class of anticancer cytotoxic agents to emerge. They represent antiproliferative drugs that act by disrupting DNA replication and protein synthesis through the formation of covalent bonds with the DNA. Alkylators react via alkyl groups with different nucleophilic atoms on DNA bases but normal they generate adducts with the N7 position of guanine and/or adenine chemical bases (Kondo et al., 2010; Oronsky et al., 2012; Zhao et al., 2014b). Beyond DNA lesions, these electrophilic agents can also damage proteins, including membrane proteins and DNA repair enzymes (Oronsky et al., 2012).

Platinum-based agents, such as Cis (cis-diamminedichloroplatinum II), carboplatin and oxoplatin, are frequently classified as alkylating agents, although they do not mediate alkylation reaction due to the lack of the alkyl group. Instead, platinum analogues bind to the DNA through a platinum atom (Oronsky et al., 2012). Among this type of agents, Cis stands out for being the first platinum-containing compound approved by the Food and Drug Administration (FDA) for cancer treatment, namely cervical, ovarian, small cell lung, testicular and breast cancers (Kelland, 2007; Prabhakaran et al., 2013). The interest in using Cis as a chemotherapy agent arose when scientists discovered that this compound was able to form electrolysis by-products that inhibited *Escherichia coli* proliferation (Rosenberg et al., 1965). Nowadays, Cis is commonly administrated with other anticancer agents, such as 5-fluorouracil, taxanes and vinca alkaloids, especially in the treatment of BC (Prabhakaran et al., 2013).

Its chemical structure consists in a square planar complex composed of a central platinum ion (Pt2+ or Pt4+) bounded to leaving groups and carrier ligands represented, respectively, by two chloride ions (Cl-) and two ammine ligands (NH3) (Fig. 3A) (Petrovic & Todorović, 2016).




(A) Cisplatin (B) Doxorubicin

**Figure 3** – Chemical structure of 2 anticancer drugs: Cisplatin (A) and Doxorubicin (B).

Drug activation is mediated within the cell as a result of hydrolysis reactions that cause the replacement of chloride ligands by water molecules. This new molecule is

extremely electrophilic and for that reason, it can form platinum-DNA adducts and crosslinks between the N7 reactive center of purine bases (guanines and adenines) from the same or opposite strands. The intrastrand 1,2-d(GpG) crosslinks are more incident (70%) and cytotoxic than d(ApG) intrastrand crosslinks that represent 20% of all the genetic damages (Petrovic & Todorović, 2016). Consequently, the formation of DNA adducts will lead to cell cycle arrest at G1, S or G2 phases, and activation of the DNA repair mechanisms. However, in the absence of adequate damage repair, cells will undergo apoptosis (Eastman, 2006).

Additionally, Cis cytotoxicity is also related to oxidative stress. The decrease of the mitochondrial antioxidant glutathione (GSH) after Cis treatment promotes the formation of hydroxyl radicals and results in mitochondrial dysfunction evidenced by a substantial decrease in calcium influx and depolarization of the mitochondrial membrane potential (Saad et al., 2004).

Nevertheless, despite being a highly effective drug, the side effects induced by Cis (e.g nephrotoxicity, neurotoxicity and hearing impairments) and the development of drug resistance are barriers to a successful treatment outcome (Amable, 2016). In fact, acquired resistance to Cis has been reported in several types of cancer, including BC (Smith et al., 2007) and it is thought that it might be related with mechanisms involving the reduction of drug accumulation, enhanced detoxification activity, increased DNA repair ability and inactivation of apoptotic signalling pathways (Chen & Chang, 2019).

However, the details about these mechanisms are still not well elucidated and the existing information is quite limited. A better understating of the mechanisms involved in drug resistance is urgently needed to improve the effectiveness in the management of BC.

#### 2.2.1.2. Anthracycline Antibiotics

Anthracyclines are a group of broad-spectrum anticancer drugs that are used in the treatment of several types of cancer, including BC, and are integrated in the World Health Organization (WHO) Model list of essential medicine (Verrill, 2001; WHO, 2015). The first anthracycline to be identified was Daunorubicin in 1963 with its derivate Adryamicin, generic name Doxorubicin (Dox), and Epirubicin (EPI) being later discovered in 1968 and 1975, respectively (Verrill, 2001). Dox was originally isolated from the soil actinobacterium *Streptomyces peucetius* (Yang et al., 2014).

The chemical structure of anthracyclines consists in a planar anthraquinone ring system bound to an amino sugar called daunosamine. The quinone moiety is responsible for anthracyclines' cytotoxic character since it is involved in multiples reduction-oxidation reactions that will ultimately result in reactive oxygen species (ROS) induction and consequent oxidative damages. (Cortes-Funes & Coronado, 2007) Dox and EPI differ from

the anthracycline daunorubicin only by a single (C-14) hydroxyl group (Burney, 2011) (for more detail about the chemical structure of Dox see Fig. 3B).

Taking into account its extremely high efficacy to treat solid tumors, Dox represents one of the most in-demand antibiotics for use in BC adjuvant and neoadjuvant chemotherapy (Shevchuk et al., 2012). Considering its extremely wide therapeutic range, this antibiotic can also be applied for the treatment of osteosarcoma, gastric, thyroid, liver cancers and ovarian carcinoma (Cox & Weinman, 2016; Rastogi et al., 2018; Sherman et al., 2011; Strother & Matei, 2009; Zhou et al., 2018).

Two main mechanisms of action of Dox in cancer cells have been proposed: 1) Intercalation of Dox into DNA and inhibition of the topoisomerase II action and 2) Generation of ROS and oxidative damages (Taymaz-Nikerel et al., 2018). Topoisomerase II represents an ATP-dependent enzyme that promotes DNA helix unwinding to resolve DNA tangles and supercoils formed during DNA transcription and replication (Thirumaran et al., 2007). Topoisomerase II inhibitors act by simultaneously blocking topoisomerase II action and intercalating between DNA base pairs therefore forming stable irreversible DNA-drug-enzyme complexes (Beretta & Zunino, 2008). These ternary complexes will prevent the resealing step of the topoisomerase II catalytic cycle and consequently stall DNA replication (Beretta & Zunino, 2008; Rivankar, 2014). Therefore the persistence of the DNA breaks results in a large number of DNA fragments that will eventually lead to the cancer cells' apoptosis (Gruber et al., 2007).

Free radicals generation has been considered as a secondary mechanism of action of Dox. During Dox metabolism occur the production of superoxide anions and other ROS (Angsutararux et al., 2015). These ROS will cause DNA damage and lipid peroxidation, resulting in oxidative stress that can trigger cancer cells' death (Minotti et al., 2004).

Similarly to other chemotherapeutic drugs, Dox also induces associated adverse effects (e.g cardiotoxicity, myelosuppression, intestinal epithelium lesions and depression of the reproductive capacities) and drug resistance (Cortes-Funes & Coronado, 2007; Shevchuk et al., 2012). Although the mechanisms of Dox resistance still need further elucidation, there are some evidences that suggest that they might be related to altered drug transport, decreased topoisomerase II levels or alteration of its enzymatic activity, overexpression of antioxidant defences and impairments in apoptotic signalling pathways and cell cycle regulation (Beretta & Zunino, 2008; Burger et al., 2003; Li et al., 2015; Thirumaran et al., 2007).

Regarding the low drug efficacy and tumor resistance in cancer therapy, new drugs, more effective and with fewer side effects, as well as improvement of the conventional therapeutic strategies are needed. Strategies to overcome chemotherapy-associated

limitations include the administration of conventional chemotherapy drugs in combination with natural products, namely from marine origin (Abudabbus et al., 2017). This type of combinatorial treatment can stimulate the occurrence of synergistic interactions along with potentiation of drug efficacy and still allow the reduction of the administered drug dose, mitigation of adverse toxic effects and prevent the development of resistances (Pádua et al., 2015). However, in BC, the combination of natural compounds with chemotherapy drugs is poorly explored, suggesting the need for more studies to evaluate the relevancy of these combinations in BC treatment.

## 3. Marine Natural Compounds

Nature has always been a source of active substances for drug development, and, despite the advances in the synthetic biology field, most of the currently approved medicines are based on natural products (Harvey, 2008; Koparde et al., 2019; Newman & Cragg, 2016; Wright, 2019). This can be related to the fact that natural products, some with a complex chemical structure, present high bioavailability, high affinity to target and reduced loss of entropy when binding to proteins (Kim, 2012).

The focus is now turning towards the marine ecosystem that covers almost 70% of the Earth's surface and harbors a vast number of marine organisms, accounting for more than 95% of the whole biosphere (Dalmaso et al., 2015). The extreme physicochemical conditions found in this environment (e.g salinity, pressure, temperature, light and nutrient and oxygen concentrations) along with the lack of naturally defence systems specially in many marine invertebrates, give marine species the ability to produce various biological compounds that structurally and chemically differ from natural terrestrial products (Hu et al., 2011; Sawadogo et al., 2015; Schumacher et al., 2011; Senthilkumar et al., 2014). Over 3000 novel marine-derived products emerged during the last decade and till date, more than 22 000 natural products of marine origin have been reported (Pacheco et al., 2018; Sawadogo et al., 2015). Hereupon, oceans constitute endless sources of unknown bioactive compounds with promising pharmaceutical potential that must be assessed. According to several studies, marine natural products can display a wide range of health-promoting effects, such as antioxidant, anti-inflammatory, antidiabetic, antibacterial, and anticancer (Almeida et al., 2018; Khalid et al., 2018; Wali et al., 2019). In 2017, seven marine-derived pharmaceutical substances were approved by the FDA for use as clinical drugs. Among these, four were accepted for the treatment of cancer, including cytarabine (Cytosar-U®, for the treatment of leukemia), eribulin mesylate (Halaven® for the treatment of metastatic breast cancer), trabectidine (Adcetris® for the treatment of tissue sarcoma and ovarian cancer) and brentuximab vedotin (Yondelis® for the treatment of anaplastic large cell lymphoma and Hodgkin's lymphoma) (Dyshlovoy & Honecker, 2018). At present, a large

number of other marine-derived sources with anticancer potentialities are under pre-clinical and clinical trials (Sarfaraj et al., 2012).

These marine-derived compounds are essentially produced from sponges (37%), coelenterates (21%), microorganisms (18%), algae (9%), echinoderms (6%), tunicates (6%), mollusks (2%), bryozoans (1%) and others (Blunt et al., 2004).

### 3.1. Seaweed as a source of bioactive compounds

Among marine organisms, seaweeds (or macroalgae) are becoming a focus of great interest to the scientific and medical community due to its promising therapeutic and preventive properties, especially in the oncology field (Wali et al., 2019). This group of organisms, commonly abundant in intertidal zones, constitutes the basis of the marine food chain and is known for bearing a high content of unique bioactive molecules, namely carotenoids, polyphenolic compounds (e.g phlorotannins), sterols, polysaccharides, lipo and hydrosoluble vitamins, and polyunsaturated fatty acids) (Almeida et al., 2018; Khalid et al., 2018; Kim, 2012; Miranda-Delgado et al., 2018). Seaweeds present specific photosynthetic pigments that enable their classification into three major groups: Clorophyta (green algae), Rhodophyta (red algae) and Phaeophyra (brown algae). Within the three taxonomic groups, brown algae present the highest phytochemical content (e.g terpenes, carotenoids and phenolic compounds) (Gupta & Abu-Ghannam, 2011).

Brown seaweeds, such as hijiki (*Sargassum fusiforme*) Nori *(Porphyra spp.)*, wakame (*Undaria pinnatifida*) and kombu (*Laminaria japonica*), have been used for human consumption in Asian countries, namely in Japan, Korea and China, since the ancient times (Mebrahtu et al., 2015; Moghadamtousi et al., 2014; Satomi, 2017). Epidemiological studies demonstrated that the daily consumption of seaweeds decreased the incidence of BC, which explains the low rate of this malignancy in Asiatic women, when compared to women in the western world (Pádua et al., 2015; Teas et al., 2013). Thus, several brown seaweed-related compounds have been isolated and studied in recent years (Moghadamtousi et al., 2014).

#### 3.1.1. Carotenoids - Fucoxanthin

Fx is one of the most abundant xanthophyll carotenoids of the marine environment, that accounts for more than 10% of the total amount of carotenoids produced in nature (Rwigemera et al., 2014). As well as other pigments, namely chlorophyll a and c and β-carotene, this orange-colored pigment is widely found in the chloroplasts of brown seaweed. It presents light-harvesting ability by forming a complex with chlorophyll (Fucoxanthin-chlorophyll protein) and photoprotective functions, especially against photooxidative stress (Heo & Jeon, 2009; Martin, 2015; Mikami & Hosokawa, 2013; Peng et al., 2011). Its

molecule displays an unusual allenic bond, responsible for the high radical scavenging activity, and oxygenic functional groups in the polyene hydrocarbon chain, namely epoxy, carboxyl, carbonyl and hydroxyl groups (Kumar et al., 2013; Sachindra et al., 2007). However, since these functional groups are highly unstable and susceptible to isomerization and oxidation, Fx can be easily degraded as a result of heating, light and aerial exposure (Zhao et al., 2014a).

Evidences from tissue culture and animal experiments suggest that dietary Fx is mostly metabolized to fucoxanthinol in the gastrointestinal tract by digestive enzymes (lipase and cholesterol esterase), which in turn is converted in the liver into amarouciaxanthin A (Asai et al., 2004; Beppu et al., 2009). After entering the blood circulatory system, fucoxanthinol is preferably accumulated in visceral organs such as liver, lungs, kidney, heart and spleen, while amarouciaxanthin A accumulates mainly in the adipose tissue (Airanthi et al., 2011; Hashimoto et al., 2009; Peng et al., 2011).

Currently Fx, as well as its metabolite fucoxanthinol, are seen as a promising marine drug, since various studies have highlighted their health-promoting activities, including anti-inflammatory, antioxidant, antidiabetic, and anticancer activities, besides hepatic, cardiovascular and cerebrovascular protective effects (Zhang et al., 2015).

Since cancer is an oxidative stress-induced disease, it is thought that fucoxanthin's antioxidant role as a free radical and ROS scavenger is the main mechanism underlying its chemopreventive activity. In addition, Fx can also have a prooxidant action on cancer cells, increasing ROS. This is thought to be a protective mechanism to induce oxidative stress and, in that sense, promote the activation of cell death signalling pathways in malignant cells (Kumar et al., 2013; Liu et al., 2011; Pádua et al., 2015; Peng et al., 2011). Besides the antioxidant activity, some other mechanisms mediated by the regulation of molecules involved in the induction of cell cycle arrest, promotion of apoptotic processes or metastasis inhibition are potentially involved in Fx anticancer activity (Martin, 2015).

Several researchers reported the *in vitro* tumor-inhibitory effects of this carotenoid against some forms of leukemias (Ishikawa et al., 2008; Kim et al., 2010) and other types of cancers, including liver (Liu et al., 2009), lung (Mei et al., 2017), colon (Hosokawa et al., 2004), prostate (Satomi, 2012) and breast cancers (Rwigemera et al., 2015). Despite inducing toxicity effects against malignant cell lines, Fx and its metabolite, do not seem to induce adverse effects on normal cells (Ishikawa et al., 2008; Peng et al., 2011).

Particularly in BC, Fx has evinced to present cytotoxicity and antioxidant properties, namely against the estrogen-sensitive MCF-7 and estrogen-resistant MDA-MB-231 BC cell lines (Ayyad et al., 2011; de la Mare et al., 2013; Rwigemera et al., 2014, 2015; Yousefi et al., 2018).

Recent studies performed by Rwigemera et al., (2014; 2015) showed that Fx and its main metabolite fucoxanthinol decreased cells viability and increased the number of apoptotic cells in MCF-7 and MDA-MB-231 cell lines. Besides, it was reported that fucoxanthinol had higher antiproliferative and apoptosis-inducing activity in MCF-7 cells than its parent compound, Fx, probably due to the presence of a hydroxyl moiety in its structure (Konishi et al., 2006; Rwigemera et al., 2014, 2015). Evidences indicate that in MDA-MB-231 cells, fucoxanthinol apoptosis-inducing activities are correlated to the disruption of the Nuclear Factor kappa B (NF-kB) signalling pathway, which regulates apoptosis by controlling the transcription of anti-apoptotic genes. In addition, two apoptotic hallmarks were detected: PARP (Poly (ADP-ribose) polymerase) cleavages following Fx and fucoxanthinol treatment; and procaspase-3 fragmentation in response to Fucoxanthinol exposure (Konishi et al., 2006; Rwigemera et al., 2014). Konishi et al., also demonstrated that Fucoxanthinol induced apoptotic effects in MCF-7 cells by prompting nuclear condensation, DNA fragmentation and formation of apoptotic bodies (Konishi et al., 2006). Other studies reveal that these carotenoids do not modulate necrotic pathways (Rwigemera et al., 2015). Moreover, Ayyad and colleagues evaluated the antioxidant potential of Fx, amongst other compounds extracted from *Sargassum sp.*, and discovered that Fx displayed the highest antioxidant activity against the MCF-7 cells (72% inhibition) (Ayyad et al., 2011). According to recent *in vivo* and *in vitro* experiments, Fx extracted from *Undaria pinnatifida* (Wakame) exhibits a suppressor role in the occurrence of lymphangiogenesis in metastatic BC as it decreases the expression and secretion of the vascular endothelial growth factor C (VEGF-C) in MDA-MB-231 cells (Wang et al., 2019).

### 3.1.2. Polysaccharides - Fucoidan

Fc is a sulphated polysaccharide molecule commonly found in the cell walls of brown seaweed, such as *Fucus vesiculosus*, *Cladosiphon okamuranus* and *Laminaria saccharina*, and in some marine invertebrates like sea cucumbers (Hsu & Hwang, 2019). The structure of Fc is extremely variable as it highly depends on the seaweed species from which the compound is extracted from, the harvested season and the purification method used, but it is generally composed by L-fucose, sulphate and low quantities of galactose, mannose, xylose and uronic acid (Li et al., 2008). Over time several biological activities of Fc have been discovered and reported in the literature. Those bioactivities are cell-type specific and include antioxidant, anticoagulant, antiviral, antilipidemic, immunomodulatory, anti-inflammatory and antiproliferative effects (Lu et al., 2018; Pádua et al., 2015). Accumulating evidences suggests that Fc has anticancer activities against several human cancer cell lines, including colorectal (Han et al., 2015), bladder (Park et al., 2014), lung (Lee et al., 2012) and breast cancers (Zhang et al., 2013a) which candidates Fc as a potential

compound for replacing high toxic conventional chemotherapy drugs used in the clinical practice. Indeed, clinical studies registered tumor regression (partial or complete remission) and consequently an improvement in the overall survival of patients with cervical, hepatic, renal and breast cancer treated with Fc (Zhang et al., 2011; Zhang et al., 2013b).

Nevertheless, establishing a general cellular mechanism for fucoidan's anticancer activity is a difficult task, especially due to its structural variety and complexity. According to *in vitro* and *in vivo* experiments, various signalling pathways have been postulated to underlie the anticancer activity of Fc in BC.

Yamasaki-Miyamoto et al. (2009) reported that Fc isolated from *Cladosiphon okamuranus* affected MCF-7 cells' proliferation in a dose-dependent manner and triggers apoptosis through the activation of a caspase-8-dependent pathway, without affecting the viability of normal human mammary epithelial cells (Yamasaki-Miyamoto et al., 2009). In accordance, low molecular weight Fc extracted from *Undaria pinnatifida* and *Cladosiphon navae-caledoniae* also demonstrated to induce apoptosis and growth inhibitory effects on both ER-negative (MDA-MB-231) and ER-positive (MCF-7) BC cells (Lu et al., 2018; Zhang et al., 2011). Also, Zhang and colleagues verified that Fc from *C. navae-caledoniae* induced apoptosis in MCF-7 cells; however, by a caspase-independent mitochondria-mediated pathway, involving the phosphorylation of MAP kinases, depletion of the mitochondrial membrane potential, the decrease of anti-apoptotic proteins expression (Bcl-2 and Bcl-x) and the release of cytochrome c and apoptosis-inducing factor (AIF) (Zhang et al., 2011). Regarding apoptosis in the MDA-MB-231 cell line, the same researchers reported that it also occurs via a mitochondrial-dependent pathway, as it was observed in MCF-7 cells. However, these cells required the activation of caspases, including caspase-3, caspase-7, caspase-8 and caspase-9 and PARP, a hallmark of caspase-activation (Zhang et al., 2013a).

Additionally, differences between these two breast cancer cells' sensibilities to Fc cytotoxic effects were registered. Studies postulated that MCF-7 cell line is more sensitive to Fc anticancer activity (60% cell viability inhibition) in comparison to MDA-MB-231 cells (40% cell viability inhibition) with a nearly 20% higher inhibitory effect (Lu et al., 2018; Zhang et al., 2011).

Meanwhile Fc isolated from *Saccharina japonica*, *Undaria pinnatifida* and *Sargassum binderi* Sonder were cytotoxic against T47D breast cancer cell line, affecting proliferation and colony formation (Saepudin et al., 2018; Vishchuk et al., 2011). Similar results were observed in MDA-MB-231 and 4T1 BC cells treated with Fc from *Fucus vesiculosus* (Hsu et al., 2013).

Xue et al. (2012) demonstrated that Fc extracted from *Fucus vesiculosus* was able to inhibit the expression of the extracellular signal-regulated protein kinases ERK1/2 (MAP

kinases), Bcl-2 and survivin (inhibitor of apoptosis protein),and increase activation of caspase-3 in mouse breast cancer 4T1 cells, which resulted in decreased proliferation and apoptosis (Xue et al., 2012).

Fc may also have a regulatory role in controlling migration and invasion of BC cell lines. Findings suggest that Fc derived from *Sargassum hemiphyllum* decreases MCF-7 and MDA-MB-231 invasiveness, while Fc derived from *Fucus vesiculosus* and *Ascophyllum nodosum* only inhibits the invasion ability of MDA-MB-231 cells. (Haroun et al., 2002; Hsu et al., 2013; Wu et al., 2016). As a miRNA regulator, Fc proved to be able to epigenetically control the migration and invasion of these cells by affecting specific miRNAs expression (miRNA-29c and miR-17-5p) with crucial functions in tumorigenesis and metastasis (Wu et al., 2016). It was also demonstrated that Fc inhibits triple-negative breast cancer cells' (MDA-MB-231) adhesion to platelets, conducing to tumor metastasis suppression (Cumashi et al., 2007).

Since Fc has proved to have cytotoxic effects *in vitro* and *in vivo*, experiments combining fucoidan with conventional chemotherapeutic drugs might be a promising option for treating cancer patients. Zhang et al. (2013) reported that the therapeutic effect of Cis, tamoxifen and paclitaxel was enhanced when used along with Fc extract (*Cladosiphon navae-caledoniae*), since MDA-MB-237 and MCF-7 cell lines presented cell cycle arrest and higher apoptotic levels when exposed to the combinatorial treatments. Remarkably, Fc extract also exerted protective effects on healthy human fibroblast, diminishing drugs cytotoxicity on these cells (Zhang et al., 2013b). According to Tocaciu and collaborators (2016), co-administration of Fc with the conventional anticancer drugs like letrozole and tamoxifen in breast cancer patients, do not induce clinical adverse effects neither do alter drug plasma concentrations (Tocaciu et al., 2018).

### 3.1.3. Phytosterols - Fucosterol

Phytosterols represent a class of cholesterol-like molecules that integrate the cellular membranes of plants and algae. These compounds play an important physiological role in regulating membrane fluidity and permeability through the stabilization of the phospholipid bilayers, besides serving as hormones or precursors to steroids hormones in certain cell signalling pathways (Lopes, 2013). Within the marine environment, sterols are mostly found in seaweeds and can serve as biomarkers for distinguishing organisms of the three principal algal divisions. In brown seaweed (Phaeophyceae), the most abundant sterols are Fct (accounting for 83 to 97% of the total sterol content) and its derivates (Abdul et al., 2016), while red seaweed (Rhodophyceae) mostly contains cholesterol and derivates, and green seaweed (Chlorophyceae) mainly comprises ergosterol and 24-ethylcholesterol (Guedes et al., 2019; Sanchez-Machado et al., 2004).

As a phytosterol, the chemical structure of Fct presents strong resemblances with cholesterol molecule present in vertebrate animals, and it includes four rings, a hydroxyl group at C-3 and a side chain with a unique alkyl group at C-24 (Lopes, 2013).

Recently, studies demonstrated that Fct exhibits several beneficial biological properties, including antioxidant, anti-inflammatory antifungal, anticholinergic, antiphotodamaging, antidiabetic, antidepressant, antihyperlipidemic, antibacterial and anticancer (Abdul et al., 2016; Kim & Ta, 2011).

Considering the oncology field, there are only few reports in the literature describing the antitumoral effects of Fct in BC models, which highlights the urgency of conducting studies exploring Fct potential chemotherapeutic or chemopreventive effects on this type of cancer.

According to Ayaad et al. (2011) Fct extracted from *Sargassum sp.* showed weak to moderate antioxidant and antitumoral activities against the MCF-7 cells (Ayyad et al., 2011). Khanavi and co-authors (2012) demonstrated that fucosterol-containing fractions of the seaweed *Sargassum angustifolium, Sargassum swartzii* and *Cystoseira myrica* presented cytotoxicity against human colon carcinoma cells (HT29 and Caco-2 cells) and the T47D BC cell line, without inducing cytotoxic effects on the normal cell line NIH3T3 (Khanavi et al., 2012; Khanavi et al., 2010).

Lipid extracts from Antarctic seaweed where Fct was identified showed ability to reduce proliferation and enhance apoptosis in MDA-MB-231 and MCF-7 cell lines and to a much lesser extent in the non-tumoral cell line CHO (Pacheco et al., 2018).

Meanwhile, Caamal-Fuentes et al. (2014) investigated the antitumoral potential of hexane fractions (comprising Fct) isolated from the brown seaweed *Dictyota ciliolata*, *Padina sanctae-crucis*, and *Turbinaria tricostata* on different cancer cell lines. The results showed that Fct induced antiproliferative effects on the MCF-7 BC and SiHa cervical cancer cell lines (Caamal-Fuentes et al., 2014). Besides, a crude extract of the seaweed *Dictyota dichotoma*, from which Fct and other metabolites were isolated, also showed *in vitro* cytotoxicity toward the MCF-7 cell line (Abou-El-Wafa et al., 2013).

## 4. Two-Dimensional (2D) and Three-Dimensional (3D) in vitro Cell Culture Models in Drug Discovery

Drug discovery and development is a time-consuming and costly process. It may take up to about 15 years to bring a newly developed pharmaceutical into the market with a cost of at least 5 billion dollars (Benton et al., 2015; Joseph et al., 2018). Any medical drug that is discovered must undergo pre-clinical and clinical trials before it can be approved for clinical use. However, despite showing initial promise in the pre-clinical trials, many drugs fail in Phase II and Phase III of the clinical trials as they exhibit lack of therapeutic

efficacy (Edmondson et al., 2014; Langhans, 2018). In fact, it is reported that the average success rate in drug development for all the therapeutic areas is around 11%, while for the oncology field, the rate accounts for only 5% of success. Researchers believe that one of the main reasons behind the high attritions rates of new anticancer drug candidates in clinical trials is related to the use of inadequate preclinical models (Carvalho et al., 2017).

Cell-based assays have been used for decades in medical and pharmaceutical research as they represent simple, fast, inexpensive and reproducible tools for testing cellular responses to certain anticancer drug candidates. In addition, the use of cultured cells represents a great alternative to avoid or reduce the number of experiments performed on animal models, at a time when ethical concerns are increasing (Edmondson et al., 2014; Langhans, 2018; Nguyen et al., 2016).

Traditionally, monolayer *in vitro* cell cultures (2D cultures) are used as a standard cell-based model in pre-clinical studies, in which cells grow adhered to a flat surface such as culture flasks or Petri dishes (Breslin & O'Driscoll, 2013; Costa et al., 2016). Hundreds of cell lines isolated from tumors with specific genetic characteristics have been used in 2D culture with well-defined culture conditions. For the study of BC, several cell lines are available with different genetic characteristics that represent the different subtypes of BC. MCF-7 and MDA-MB-231 cells line are two examples of commonly used BC cell models, that are representative of the luminal A and triple-negative subtypes of BC. The study of these two cell lines is important to evaluate the influence of the hormone receptor status in the efficacy of anticancer compounds. Another cell line is the SKBR3 that is characterized for lacking hormone receptors and having HER2 amplification and constitutes an effective cell model to test HER2-targeted therapies (Holliday & Speirs, 2011; Subik et al., 2010).

However, despite being able to provide valuable information in the scope of oncology drug discovery, the 2D cell culture models present several limitations in predicting drug activity and toxicity *in vivo*, for not taking into consideration the natural tumor microenvironment and its 3D structure (Kim et al., 2004; Verjans et al., 2018).

As opposed to *in vivo*, in 2D monolayer cultures cells are usually flatter and more stretched, and their bidimensional morphology allows them to have unlimited access to nutrients, oxygen and growth factors from the cell culture medium. Besides, the monolayer essentially contains cells in proliferation, since detached dead cells are easily discarded during cell culture medium changes (Edmondson et al., 2014; Kapalczynska et al., 2018).

Nonetheless, one of the main disadvantages of 2D models consists in the lack of cell-cell interactions and cell-extracellular environment interactions, normally found in solid tumors, which consequently affects cell polarity and other related cellular functions, including cell proliferation and differentiation, cell viability, apoptosis, proteins and gene expression, response to stimuli and drug metabolism (Kapalczynska et al., 2018). The lack

of the complexity observed in 2D cultures leads researchers to take inaccurate information and therefore overestimate (or sometimes underestimate) the efficacy of some potential antineoplastic drugs (Imamura et al., 2015; Vinci et al., 2012).

In this regard, 3D culture techniques have emerged in order to realistically mimic *in vivo* physiological conditions and therefore bridge the existent gap between the conventional monolayer cell culture techniques and in *vivo* studies (Costa et al., 2018).

Accumulating evidences confirm that cells grown in a 3D physical shape have a better predictive capacity of *in vivo* cellular responses than cells grown as a monolayer (Santo et al., 2017). Different methodologies are used for 3D culture and can be divided into two groups: 1) scaffold-based, where cells are grown attached to hydrogel-based or polymeric matrices, or 2) scaffold-free (Langhans, 2018; Nunes et al., 2019a). Contrarily to the scaffold-based models, the scaffold-free technique does not use artificial substrates for cell attachment, allowing cells in suspension to self-assemble and form spheroidal multicellular aggregates usually named spheroids. The 3D configuration of spheroids models is more similar to the *in vivo* structure of tumors, favouring cell-to-cell contact, intercellular signalling networks, and extracellular matrix (ECM) proteins secretion and deposition (Joseph et al., 2018; Mehta et al., 2012). Multicellular spheroids display gradients of oxygen, nutrients, metabolites and soluble signals from the outside to the core, generating heterogeneous cell populations with different expression patterns, similar to what occurs in a tumor mass (Amaral et al., 2017; Fang & Eglen, 2017). Typically, spheroids are described as presenting three distinct zones of cells (Fig. 4): 1) The external layer of the spheroids corresponds to the proliferative zone, since cells located in this layer have easier access to nutrients, oxygen and essential metabolites from the culture medium; 2) the intermediate layer represents the hypoxic zone, comprising viable senescent cells, while 3) the inner layer presents necrotic cells in an acidic pH environment resultant of the limited diffusion of oxygen and nutrients (Carvalho et al., 2017; Costa et al., 2016; Mehta et al., 2012).

Furthermore, the level of compactness and morphology of spheroids vary according to several parameters including the cell lines used, the applied methodology, the formation period and initial cell density. Hence, according to Froehlich et al., (2016) spheroids can be classified as compact spheroids, multiple small spheroids, compact aggregates, loose aggregates and single cells suspensions (if no cell aggregation occurs) (Froehlich et al., 2016; Gencoglu et al., 2018).

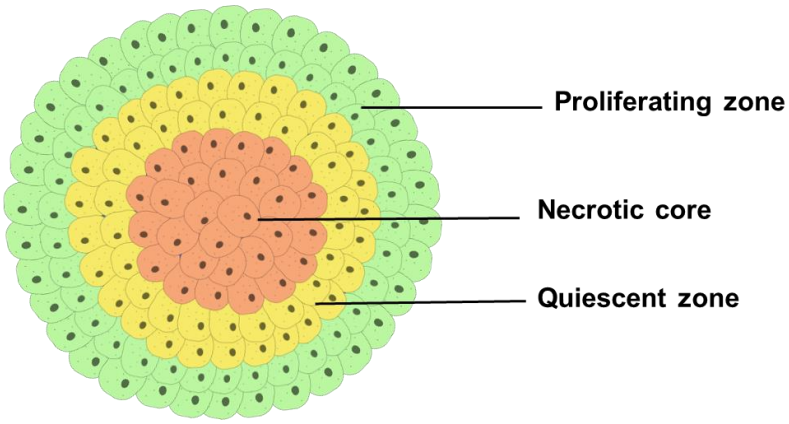



**Figure 4-** Schematic representation of the typical three-layer structure of a spheroid.

Amongst all the 3D scaffold-free culture approaches (e.g. hanging drop method, micro-based techniques and agitation-based approaches), the liquid overlay or forced floating method is considered one of the simplest and most suitable system for spheroids formation (Costa et al., 2018; Metzger et al., 2011). This technique entangles the use of non-adhesive surfaces, such as the commercially available ultra-low attachment (ULA) plates with U-shaped, tapered or V-shaped bottomed wells in order to minimize cell-substrate adhesion and ultimately promote, along with a centrifugation step, cells' self-aggregation into spheroids (a single spheroid per well) (Amaral et al., 2017; Fang & Eglen, 2017). The size of spheroids obtained via ULA plates can be easily managed since it is directly proportional to the initial seeding density plated. One of the key advantages of this approach is the generation of reproducible spheroids of uniform size and shape, suitable for high-throughput drug screening (Breslin & O'Driscoll, 2013).

The generation of 3D models from different BC cell lines (e.g. BT474, MCF-7, MDA-MB-231, T-47D and MDA-MB-157), has been investigated over recent years to better understand the mechanisms underlying the disease and screen the best anticancer drugs for its treatment (Benton et al., 2015; Breslin & O'Driscoll, 2016; Ham et al., 2016; Imamura et al., 2015). However, there are still some limitations regarding the application of 3D models as effective drug screening methodologies in the field of biomedical/cancer research, including the lack of standardized and consistent protocols for each cell line (Froehlich et al., 2016).

Therefore, more studies are needed in order to validate 3D culture systems and more accurately predict the clinical efficacy of anticancer drugs, minimizing the cost of failed clinical trials.

# – CHAPTER II –
Objectives

## Objetives

The aim of the present investigation was to evaluate the *in vitro* anticancer activity of three seaweed-derived bioactive compounds – Fx, Fc and Fct – alone and in combination with the conventional anticancer drugs Dox and Cis, in 2D and 3D cultures of a panel of 3 human BC cell lines – MCF-7, SKBR3 and MDA-MB-231 - and one non-tumorigenic epithelial breast cell line – MCF-12A. In light of the main aim of this research, the specific objectives to be achieved were:

- Test the cytotoxic, genotoxic and cell death induction effects of Fx, Fc and Fct, alone or in combination with the anticancer drugs (Dox and Cis), on the panel of 4 breast cell lines cultured in 2D.

- Optimize a 3D culture technique for the generation of MCAs from the tumor and non-tumor BC cell lines under investigation to be used in drug screening.

- Characterize MCAs morphology and ultrastructure using light and electron microscopy. Also, evaluate the expression of proteins related to proliferative and death pathways using immunocytochemistry in MCAs.

- Select the compounds that showed more promising effects on 2D cultures and evaluate their cytotoxic, antiproliferative and cell death effects on 3D cultures generated from the 4 breast cell lines, using colorimetric assays as well as morphological and immunocytochemistry analysis.

- Evaluate the possibility of using the panel of breast cells in 3D culture to assess the anticancer effects of natural compounds generating more predictive data.

# – CHAPTER III –
Material and Methods

# Material and Methods

## 1. Chemicals and Cell Culture Reagents

Dimethyl sulfoxide (DMSO) was purchased from VWR Chemicals (Solon, OH, USA). 3-(4,5-Dimethyl-2-thiazolyl)-2,5-diphenyl-2H-tetrazolium bromide (MTT), 4',6-diamidino-2-phenylindole (DAPI), Cis, cholera toxin, Dox, Fc, Fct, Fx, insulin, hydrocortisone, EGFR and Triton X-100 were obtained from Sigma Aldrich (St.Louis, MO, USA). Dulbecco's Modified Eagle's Medium (DMEM) without glutamine and without phenol red, fetal bovine serum (FBS), streptomycin and penicillin solution and trypsin/ ethylenediaminetetraacetic acid (EDTA) solution were acquired from Biochrom KG (Berlin, Germany). Dulbecco's Modified Eagle's Medium/Ham's Nutrient Mixture F12 (DMEM/F-12) medium without phenol red was obtained from GE Healthcare (Chicago, IL, USA). All other reagents and chemicals used were analytical grade.

Stock solutions of Dox, Fct and Fx were prepared in DMSO and Fc was prepared in cell culture medium. Stock solution of MTT was prepared in phosphate buffer saline (PBS) at a final concentration of 5 mg/ml. All those stock solutions were kept at –20ºC until used, except for the stock solution of Fc that was prepared immediately before use. Stock solution of Cis was prepared in 0.9% NaCl solution and kept at 4ºC up to 1/2 months. Exposure solutions were prepared before each experiment by diluting the appropriate volume of the stock solution into the respective fresh culture medium.

## 2. Cell Cultures

In this study, a panel of three BC cell lines was investigated: MCF-7, SKBR3, MDA-MB-231, along with a non-tumorigenic breast cell line, MCF-12A. MCF-7 was acquired from the European Collection of Authenticated Cell Cultures (ECACC). MCF-12A and MDA-MB-231 cell lines were purchased from the American Tissue Culture Collection (ATCC) and SKBR3 cell line was kindly provided by Professor Carmen Jerónimo of the Portuguese Oncology Institute - Porto. MCF-7, SKBR3 and MDA-MB-231 cell lines were cultivated with DMEM with high glucose content deprived of phenol red, supplemented with 10% of FBS and 1% of an antibiotic solution of streptomycin and penicillin. MCF-12A cell line was cultured with DMEM/F-12 supplemented with 20 ng/ml of EGFR, 100 ng/ml of cholera toxin, 0.01 mg/ml of human insulin and 500 ng/ml hydrocortisone, 10% FBS and 1% of an antibiotic solution containing streptomycin and penicillin. All the cell lines were maintained as monolayer cultures in T75 $cm^3$ culture flasks (Orange Scientific, Belgium) and were kept in the incubation chamber MCO 19AIC (Sanyo, Japan) at 37ºC with 5% $CO_2$. For cells growth and maintenance, the culture medium was replaced every two days. Cells were regularly observed using the Olympus CKX41 inverted phase-

contrast microscope (Olympus, Tokyo, Japan) in order to verify cell density and assure there were no signs of contamination or deterioration. At 80% of cell confluence, monolayer cells were subcultured (see protocol below in sub-section 2.2.). All the experiments were performed with cells in the logarithmic phase of growth. When the passage number went over 20 after the beginning of the experiments, new vials from the same stock cells were thawed (as described in sub-section 2.1.) and plated in new culture flasks.

### 2.1. Thawing of Frozen Cell Lines

To start a new cell culture, an aliquot of frozen cells was thawed at 37ºC and immediately mixed with the appropriate cell culture medium. Then, cells were transferred into a sterile T75 $cm^3$ cell culture flask and 14 ml of pre-warmed medium was added. The flask was incubated at 37ºC and 5% $CO_2$ and after 24 h, the medium was changed in order to remove all traces of DMSO in the culture. The medium was renewed every two days, and cells were subcultured when reached 80% of confluence.

### 2.2. Subculture of Adherent Cells

Prior to manipulation, the flasks were observed for confluence and contamination under an inverted microscope. The medium was carefully removed, and cells were washed twice with 4 ml of pre-warmed PBS at 37ºC. Then, 3 ml of Trypsin-EDTA solution (0.25% Trypsin and 0.02% EDTA) were added into the flask which was subsequently incubated at 37ºC for 5-7 min. When the cells started to be detached (observed under an inverted microscope), 7 ml of the corresponding cell culture medium were added to the flasks in order to stop trypsin action. Some of the cell lines, especially SKBR3 required extended trypsinization time and mechanical shearing to detach and disaggregate. After trypsinization, cell density and viability were assessed by the Trypan Blue Exclusion Method (see protocol below in sub-section 2.3). For sub-cultivation, around 1000 µl (MCF-7 and MDA-MB-231), 2500 µl (SKBR3) and 500 µl (MCF-12A) of cell suspension were added in new flasks along with the adequate amount of fresh culture medium to make up to a volume of 15 ml. The new flasks were kept at 37ºC and 5% $CO_2$ in a dry incubator.

### 2.3. Cell quantification by Trypan Blue Exclusion Method

To determine the number of pre-detached cells, 20 µl of cell suspension was mixed at 1:1 with 0.1% Trypan blue in PBS and then 10 µl of the mixture were loaded in a Neubauer Chamber. Cell quantification was performed on the inverted phase-contrast

microscope and the number of viable cells (cells with clear cytoplasm) and non-viable cells (blue-stained cells due to uptake of trypan blue) were registered. Cell density and cell viability were calculated using the following equations:

$$\textbf{Cell density (Nº cells/ ml)} = \text{Average Nº of counted cells} \times 2\ \textbf{(dilution factor)} \times 10^4\ \text{(Chamber conversion factor for Neubauer)}$$

$$\textbf{Cell viability (\%)} = \frac{\text{Nº of viable cells}}{\text{Nº of total cells}} \times 100$$

# 3. 2D Cultures

## 3.1. Determination of Cell Viability by MTT Reduction Assay

To assess the effects of seaweed compounds (Fx, Fct and Fc) alone and in combination with anticancer drugs (Dox and Cis) on cell viability, cells were plated in 96-multiwell culture plates (Orange Scientific, Braine-l'Alleud, Belgium) at a density of 0.5 x $10^5$ cells/ml ,100 µl/ well, and kept in the incubator at 37ºC and 5% $CO_2$. After 24 h, plated cells were exposed and co-exposed to various concentrations of Dox, Cis, Fx, Fct, and Fc (see Table 1).

Table 1- Experimental concentrations of Dox, Cis, Fx, Fct and Fc tested on each breast cell line.

| *Cell lines* / *Compounds* | MCF-7 | SKBR3 | MCF-12A | MDA-MB-231 |
|---|---|---|---|---|
| Dox | 0.01; 0.1 µM | | | 0.1; 1 µM |
| Cis | 10; 20 µM | | 1; 10 µM | 10; 20; 50 µM |
| Fx | 1; 10 µM | | | |
| Fct | 1; 5 µM | | | |
| Fc | 10; 50 µg/ml | | | |

Also, several controls were added in this assay: untreated cells were used as negative control (cells incubated with culture medium only); cells treated with 0.1% (v/v) DMSO or 0.9% (v/v) NaCl, and cells treated with both solvents simultaneously were used as solvent controls. After 72 h of exposure, images were captured by the phase-contrast microscope and effects on cell viability were assessed by the MTT assay. The MTT colorimetric assay measures the cell metabolic activity based on the ability of mitochondrial dehydrogenases (namely succinate dehydrogenase) to reduce MTT, a

yellow water-soluble tetrazolium dye, into purple-colored formazan crystals, in living cells. Therefore, the amount of formazan crystals formed during the reduction reaction reflects the number of originally viable cells in culture (Lim et al., 2015; Sliwka et al., 2016).

To perform this assay, 10 µl of MTT (0.5 µg/ml) were added per well in the dark, since MTT is light-sensitive (Bahuguna et al., 2017), and incubated at 37ºC and 5% $CO_2$. After 2 h of incubation, the exposure medium was removed, and the formazan crystals were dissolved in 150 µl of DMSO under slight agitation during approximately 30 min. After crystals dissolution, absorbance (A) was measured at 570 nm using a microplate reader Multiskan GO (Thermo Fisher Scientific, Waltman, MA, USA). The percentage of cell viability was calculated using the following equation:

$$\textbf{Cell viability (\%)} = \frac{A_{Sample}}{A_{Control}} \times 100$$

The results correspond to the mean of five independent experiments, each one performed on different days. After the statistical data analysis, the conditions that induced significant effects on cell viability were selected for further testing by nuclear condensation and comet assays (see subsections 3.2 and 3.3).

### 3.2. Cell Death Assessment by Nuclear Condensation Assay

The nuclear condensation assay enables the identification of cell death through the evaluation of the chromatin condensation state. Cells undergoing cell death display highly condensed nuclei in comparison with viable cells (Kroemer et al., 2009). Therefore, this assay was performed to determine the ability of the compounds to induce cell death. All the cell lines were seeded in 24-multiwell culture plates with flat bottom (Orange Scientific, Belgium) at a density of 0.5 x $10^5$ cells/ml and 0.3 x $10^5$ cells/ml for the tumorigenic (MCF-7, SKBR3 and MDA-MB-231) and normal cell lines (MCF-12A), respectively, and cultured during 24 h under standard cell culture conditions (37ºC and 5% $CO_2$). After adhesion, cells were exposed for 72 h to the experimental conditions selected. Subsequently, both adherent and non-adherent cells were collected, washed, centrifuged and fixated with 4% (w/v) paraformaldehyde (Sigma Aldrich, St.Louis, MO, USA) in PBS. Then, cells were attached into silane adhesive microscope slides (VWR International B.V, Amsterdam, The Netherlands) using Shandon Cytospin 3 cytocentrifuge (Thermo Fisher Scientific, Waltham, MA, USA) at 500 rpm for 5 min. The local of each sample was promptly circled with a diamond-tipped pen (in the back of the slide) and left to air dry. For the nuclear staining, samples were incubated with 20 µl of DAPI staining solution (1 µg/ml) for 10 min in the dark. DAPI forms a fluorescent complex with double-stranded DNA (Pacheco et al., 2018) allowing the observation of nuclear

morphology of the cells. Samples were blindly selected to avoid experimental bias and at least 300 cells per sample were counted under a fluorescence microscopy (Olympus IX71, Tokyo, Japan) using the total magnification of 200X (20X objective lens plus 10X eyepiece lens). The percentage of cells with condensed nuclei was calculated according to the following equation:

$$\textbf{\% of condensed nuclei} = \frac{\text{Nº cells with nuclear condensation}}{\text{Nº total cells}} \times 100$$

The results correspond to the mean of at least three independent experiments, each one performed on different days.

### 3.3. Genotoxicity Assessment by Comet Assay

The single cell gel electrophoresis (SCGE) assay, also known as comet assay, is a method for measuring the level of DNA damage in single cells. The alkaline version of this assay (pH > 13) allows the specific detection of alkali-labile sites and DNA strand breaks (Collins, 2004). Since cytotoxicity can be a confounding factor on the comet assay (Zarifi et al., 2018), the cytotoxic effects were evaluated after 24 h of exposure by the MTT assay and only the conditions with cell viability over 80% were selected for genotoxicity assessment by comet assay. Briefly, cells were seeded in a 96-multiwell culture plate at a density of 0.5 x $10^5$ cells/ml and after cell adhesion (24 h) at 37ºC and 5% $CO_2$, cells were treated for 24 h with the selected experimental conditions. Then, the MTT assay was performed as described before (see the sub-section 3.1.). The results correspond to the mean of at least three independent experiments, each one performed on different days**.**

For the alkaline comet assay, cells were seeded at 0.5 x $10^5$ cells/ml in 24-multiwell culture plate and allowed to adhere for 24 h in an incubator at 37ºC and 5% $CO_2$. Subsequently, cells were treated for 2 h with the conditions selected and by the end of the treatment, each sample was washed with PBS, trypsinized with 0.25% Trypsin/EDTA solution, collected (approximately 50.000 cells per well) and centrifuged at 5000 rpm for 1 min using the Micro Star 12 microcentrifuge (VWR International, Pennsylvania, USA). After centrifugation and removal of the supernatant, the cells were mixed with 100 µl of Low Melting Point Agarose (0.5%) and 70 µl of the mixture was applied on the microscope slide previously coated with 1% (w/v) Normal Melting Point Agarose. Immediately the coverslip was placed over the drop and slides were maintained at 4ºC. The slides were then incubated in a lysis solution [2.5 M NaCl, 100 mM $Na_2EDTA$, 10 mM Tris Base, pH 10 plus 1 % (v/v) Triton X-100, pH 10] during 1 h, at 4ºC, to lysate

the cells and release the DNA. After, slides were washed with distilled water, transferred into a horizontal electrophoresis tank and immersed in electrophoresis buffer (300 mM NaOH and 1 mM $Na_2EDTA$, pH ≥ 13) for 40 min at 4ºC for DNA unwinding. Electrophoresis ran for 20 min at 4ºC under a voltage gradient of 1V per cm (20V). Following electrophoresis, slides were rinsed in distilled water, dehydrated with absolute ethanol and lastly air-dried. Before analysis, slides were rehydrated in Tris-EDTA (TE) Buffer (Tris-HCl 10 mM and EDTA 1 mM) for 15 min under slight agitation and then 20 µl of SYBR Gold staining solution (Thermo Fisher Scientific, Waltman, MA, USA) was added to the buffer. Slides were stained for 30 min in the dark and under slight agitation. After staining, slides were analysed with a Nikon Eclipse E400 microscope (Nikon, Tokyo, Japan) connected to an epi-fluorescence illuminator Nikon C-SHG1 power supply for HG 100 W with 250x magnification (Semrock SYBRGold-A-NQF filter). The Comet Assay IV software (Perceptive Instruments, Haverhill, UK) was used to calculate the parameter % tail intensity. A hundred randomly selected cells were analysed per sample. Three independent experiments were performed, each on different days, in order to obtain feasible results.

# 4. 3D Cultures

## 4.1. Generation and Characterization of 3D MCAs Cultures

To determine the optimal conditions for MCAs formation, preliminary tests were performed where different cell densities and formation periods were tested. 3D MCAs of the MCF-7, SKBR3 and MDA-MB-231 human BC cell lines and the MCF-12A non-tumor breast cell line were generated by a forced-floating method using 96-well conical bottom Ultra-Low Attachment (ULA) microplates (Corning, New York, USA) and grown as single entities in each well.

Cells were first trypsinized (as described in 2.2. sub-section) and then several seeding concentrations were experimented: MCF-7 and SKBR3 cells were seeded at 5, 10, 20 and 40 x $10^4$ cells/ml; MDA-MB-231 cells were seeded at 10, 20, 40 and 50 x $10^4$ cells/ml; MCF-12A cells were seeded at 5, 10 and 20 x $10^4$ cells/ml. A working volume of 200 µl of cell suspension was used per well. After seeding, microplates were centrifugated at 200 g during 10 min using a ROTINA 380R centrifuge with swinging buckets (Hettich, Germany) and incubated at 37ºC in a 5% $CO_2$ atmosphere. Additionally, incubations periods of 3, 4, 7 (with medium change at day 5), 10 (with medium changes at day 5 and day 7) and 12 days (with medium changes at day 5 and day 7) were tested. The selection of the mentioned formation periods and cell densities relied on the results of past studies carried out in our laboratory (data not published) as

well as on the existent data in the literature (Dubois et al., 2019; Ho et al., 2012; Vinci et al., 2012).

The optimization process consisted in three different independent experiments. During all the experiments stereomicroscope images were captured. The MCAs formed at the selected optimal conditions were also photographed and the captured images were further analysed by a specialized software program (see subsection 4.3). Besides image analysis, these MCAs were harvested for assessment by light microscopy (see subsection 4.7), transmission electron microscopy (TEM) (see subsection 4.8) and immunocytochemistry (see subsection 4.9). Data obtained from image analysis, light microscopy, TEM and immunocytochemistry correspond to the evaluation of one single replica.

## 4.2. Exposure

According to the selected optimal conditions, MCAs were formed and exposed for 4 days under standard cell culture conditions (at 37ºC and 5% $CO_2$) to the experimental treatments that exhibited the most promising effects on 2D cultures. Cells treated with 0.1% DMSO were included as solvent control. MCAs were photographed after the formation period (start of the exposure) and at the end of the exposure for further automated image analysis (see subsection 4.3). Effects on cell viability and proliferation were assessed by the MTT (see subsection 4.4), Lactate dehydrogenase (LDH) (see subsection 4.5) and 5′-bromo-2′-deoxyuridine (BrdU) (see subsection 4.6) assays and selected MCAs were harvested for later analysis by light microscopy (see subsection 4.7) and immunocytochemistry (see subsection 4.9). Data obtained from the cell-based assays, image analysis, light microscopy and immunocytochemistry correspond to the analysis of four independent replicas.

## 4.3. Image Analysis

Photographs of the MCAs were taken using the Olympus SZX10 stereomicroscope, equipped with a digital camera DP21 (Olympus, Tokyo, Japan). Stereoscope images were analysed using the free download AnaSP software (Piccinini, 2015) and several morphological parameters were measured: area, convexity, diameter, volume, sphericity and solidity.

## 4.4. Determination of Cell Viability by MTT Reduction Assay

Cell viability was evaluated by the MTT assay accordingly to the method described for 2D cultures, with slight modifications. MCAs were incubated in the dark at

37ºC in a 5% $CO_2$ atmosphere with 20 µl of the MTT reagent per well during 4 h. After incubation, the formazan crystals along with the respective exposure medium were transferred from the ULA 96-well microplates into 96-well flat-bottomed microplates and centrifugated at 2000 g for 5 min in ROTINA 380R centrifuge with a 96-well plate rotor (Hettich, Germany). Briefly, 100 µl of the supernatant were removed (from a total of 200 µl/well) and, in order to prevent crystals loss, microplates were incubated overnight at 37ºC to promote evaporation of the remaining supernatant. Formazan crystals were dissolved in 100 µl of DMSO and, after 30 minutes under slight agitation, absorbance was measured and the percentage of cell viability calculated in the same manner as described for 2D cultures (see sub-section 3.1).

### 4.5. Determination of Cell Viability by LDH Assay

LDH release, which occurs in response to cellular damage, was assessed as a biomarker for cellular cytotoxicity following the manufacturer's instructions and using the reagents from the Pierce™ LDH Cytotoxicity Assay Kit (Thermo Fisher Scientific, Waltham, MA, USA). This cytoplasmatic enzyme is responsible for the conversion of lactate to pyruvate via NAD+ reduction to NADH. Subsequently, NADH reduces iodonitrotetrazolium chloride to formazan, a water-soluble red-colored product that can be measured at 490 nm (Kaja et al., 2017).

Prior to the assay, 20 µl of lysis buffer (10X) was added to the wells containing the MCAs from the solvent control group to promote maximum LDH release. These MCAs were included as a positive control. After 45 min of incubation, 50 µl of the medium from each well (including medium from the solvent control, treated and maximum LDH release groups) was transferred to a flat-bottom 96-well microplate and incubated for 30 min in the dark with 50 µl of the reaction mixture. Lastly, 50 µl of stop solution was added and after 5 min under slight agitation, the absorbance (A) was measured at 490 nm and 680 nm in a microplate reader Multiskan GO (Thermo Fisher Scientific, Waltman, MA, USA). The percentage of LDH release relative to the positive control (maximum LDH release) was calculated according to the following equation:

$$\text{LDH Release (\%)} = \frac{A_{\text{sample at 490nm-680nm-Blank}}}{A_{\text{control at 490nm-680nm- Blank}}} \times 100$$

### 4.6. Cell Proliferation Assessment by BrdU Assay

Effects on cell proliferation were evaluated by BrdU assay using the Cell Proliferation ELISA, BrdU (colorimetric) (Roche, Switzerland), however, the manufacturer's instructions were adapted for our 3D culture model. This method is based on the incorporation of the thymidine analogue 5′-bromo-2′-deoxyuridine (BrdU) into the

DNA of proliferating cells, followed by ELISA-based detection. The amount of BrdU incorporated during DNA synthesis reflects the number of replicating cells in culture (Gauthier et al., 2003).

Briefly, after MCAs exposure, 100 µl of each well medium was removed and MCAs were incubated with 10 µl of BrdU labelling solution (final concentration = 10 µM BrdU) for 5 h, at 37ºC. Then, MCAs were transferred into a flat-bottom 96-well microplate and following the removal of the labelling medium, they were incubated overnight at 4ºC. The next day, cells were fixed and DNA denatured by adding 100 µl of the FixDenant Reagent (30 min). After the removal of the FixDenant Reagent, BrdU incorporation into cellular DNA was detected by cells incubation with anti-BrdU-POD working solution (100 µl/well) for 90 min. Then, wells were rinsed with washing solution (PBS 1x) and 100 µl of substrate solution was added in order to perform photometric detection. Following 30 min of incubation, the absorbance (A) was measured at 370 nm and 492 nm in the microplate reader MultiskanGO. Cell proliferation relative to the control was calculated according to the following formula:

$$\text{Cell proliferation } (\%) = \frac{A_{\text{sample at 370 nm-492nm}}}{A_{\text{control at 370nm-492nm}}} \times 100$$

## 4.7. Histological Analysis

MCAs were fixed directly in their respective well of the 96-well microplate, after culture medium removal, by adding 200 µl of 10% buffered formalin. MCAs were then harvested with a micropipette and transferred into 1.5 ml tubes also containing 10% buffered formalin. During the harvesting of larger sized MCAs, the micropipette tip needed to be previously cut in order to avoid the destruction of their structure. After 24 h of fixation at room temperature, formalin was discarded and replaced by ethanol 70%. Prior to the histologic processing, ethanol was removed, and MCAs were enveloped in Histogel ™ (Thermo Fisher Scientific, Waltman, MA, USA) according to the manufacturer's instructions. MCAs were subsequently processed for paraffin embedding in an automatic tissue processor Leica TP1020 (Leica, Nussloch, Germany), according to a standardized protocol that consisted in three main steps: 1) dehydration with ethanol (Proclínica, Portugal) (incubation with ethanol 70%, ethanol 90%, ethanol 96%; absolute ethanol; absolute ethanol; 1 h each); 2) clearing with xylene (VWR, France) (incubation with absolute ethanol : xylene (1:1); xylene; xylene;1 h each) and 3) impregnation in paraffin (Thermo Fisher Scientific, Waltman, MA, USA) (Two baths of liquid paraffin, 1 h each). Posteriorly MCAs were embedded in paraffin blocks using the tissue-embedding workstation EG1140H (Leica, Germany). Each block contained two to three MCAs. Paraffin blocks were manually sectioned at 3 µm-thickness on a rotatory microtome Leica

RM2255 (Leica, Germany) into non-serial sections, which were placed on adhesive glass microscope slides (Klinipath, Belgium). Slides were incubated in an oven at 60ºC for at least 30 min and then placed at 37ºC until the histological staining or immunocytochemistry. The sections were stained with the haematoxylin and eosin (HE) staining technique, commonly used in histopathology, which started with the deparaffinization of the sections with xylene (two baths, 10 min each). As the dyes used for staining are aqueous, it was essential to previously rehydrate the sections by using descending alcoholic concentration solutions (absolute ethanol, ethanol 95% and ethanol 70%, 5 min each) and running tap water. Then, sections were stained with Mayer's haematoxylin (Merck, Darmstadt, Germany), for purple nuclear staining (2 min), rinsed in tap water, and counterstained with eosin Y 1% aqueous solution (Merck, Darmstadt, Germany) (5 min) to stain the cytoplasm and connective tissue fibres (Bancroft & Layton, 2019). Following the HE staining and a washing step, slides underwent processes of dehydration (three baths of absolute ethanol, 5 min each) and diaphanization (two baths of xylene, 3 min each). Finally, slides were mounted using Coverquick 2000 mounting medium (VWR International, France) and glass coverslips (Thermo Fisher Scientific, USA). The slides were allowed to dry at room temperature and then observed under an Olympus BX50 microscope (Olympus, Japan). Representative images were taken using a DP21 camera (Olympus Japan).

### 4.8. Transmission electron Microscopy (TEM)

MCAs were harvested and processed for TEM with the aim of assessing the ultrastructural morphology. Fixation was conducted directly within wells, after the removal of the medium, by adding 200 µl/well of 2.5% Glutaraldehyde in Cacodylate buffer 0.15 M, pH 7.2 (always prepared prior to use). MCAs were then transferred with micropipettes into 1.5 ml tubes, also containing the fixative. For the harvesting of the larger sized MCAs the micropipette tip was cut to prevent spheroid disintegration. Thus, MCAs were fixated at 4ºC during 2 to 3 h and washed with Cacodylate buffer 0.15 M, pH 7.2. Post-fixation was performed with 1% osmium tetroxide (Agar Scientific, Stansted, UK) in Cacodylate buffer for 2 h at the same temperature conditions. After the double fixation, MCAs were washed with Cacodylate buffer and dehydrated in graded ethanol series up to 100% (50% ethanol; 70% ethanol; 95% ethanol; absolute ethanol; absolute ethanol; 30 min each). The dehydrating agent was replaced for propylene oxide (Merck, Darmstadt, Germany) (two baths of propylene oxide, 30 min each), thus allowing MCAs' subsequently impregnation in epoxy resin. During impregnation, MCAs were subjected to three different mixtures of propylene oxide and epoxy resin, in which the resin concentration was gradually increased (propylene oxide + epon 3:1; 1:1; 1:3 - 1 h each

mixture) and ultimately embedded in only resin (epon – 1 h; epon – 10 min at 60ºC). Embedding was performed in silicone rubber moulds where MCAs were positioned at the bottom of the block in a horizontal position, whenever possible, and covered with epoxy resin. Polymerization occurred during 48 h at 60ºC and when polymerized, the hardened epoxy blocks were first trimmed manually with a razor blade and then sectioned with a diamond knife (Diatome, Nidau, Switzerland) on an ultramicrotome EM UC7 (Leica, Nussloch, Germany). Semithin sections of 1.25 µm thickness were collected on adhesive glass microscope slides (Klinipath, Belgium), stained for 1 min with a mixture 1:1 of 1 % methylene blue (Merck, Darmstadt, Germany) and 1 % azure II (Merck, Germany) and ultimately mounted with epoxy resin.

The 90 nm-thick ultrathin sections were deposited on 200 mesh hexagonal copper grids (Agar Scientific, Stansted, UK) and contrasted with 3% aqueous uranyl acetate (20 min) (Merck, Darmstadt, Germany) and Reynolds' lead citrate (10 min) (Merck, Darmstadt, Germany). Grids were analysed under an electron microscope JEOL 100CXII (JEOL, Tokyo, Japan), operated at 60 kV, and photographs of the representative ultrastructural changes were taken with the Orius SC1000 CCD digital camera (Gatan, Pleasanton, CA, USA).

### 4.9. Immunocytochemistry

For immunocytochemical analysis, sections of the paraffin-embedded MCAs were deparaffinised in xylene and hydrated with descending series of ethanol, tap water and distilled water (as described in section 4.7. for HE staining). Care was taken to ensure slides did not dry out throughout the experimental procedure. Next, slides underwent a heat-induced antigen retrieval step required to break the methylene bridges formed during the formalin-fixation process and expose the target antigenic sites (Kim et al., 2016). For this step, sections were heated in citrate buffer (0.01 M, pH 6.0) using a pressure cooker and incubated for 2 min after reaching the maximum pressure. Once this step is over, slides slowly cooled to room temperature and were washed with distilled water. Then slides were immersed for 10 min in a solution of 3% hydrogen peroxide in methanol, prepared immediately before use, to block endogenous peroxidase activity, and avoid non-specific background staining. After rising the slides in tris-buffered saline (TBS, pH 7.6), sections were circled with a hydrophobic pen (Leica, Biosystems, Nussloch, Germany) in order to minimize the volume of reagents used. Briefly, unspecific antibody binding was blocked for 5 min using the Protein block reagent from the NovoLink™ Max Polymer Detection System Kit (Leica Biosystems, Nussloch, Germany) and the sections were rinsed twice with TBS (5 min each). Thereafter, the sections were incubated overnight (16 h) in a humidified chamber at 4ºC with the following primary

antibodies: Rabbit monoclonal anti-Ki67, clone SP6 (Biocare Medical, Pacheco, CA, USA), dilution of 1:200; rabbit polyclonal anti-caspase-3, ab 13847 (Abcam, Cambridge, United Kingdom), dilution 1:5000. All the primary antibodies were diluted in PBS with 5% bovine serum albumin (BSA) (Nzytech, Lisbon, Portugal). As a negative control, sections were incubated with PBS and 5% BSA solution under the same conditions. The next day, sections were rinsed twice (5 min each) in TBS with 0.05% Tween 20 (Sigma Aldrich, St.Louis, MO, USA), and incubated for 30 min with the Post Primary Block solution. This step was followed by the incubation of slides with the NovoLink™ Polymer reagent (30 min) and subsequent washes in TBS with 0.05% Tween 20. Then, slides were incubated with DAB working solution (prepared before use by diluting DAB Chromogen in Novolink™ DAB Substrate Buffer, 1:20) during 2 min for signal revelation and rinsed in tap water. Lastly, slides were counterstained with haematoxylin (Merck, Darmstadt, Germany) for 1 min, washed in tap water, dehydrated in ethanol, cleared in xylene and coverslipped with Coverquick 2000 (VWR International, France) mounting medium for microscopy. Representative images were captured using an Olympus BX50 microscope (Olympus, Japan) attached to a DP21 camera (Olympus Japan).

## 5. Statistical Analysis

Descriptive and inferential statistics were performed using GraphPad Prism 6.0 software (GraphPad Software, La Jolla, CA, USA). The results are presented as mean ± standard deviation (SD) of at least 3 independent experiments. Significant differences ($p < 0.05$) were assessed by one-way ANOVA, followed by the post-hoc Holm-Šídák multiple comparison test whenever the ANOVA displayed significant results for the tested effects. The one-way ANOVA assumptions of normality and homogeneity of variance were confirmed by the Shapiro-Wilk's and Levene's tests, respectively.

# -CHAPTER IV-

Results

# Results

## 1. Effects in 2D Cultures

### 1.1. Assessment of Cytotoxic Effects – 72 h Exposure

Cytotoxic effects of Fx, Fct and Fc alone and in combination with the anticancer drugs Dox and Cis were assessed in three representative BC cell lines (MCF-7, SKBR3 and MDA-MB-231) and in a non-tumor breast cell line (MCF-12A) by the MTT assay, after 72 h of incubation. Several controls were incorporated in this assay: 1) untreated cells were used as negative control (cells incubated with cell culture medium only); while 2) cells treated with 0.1% (v/v) DMSO, 3) cells treated with 0.9% (v/v) NaCl and 4) cells exposed to both solvents simultaneously were used as solvent controls. Since no significant differences were detected in the one-way ANOVA statistical analysis, followed by post-hoc Holm-Sidak's multiple comparison test, between the percentages of cell viability of the solvent and the negative controls (data not shown), we opted to simply present in the control group the results for the negative control (untreated cells).

Following 72 h of exposure, both drugs Dox and Cis induced significant cytotoxic effects, when compared to the negative control, in all the cell lines tested (Fig. 5). In MCF-7 and SKBR3 cells, Dox at 0.1 µM (Fig. 5a and 5c), Cis at 10 and 20 µM (Fig. 5b and 5d) diminished both cell lines' viability in approximately 25%, 35% and 62%, respectively. In MDA-MB-231 cells treated with Dox at 1 µM and Cis at 50 µM (Fig. 5e and 5f), the cell viability decreased in around 47% and 65%, while in MCF-12A cells exposed to Dox at 0.1 µM and Cis at 10 µM, the reduction was about 26% and 58% (Fig. 5g and 5e), respectively.

As shown in Figure 5, Fx at 10 µM was able to significantly reduce viability (comparatively to the control), in all the cell lines tested, in about 23% (MCF-7), 31% (SKBR3), 32% (MDA-MB-231) and 37% (MCF-12A). Co-incubation of Fx with the anticancer drugs Dox and Cis also significantly reduced cell viability in: MCF-7 (Fx 1 µM + Cis 10/20 µM and Fx 10 µM + Dox 0.1 µM/ Cis 10/20 µM – Fig. 5a and 5b), SKBR3 (Fx 1 µM + Cis 20 µM; Fx 10 µM + Dox 0.1/ Cis 10/20 µM – Fig. 5c and 5d), MDA-MB-231 (Fx 1 µM + Dox 1/ Cis 20 µM; Fx 10 µM + Dox 0.1/ Cis 20 µM – Fig. 5e and 5f) and MCF-12A (Fx 1 µM + Dox 0.1/ Cis 10 µM; Fx 10 µM + Dox 0.01/0.1 µM / Cis 1/10 µM – Fig. 5g and 5h), relative to the control. However, those effects did not statistically differ from the effects of the single agents. Interestingly, only the co-incubation of Fx at 10 µM with Dox at 1 µM potentiated the cytotoxic activity of this anticancer drug in MDA-MB-231 cells, showing significant differences relative to the negative control and to the agents individually (Fig. 5e).

The results for Fct exposure (Fig. 6) showed that the compound alone did not induce cytotoxic effects in any of the cell lines tested. However, when combined with Dox at 0.1 µM, Fct at 5 µM presented marked effects in MDA-MB-231 cells' viability compared with cells incubated with Dox and Fct alone (Fig 6e). Also, some other combinations of Fct with Dox or Cis produced significant effects relative to control, but not when compared to the isolated compounds, for instance in: MCF-7 (Fct 1 µM + Dox 0.01/0.1 µM/ Cis 10/20 µM; Fct 5 µM + Dox 0.01/0.1 µM/ Cis 10/20 µM – Fig. 6a and 6b), SKBR3 (Fct 1 µM + Dox 0.1 µM/ Cis 10/20 µM; Fct 5 µM + Dox 0.1 µM/ Cis 10/20 µM – Fig. 6c and 6d); MDA-MB-231 (Fct 5 µM + Dox 1 µM – Fig. 6e) and MCF-12A cell lines (Fct 1 µM + Cis 10 µM; Fct 5 µM + Cis 10 µM – Fig. 6h).

Regarding the data obtained for Fc treatments (Fig. 7), it is possible to observe that cells' incubation with Fc alone did not reveal cytotoxic effects at any of the concentrations tested in any of the cell lines. In MDA-MB-231 cells, it was observed that Fc at 10 µg/ml attenuated the cytotoxic effects promoted by Dox at 1 µM, since there was a significant increase in cell viability when these two compounds were combined, relative to Dox alone (Fig. 7e). In contrast, the combination of Fc at 50 µg/ml and Dox at 1 µM significantly decreased the viability of MDA-MB-231 cells compared with Fc and Dox alone (Fig. 7e). Additionally, significant differences, relative to the negative control, were registered in certain co-exposures in: MCF-7 (Fc 10/50 µg/ml + Cis 10/20 µM – Fig. 7b), SKBR3 (Fc 10 µg/ml + Cis 20 µM; Fc 50 µg/ml + Cis at 10/20 µM – Fig. 7d), MDA-MB-231 (Fc at 10/50 µg/ml + Cis 20 µM – Fig. 7f) and in MCF-12A cells (Fc 10/50 µg/ml + Cis 10 µM; Fc 10 µg/ml + Cis 1 µM Fig. 7h). Despite having marked differences relative to control, the cytotoxicity induced by these conditions did not differ statistically from the single effects of those agents.

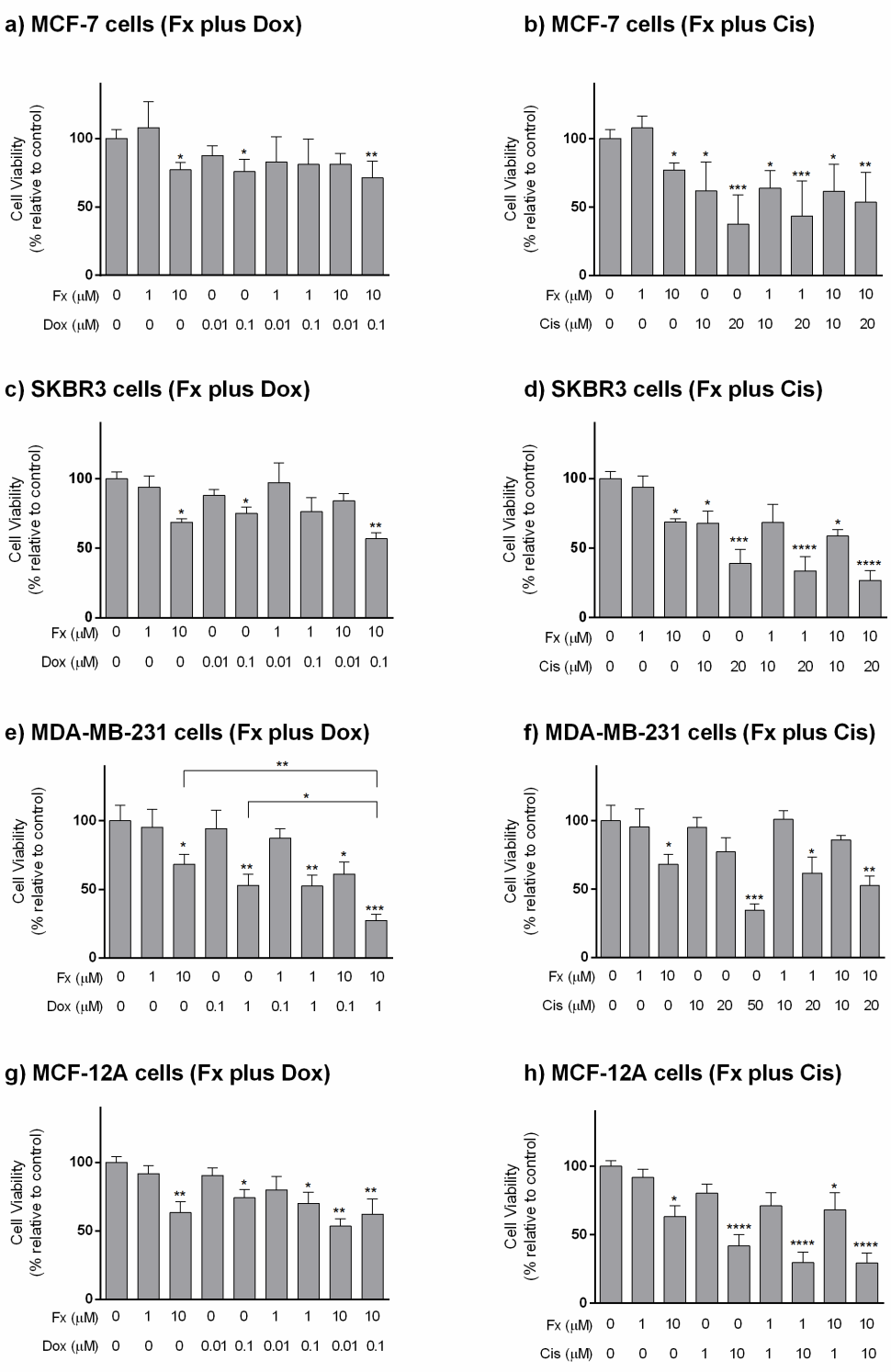



**Figure 5 -** Effect of Fx alone or co-incubated with Dox or Cis on cell viability, after 72 h of incubation, in MCF-7(a and b), SKBR3 (c and d), MDA-MB-231 (e and f) and MCF12A (g and h) cell lines assessed by MTT assay. Untreated cells (C) (cells in culture medium) were included as a negative control. Results are expressed as mean ± (SD) of five independent experiments. Significant differences (* P<0.05; ** P<0.01; *** P<0.001; **** P<0.0001), when compared to the control, were tested by one-way ANOVA, followed by post-hoc Holm-Sidak's multiple comparison test. Additionally, a Student's *t*-test was selectively used to access significant differences in MDA-MB-231 (Fx 10 + Dox 1 versus Dox1 and Fx 10 + Dox 1 versus Fx 10), and SKBR3 (Dox 0.1 versus C and Cis 10 versus C).

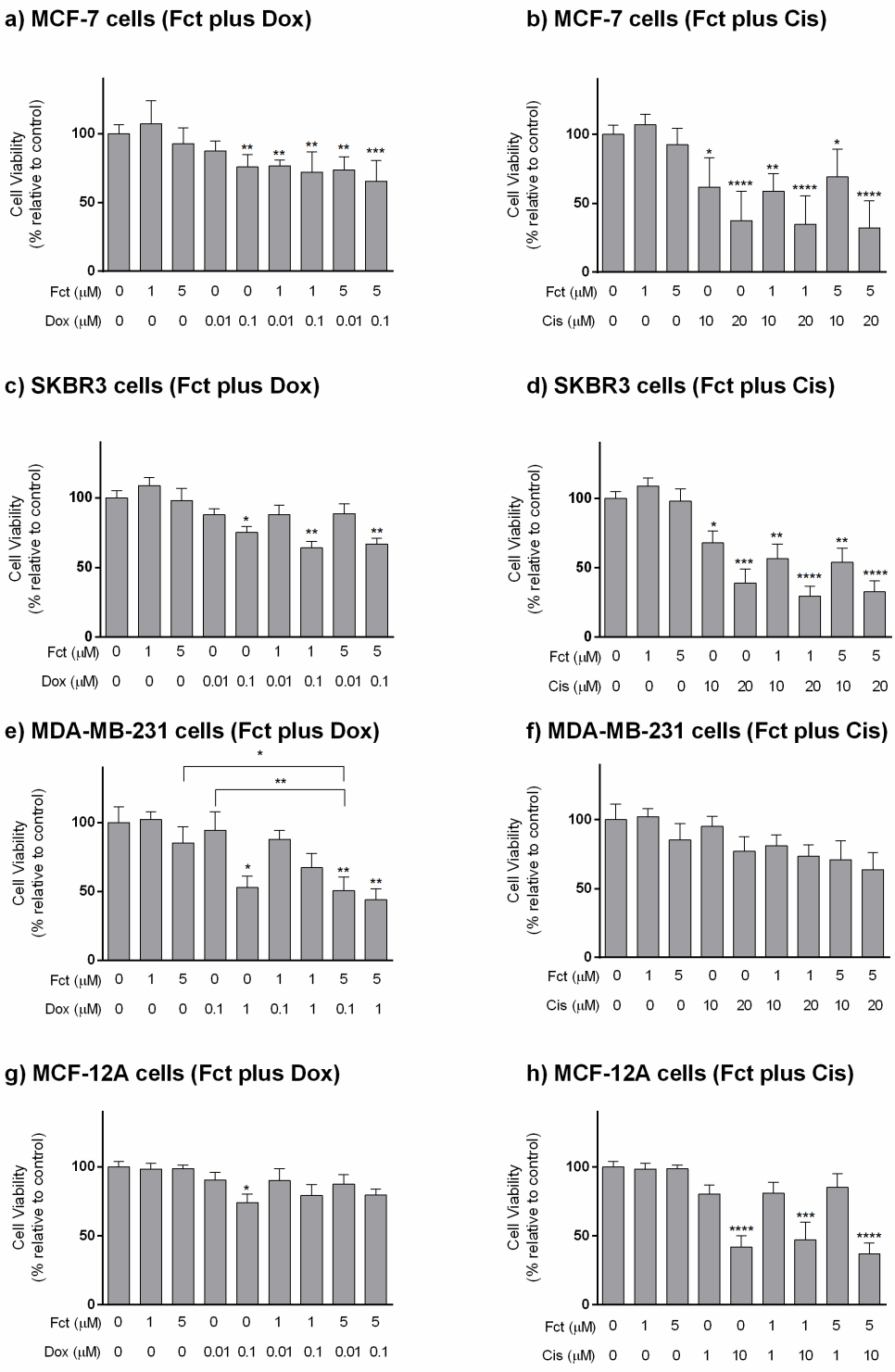



**Figure 6 -** Effect of Fct alone or co-incubated with Dox or Cis on cell viability, after 72 h of incubation, in MCF-7 (a and b), SKBR3 (c and d), MDA-MB-231(e and f) and MCF12A (g and h) cell lines assessed by MTT assay. Untreated cells (C) (cells in culture medium) were included as a negative control. Results are expressed as mean ± SD of five independent experiments. Significant differences (* P<0.05; ** P<0.01; *** P<0.001; **** P<0.0001), when compared to the control, were tested by one-way ANOVA, followed by post-hoc Holm-Sidak's multiple comparison test. Additionally, a Student's *t*-test was selectively used to access significant differences in MCF-7 (Fct 5 + Cis 10 versus C).

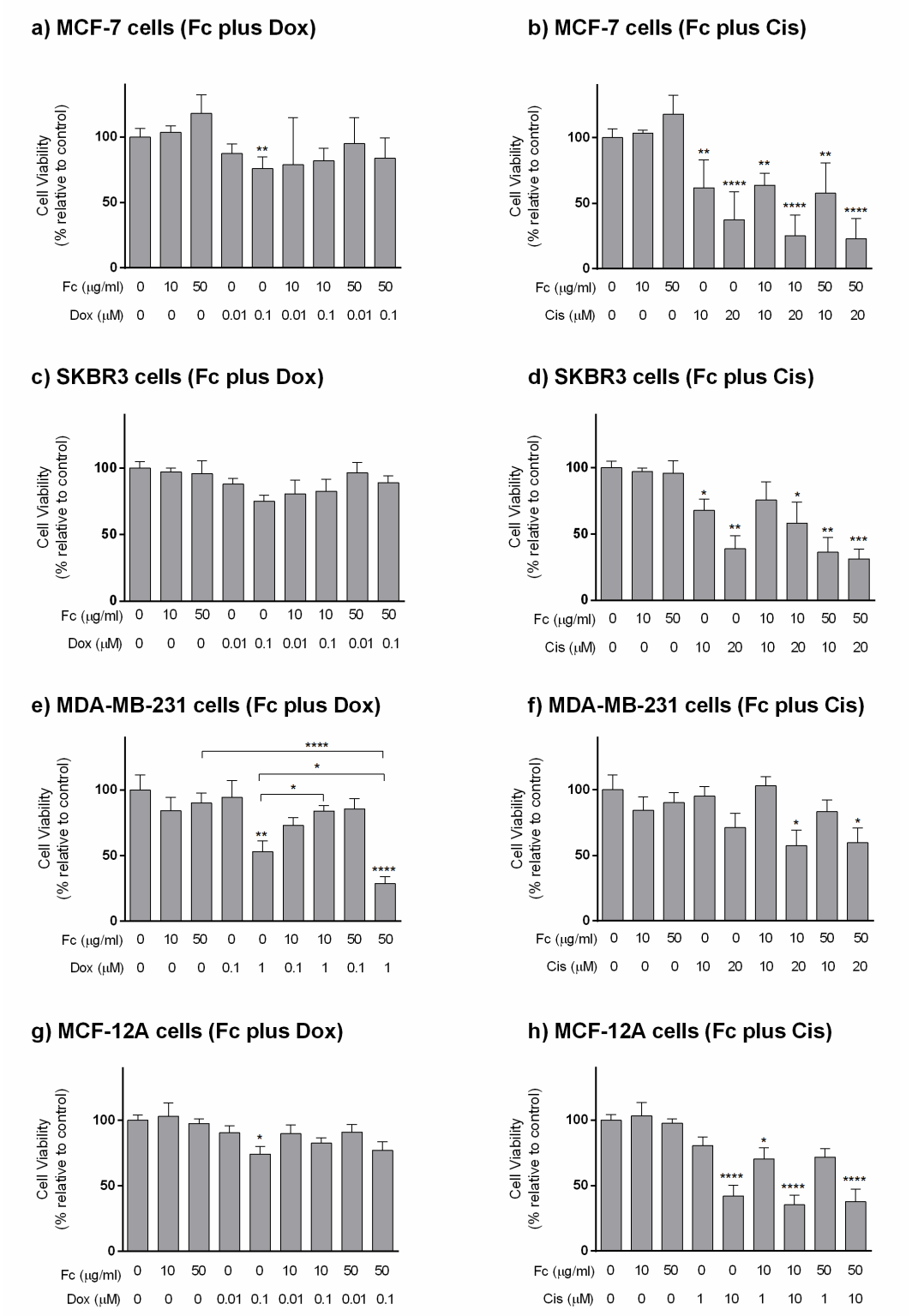



**Figure 7** - Effect of Fc alone or co-incubated with Dox or Cis on cell viability, after 72 h of incubation, in MCF-7 (a and b), SKBR3 (c and d), MDA-MB-231 (e and f) and MCF12A (g and h) cell lines assessed by MTT assay. Untreated cells (C) (cells in culture medium) were included as a negative control. Results are expressed as mean ± SD of five independent experiments. Significant differences (* P<0.05; ** P<0.01; *** P<0.001; **** P<0.0001), when compared to the control, were tested by one-way ANOVA, followed by post-hoc Holm-Sidak's multiple comparison test.

Complementarily, after 72 h of exposure, cells were analysed by phase-contrast microscopy and representative images were captured of certain selected conditions that showed evident morphological changes. These conditions were evaluated based on several cellular parameters such as: cell-substrate adhesion, cell density, presence of hypertrophic cells, vacuolization and the occurrence of finger-like protrusions (Table 2). Cis, Dox and Fx were the compounds that induced more morphological alterations, in relation to the control (Fig. 8)

According to our qualitative analysis (Fig. 8 and Table 2), Cis induced morphological effects in all the cell lines, when compared to the control, showing the presence of several dead cells and cell debris and a marked decrease in cell density. Besides, the examination of Cis-treated cells revealed an increase in the number of vacuoles (in MCF-7) and hypertrophic cells (in MCF-7, MDA-MB-231 and MCF-12A), and the occurrence of cell rounding (due to cell shrinkage) in cells that remained attached to the substrate in all the cell lines. Some MCF-12A cells exposed to Cis at 10 μM presented cell membrane extensions, identified as finger-like protrusions.

All the cell lines exposed to Dox presented lower cell density, higher level of vacuolization (except in MDA-MB-231) and cell swelling (except in SKBR3 cells) as well as a rounder shape, characteristic of injured cells. In MDA-MB-231, the number of adhered cells reduced when exposed to Dox at 1 μM. Additionally, the presence of several finger-like protrusions was frequently detected in almost all the Dox-treated cell lines, except in SKBR3 cells.

Regarding the natural compounds, Fx slightly decreased the number of cells in culture and cell adhesion (in MCF-7 and MDA-MB-231), when compared to the control, but apart from that no more morphological alterations were observed in none of the cell lines tested. Also, no evident changes were detected in most of the morphological parameters assessed in MDA-MB-231 cells exposed to Fc at 50 μg/ml, except for a slight reduction in the number of adherent cells treated with Fc. In the combinatorial treatments, the observed alterations did not markedly differ from the morphological changes registered in cells exposed to the anticancer drugs individually.

**Table 2**- Heatmap of the qualitative evaluation of the effects induced by the tested compounds (Dox, Cis, Fx and Fc) on different morphological parameters at 72 h of exposure. Comparisons were made relative to the negative control (untreated cells). The yellow color indicates no changes in relation to the control. The red and green colours indicate a decrease or an increase, respectively, of the measured parameter relative to the control.

| | Morphological parameters / Conditions | Cell-substrate adhesion | Cell density | Hypertrophy | Vacuolization | Finger-like protrusions |
|---|---|---|---|---|---|---|
| MCF-7 | Fx 10 µM | | | | | |
| | Dox 0.1 µM | | | | | |
| | Cis 20 µM | | | | | |
| SKBR3 | Fx 10 µM | | | | | |
| | Dox 0.1 µM | | | | | |
| | Cis 20 µM | | | | | |
| MDA-MB-231 | Fx 10 µM | | | | | |
| | Fc 50 µg/ml | | | | | |
| | Cis 50 µM | | | | | |
| | Dox 1 µM | | | | | |
| MCF-12A | Fx 10 µM | | | | | |
| | Dox 0.1 µM | | | | | |
| | Cis 10 µM | | | | | |

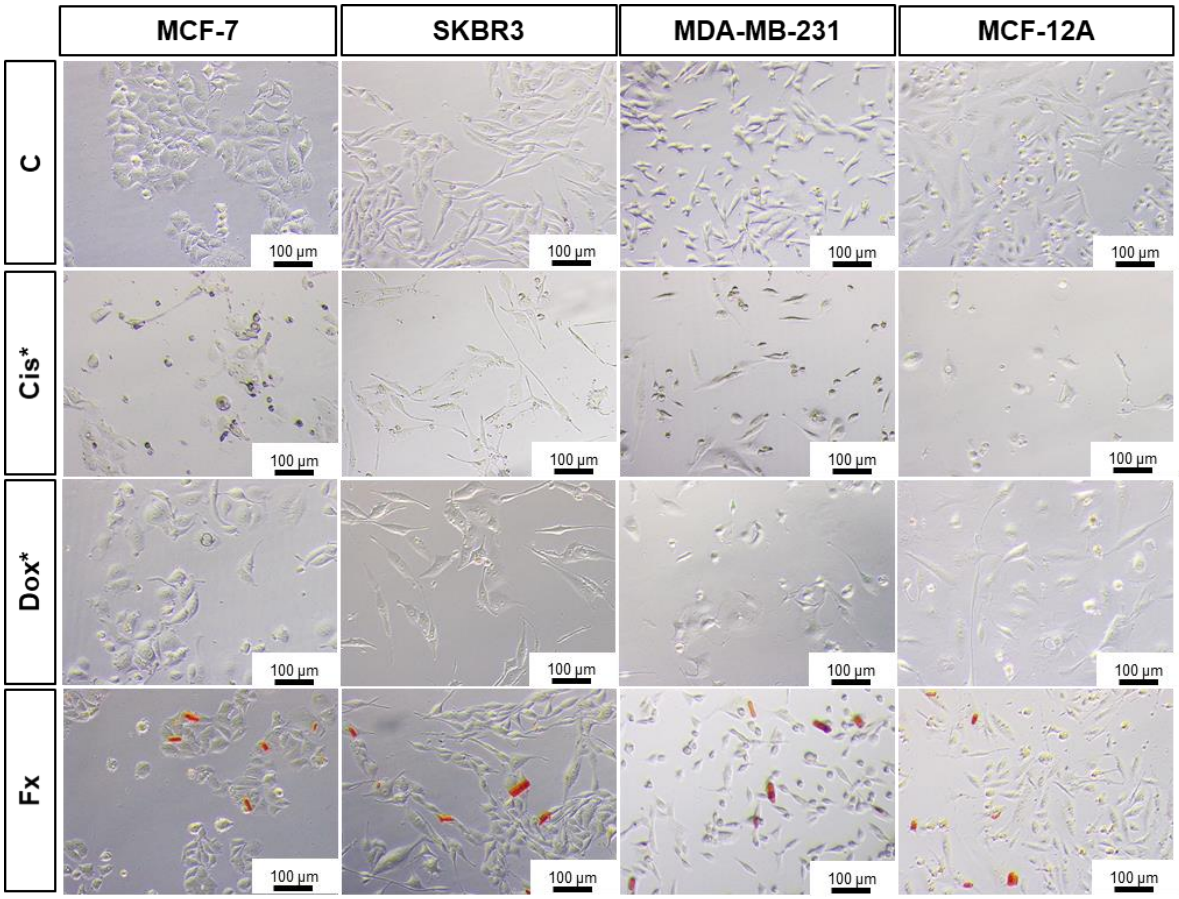



**Figure 8-** Representative images of the morphological changes in MCF-7, SKBR3, MDA-MB-231 and MCF-12A monolayer cell cultures exposed to Cis, Dox and Fx for 72h. The * indicates that exposure concentrations differed between cell lines. Cis was administrated at 10 µM (in MCF-12A), 20 µM (in MCF-7 and SKBR3) and 50 µM (in MDA-MB-231). Dox was applied at 0.1 µM (in MCF-7, SKBR3 and MCF-12A) and at 1 µM (in MDA-MB-231). Fx was tested at 10 µM in all the cell lines. Untreated cells (cells in culture medium) were included as a negative control (C). In Fx exposure conditions, it is visible some orange precipitates. Scale bar: 100 µm.

Taking all these results into consideration, we selected the statistically significant conditions (summarized in Table 3) in order to explore the mechanisms underlying the observed cytotoxic effects. Thus, solely the selected conditions were tested in subsequent assays.

**Table 3-** Summary of the conditions that induced statistically significant cytotoxic effects on the different cell lines, in comparison with the negative control or the isolated compounds, after 72 h of exposure.

| Cell lines / Compounds | **MCF-7** | **SKBR3** | **MDA-MB-231** | **MCF-12A** |
|---|---|---|---|---|
| **Dox** | Dox 0.1 µM | Dox 0.1 µM | Dox 1 µM | Dox 0.1 µM |
| **Cis** | Cis 10 µM<br>Cis 20 µM | Cis 10 µM<br>Cis 20 µM | Cis 50 µM | Cis 10 µM |
| **Fx and combinations** | Fx 10 µM | Fx 10 µM | Fx 10 µM<br>Fx 10 µM + Dox 1 µM | Fx 10 µM |
| **Fct and combinations** | - | - | Fct 5 µM+ Dox 0.1 µM | - |
| **Fc and combinations** | - | - | Fc 10 µg/ml + Dox 1 µM<br>Fc 50 µg/ml + Dox 1 µM | - |

### 1.2. Assessment of Cell Death Induction

In order to assess the ability of the isolated or combined compounds to induce cell death, the cell lines were incubated for 72 h with the previously selected conditions and the nuclear condensation assay was performed. As shown in Figure 9a and b, Cis at 10 and 20 µM significantly increased the percentage of cells with nuclear condensation in a dose-dependent manner in MCF-7 (by 8% and 12%, respectively) and SKBR3 cells (by 5% and 12%, respectively). Besides, Cis at 10 µM (in MCF-12A) and 50 µM (in MDA-MB-231) increased the percentage of cells with nuclear condensation by 5% and 9%, respectively (Fig. 9c and f). In the case of Dox at 0.1 µM, it only increased the percentage of cells with condensed nuclei in MCF-12A cells (by 13%). None of the seaweed-derived compounds showed the ability to increase nuclear condensation in any of the four cell lines used. In MDA-MB-231 cells, Fx at 10 µM plus Dox at 1 µM (Fig. 9c) showed a significant increase of nuclear condensation, when compared to Fx, but without significant differences relative to Dox alone. Furthermore, Fc at 50 µg/ml and Dox at 1 µM alone did not induce significant effects on the percentage of condensed nuclei, while the combination of these two agents caused a significant induction in cell death of MDA-MB-231 cells, when compared to the negative control and Fc (Fig 9e).

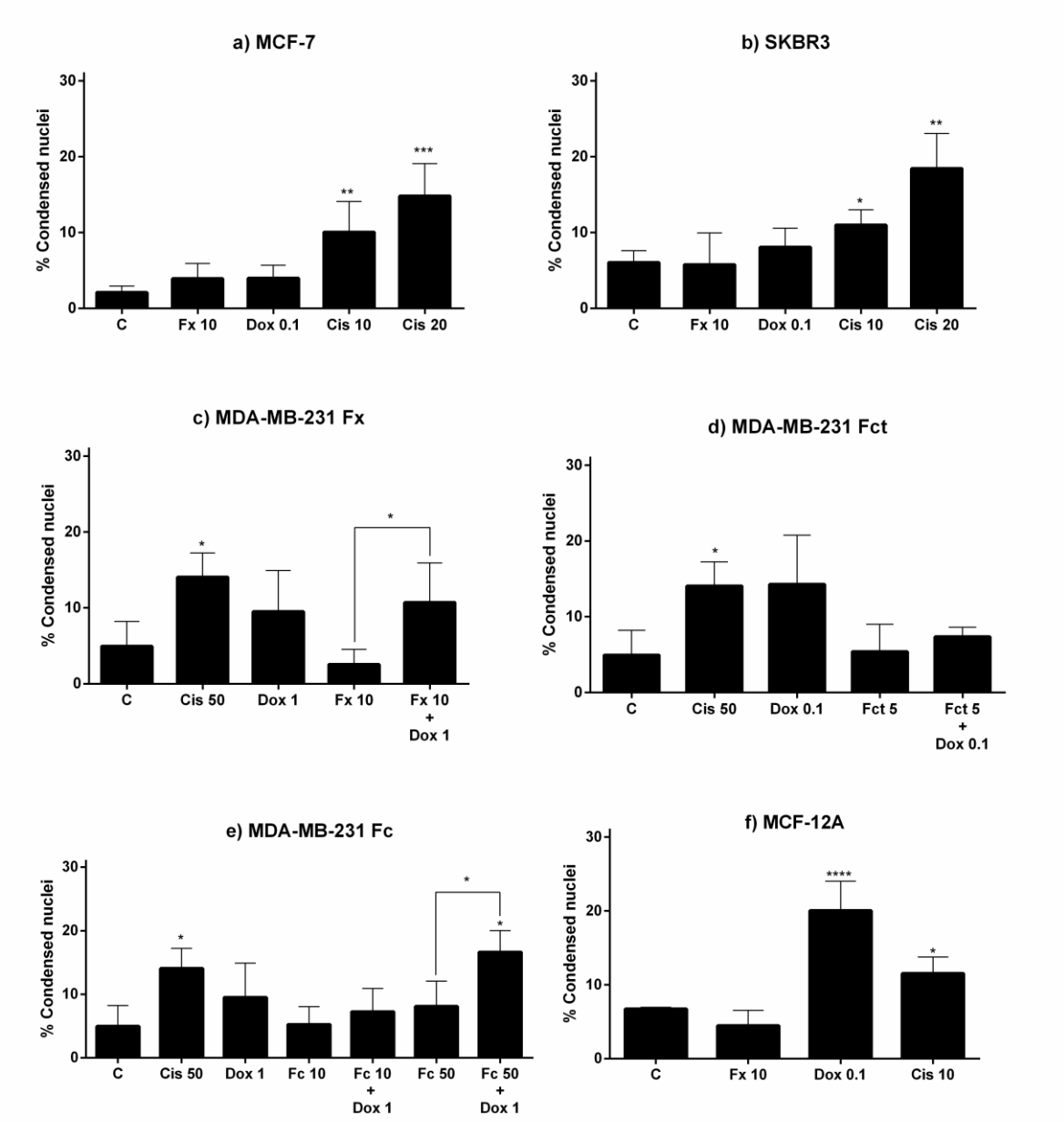



**Figure 9-** Effect of Fx (10 µM), Fct (5 µM) and Fc (10 and 50 µg/ml) alone and in combination with Dox (0.1 and 1 µM) or Cis (10, 20 and 50 µM) on induction of cell death in 2D cultures. MCF-7 (a), SKBR3 (b), MDA-MB-231(c, d, e) and MCF-12A (f) cells were incubated for 72 h and induction of cell death assessed by nuclear condensation assay. Untreated cells (cells in culture medium) were included as a negative control (C). Data are expressed as the percentage of condensed nuclei, relative to the negative control, and are presented as mean ± SD of at least three independent experiments. Significant differences (* $P < 0.05$, ** $P < 0.01$; *** $P < 0.001$; **** $P < 0.0001$), when compared with the negative control, were determined by one-way ANOVA, followed by a Holm-Sidak's multiple comparisons test. Additionally, a Student's *t*-test was selectively used to access significant differences in SKBR3 (Cis 10 versus C), MDA-MB-231 (Fx 10 + Dox 1 versus Fx 10; Fc 50 + Dox 1 versus Fc 50) and MCF-12A (Cis 10 versus C).

### 1.3. Assessment of Cytotoxic Effects - 24 h Exposure

To select the appropriate exposure conditions for the genotoxicity testing, we evaluated the cytotoxic effects after 24 h of incubation, using the MTT assay. Results were expressed as the percentage of cell viability, relative to the control. Among all the tested compounds, only Cis at 20 µM exhibited a reduction of 51% on the cell viability of MCF-7 cells, in comparison to the respective control (Fig. 10a). None of the other exposure conditions had significant cytotoxic effects at 24 h.

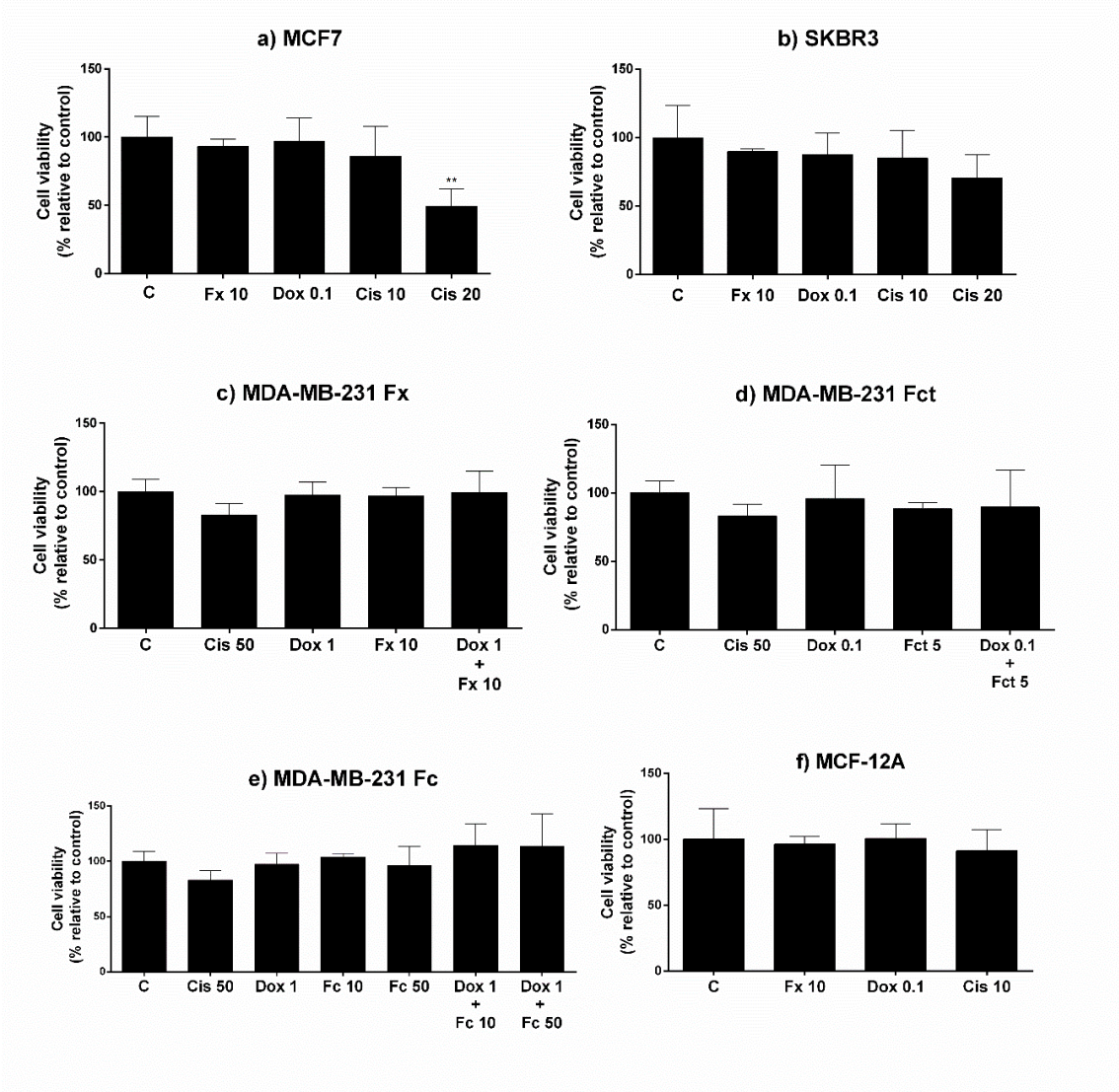



**Figure 10-** Effect of Fx (10 µM), Fct (5 µM) and Fc (10 and 50 µg/ml), alone and in combination with Dox (0.1 and 1 µM) or Cis (10, 20 and 50 µM) on cell viability in 2D cultures. MCF-7 (a), SKBR3 (b), MDA-MB-231(c, d, e) and MCF-12A (f) cells were incubated for 24 h and viability was assessed by the MTT assay. Untreated cells (cells in culture medium) were included as a negative control (C). Data are expressed as the percentage of cell viability, relative to the negative control, and are presented as mean ± SD of at least three independent experiments. Significant differences (** $P < 0.01$) when compared with the negative control were determined by one-way ANOVA, followed by a Holm-Sidak's multiple comparisons test.

### 1.4. Assessment of the Genotoxic Effects

For the genotoxicity assessment, cell viability is required to be over 70 to 80% (Ribeiro et al., 2006; Tice et al., 2000). Attending to the results obtained on the MTT assay, the only condition that caused cell viability to reduce below 80%, after 24 h of exposure, was Cis at 20 µM. Therefore, this condition was not appraised in any of the cell lines in this assay. Additionally, only the higher concentration of Fc was selected to be tested in the MDA-MB-231 cell line. Due to technical reasons, we could not evaluate the genotoxic effects of the combination Fct 5 µM + Dox 0.1 µM in MDA-MB-231 cells. Thus, cells were exposed to the selected conditions during 2 h and the amount of DNA damages (strand breaks) were analysed by the Comet assay (alkaline version). Data were expressed as the percentage of DNA in tail (Fig. 11).

Results showed that Dox at 1 µM alone or in combination with the tested marine compounds (Fx 10 µM and Fc 50 µg/ml) increased DNA damage in MDA-MB-231 cells, in relation to the control and the natural agents alone (Fig. 11c and d). However, MDA-MB-231 cells treated with the combination of Fx 10 µM plus Dox 1 µM showed a significant decrease in DNA damage when compared to cells exposed to Dox alone (Fig. 11c and Fig. 12). No statistically significant differences were detected on the remaining cell lines and tested compounds.

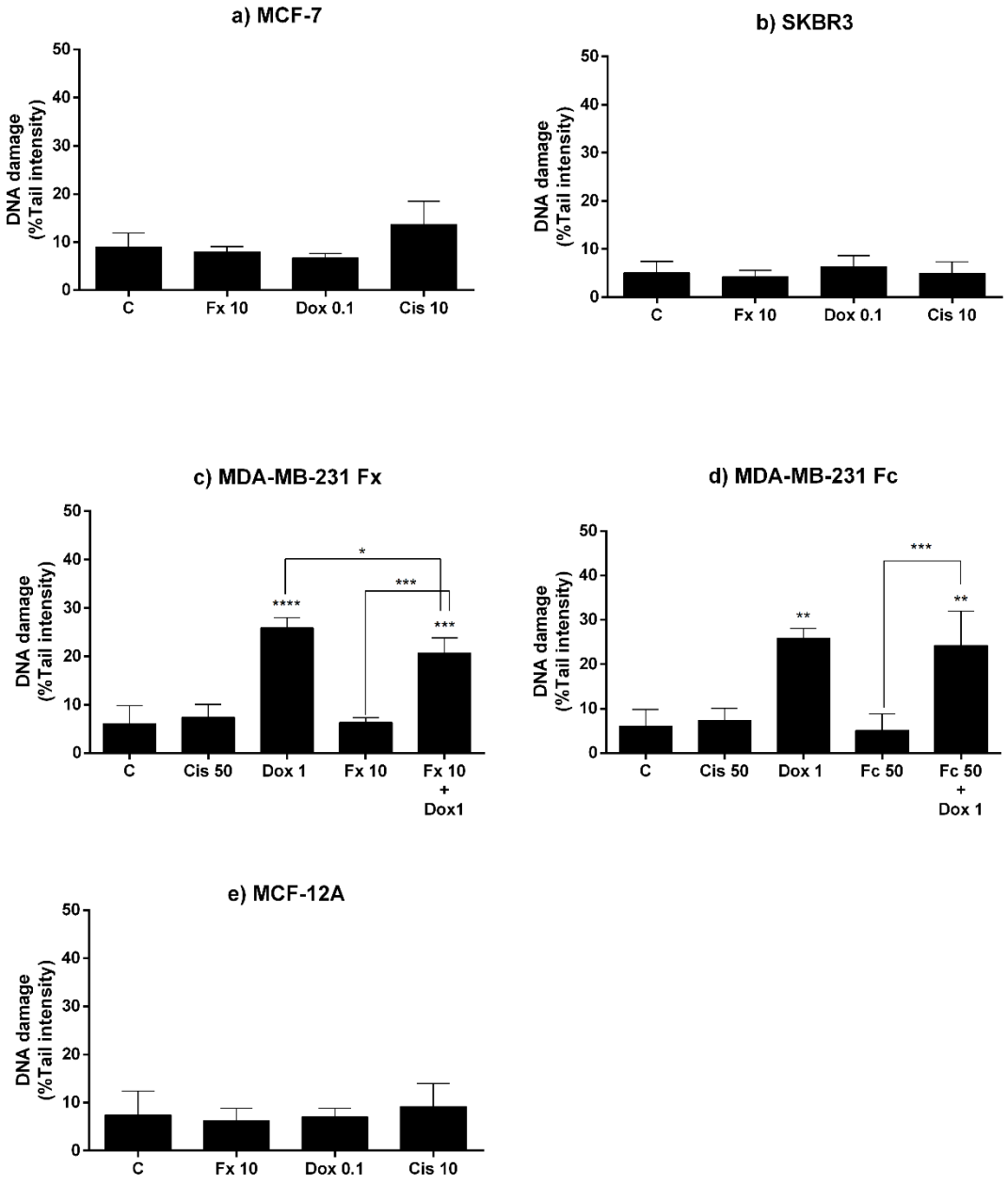



**Figure 11-** Genotoxic effect of Fx (10 µM) and Fc (50 µg/ml), alone and in combination with Dox (1 µM) or Cis (10 and 50 µM) on DNA damage in MCF-7 (a), SKBR3 (b), MDA-MB-231 (c and d) and MCF-12A (e) cells after 2 h of exposure evaluated by the Comet assay. Untreated cells (cells in culture medium) were included as a negative control (C). Data are expressed as the percentage of tail intensity, relative to the negative control, and are presented as mean ± SD of at three independent experiments. Significant differences (* $P < 0.05$, ** $P < 0.01$; *** $P < 0.001$; **** $P < 0.0001$) were determined by one-way ANOVA, followed by a Holm-Sidak's multiple comparisons test.

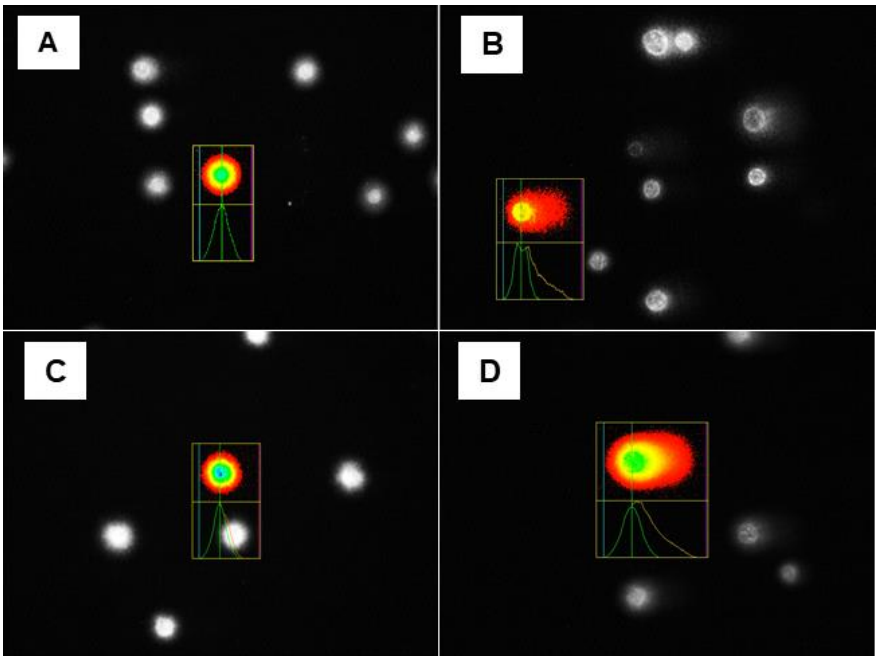



**Figure 12-** Representative images of the comet assay in MDA-MB-231 cells treated with A) Culture medium (Negative Control), B) Dox (1 µM) C) Fx (10 µM) and D) Fx (10 µM) + Dox (1 µM). Samples were analysed by the Comet Assay IV software. In the presence of low level of DNA damages, DNA occurs as a nucleoid with no or a small tail (A and C). Cells with DNA strand breaks resembles a comet structure with a head and a damaged DNA streak representing the tail (B and D). The blue line indicates the start of the comet head, the green line represents the middle of the comet head and the purple line limits the end of the comet tail. The fluorescence intensity of the comet tail, in relation to the head, is directly proportional to the extent of DNA breaks occurred. Untreated cells (A) as well as cells exposed to Fx (C) presented a low level of DNA damage, while cells incubated with Dox alone (B) and in combination with Fx (D) showed higher induction of DNA damages. Original magnification: 250x.

# 2. 3D Multicellular Aggregates (MCAs)

## 2.1. MCAs Generation and Characterization

The second part of our study aimed to optimize the generation of reproducible MCAs with enough size and compactness in order to allow their visualization during manipulation, and consequently prevent their loss throughout the experimental procedures (medium changes, exposure and histological processing). In this regard, preliminary experiments were performed for assessing the optimal cell seeding densities and formation time. We started by seeding cells (200 µl/ well) in Corning® ULA 96-well microplates at two distinct densities: 5 x $10^4$ cells/ml (D1) and 10 x $10^4$ cells/ml (D2) for all the cell lines, except for the MDA-MB-231 cells which were seeded at higher cell densities, 10 x $10^4$ cells/ml (D1) and 20 x $10^4$ cells/ml (D2), as this line generated smaller MCAs. Moreover, 4 culturing periods

were tested: 4 days (96 h), 7 days (168 h), 10 days (240 h) and 12 days (288 h) in order to assess MCAs formation and compaction level during different times of incubation.

### 2.1.1. Image Analysis

To track the development of MCAs over time, stereoscope images were taken at 4 time points: day 4 (96 h), day 7 (168 h), day 10 (240 h) and day 12 (288 h). The images from Figure 13 showed that all the cell lines, except MCF-7, seemed to form a round-shape 3D structure within 4 days (96 h) of culture. In a first attempt, MCF-7 cells did not form a consistent aggregate in any of the cell densities and formation periods tested (data not shown), which precluded their evaluation during the experimental period. Different levels of tightness were observed among MCAs formed from the SKBR3, MDA-MB-231 and MCF-12A cell lines, so therefore and considering Froelich et al. (2016) classification MCAs were grouped into two categories: compact MCAs (MDA-MB-231), and loose MCAs (SKBR3 and MCF-12A). The MCAs generated from the MDA-MB-231 cell line were the most compact and roundish. These MCAs displayed well-defined borders and individual cell margins were practically undetectable when observed under the stereomicroscope (Fig. 13). Meanwhile, the SKBR3 cell line formed loose aggregates that never fully compacted over a period of 12 days cultivation (Fig. 13). As for MCF-12A, this cell line also formed very loose MCAs (Fig.13), however, and contrarily to SKBR3, those MCAs were easily disaggregated by simple manipulation, giving rise to single cells suspensions (data not shown).

Within the same cell line, MCAs formation appeared to be consistent since they presented a similar morphology when examined under the stereomicroscope. However, the occasional appearance of small fibers inside the microplate wells impaired the correct formation of some MCAs, as they tended to grow along the fibers and did not acquire a round geometry. Yet we also noticed that the structure of MCAs seeded at higher densities were not as easily affected by those fibers as small-sized aggregates (data not shown).

As expected, D2 generated larger MCAs than D1 (Fig. 13) in all the cell lines. During manipulation, we found that MCAs seeded at D2 were more cohesive than MCAs seeded at D1, since they showed more resistance to disaggregation. Regardless of the initial cell-seeding densities used, the MCAs cultured up to 7 days (168 h) presented a round-shape with no visible signs of disintegration. Besides, it was observed a pronounced reduction in the size of the MDA-MB-231 MCAs during this time period. On the contrary, it was noticeable in all the cell lines tested (not so evident in the SKBR3 cell line) that an extended cultivation time (over 7 days) gradually decreased the MCAs' tightness and cohesion, promoting their disintegration, as shown in Figure 13.

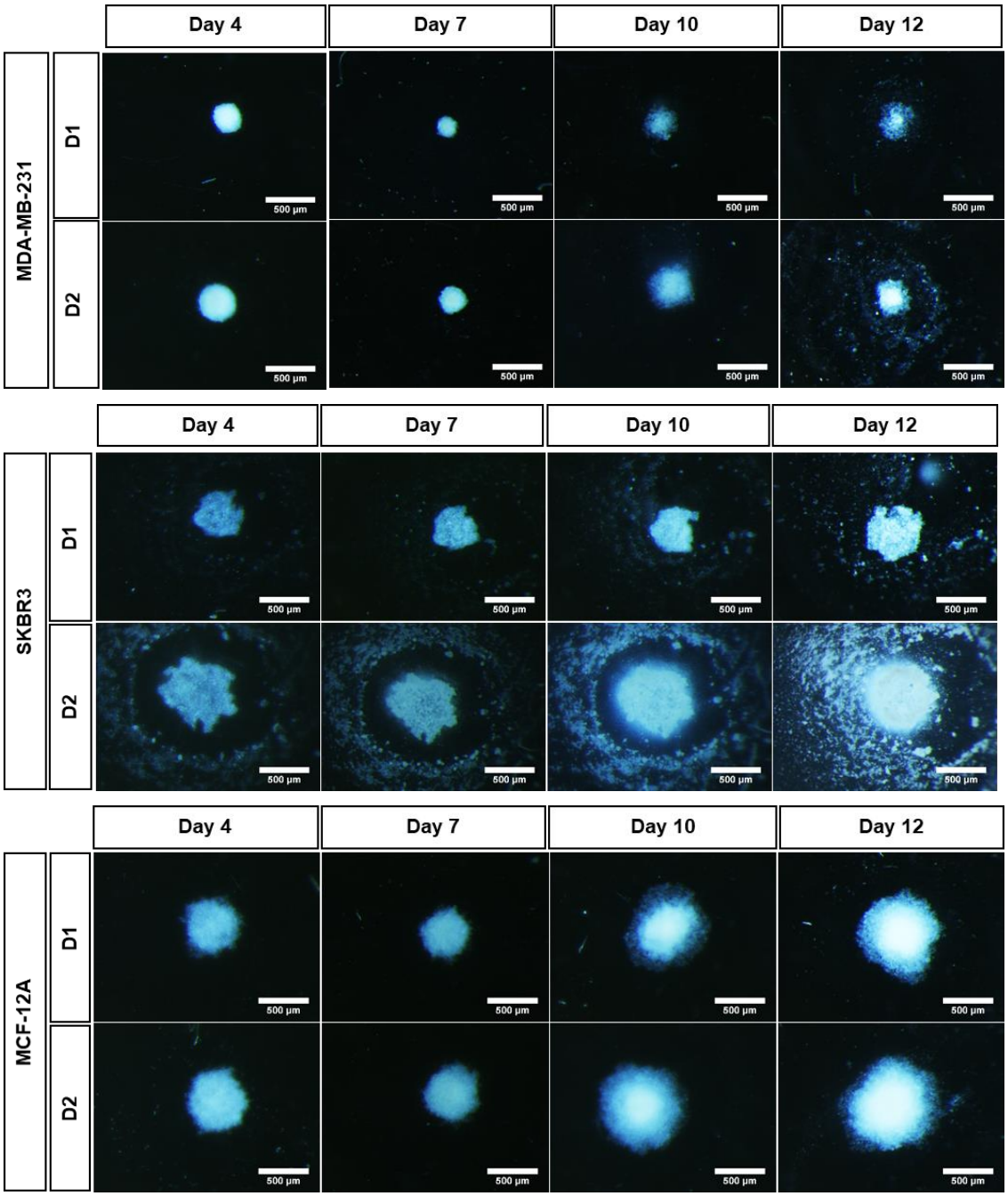



**Figure 13**- Representative morphology images of the 3D MCAs at different incubation periods. SKBR3 and MCF12-A cell lines were seeded in ULA plates at 5 x $10^4$ cells/ml (D1) and 10 x $10^4$ cells/ml (D2) while MDA-MB-231 cell line was seeded at 10 x $10^4$ cells/ml (D1) and 20 x $10^4$ cells/ml (D2). Photographs were taken in a stereomicroscope at 4 days (96 h), 7 days (168 h), 10 days (240 h) and 12 days (288 h) of incubation. Scale bar: 500 µm.

Since prolonging the incubation time did not significantly increase MCAs size and would even compromise their integrity, we decided to test higher cell-seeding densities and shorten the formation time, thus avoiding the need for manipulation (medium changes) and consequently MCAs destruction or damaging, especially in MCF-12A aggregates. Although we could not assess the suitable conditions for the MCF-7 MCAs' generation we decided to

proceed with the experiments and assume that, in accordance with the other cell lines, the period of cultivation should not exceed the 7 days.

In a second experiment, three different seeding densities were assessed for each cell line: MCF-7 and SKBR3 (D1 - 10 x $10^4$ cells/ml, D2 - 20 x $10^4$ cells/ml and D3 - 40 x $10^4$ cells/ml), MDA-MB-231 (D1 - 20 x $10^4$ cells/ml, D2 - 40 x $10^4$ cells/ml and D3 - 50 x $10^4$ cells/ml) and MCF-12A cells (D1 - 5 x $10^4$ cells/ml, D2 - 10 x $10^4$ cells/ml and D3 - 20 x $10^4$ cells /ml). Cells were incubated for 3 days (72 h) and 4 days (96 h) for MCAs formation. This time, a new aliquot of MCF-7 cells was thawed and we were able to get properly formed MCAs with visible irregular borders after 3 and 4 days culturing at all the cell densities. Despite being lesser compact than the MDA-MB-231 MCAs, MCF-7 MCAs also presented a high level of compactness which allowed their classification as compact aggregates. From the analysis of the stereomicroscope images collected, no evident differences were noted in MCAs morphology after 3 or 4 days of formation for any of the cell lines tested (data not shown), so we opted to use 3 days as the optimal formation period. Figure 14 represents the MCAs generated after 3 days at the three different densities experimented and it shows that increasing cell density, slightly improved MCAs size and cellular compaction in MCF-7, SKBR3 and MCF-12A cell lines. As for the MDA-MB-231 cell line, seeding density seems to have no influence on the MCAs appropriate formation, since they displayed a high level of compactness and cohesion regardless of the initial cell density used (Fig. 14).

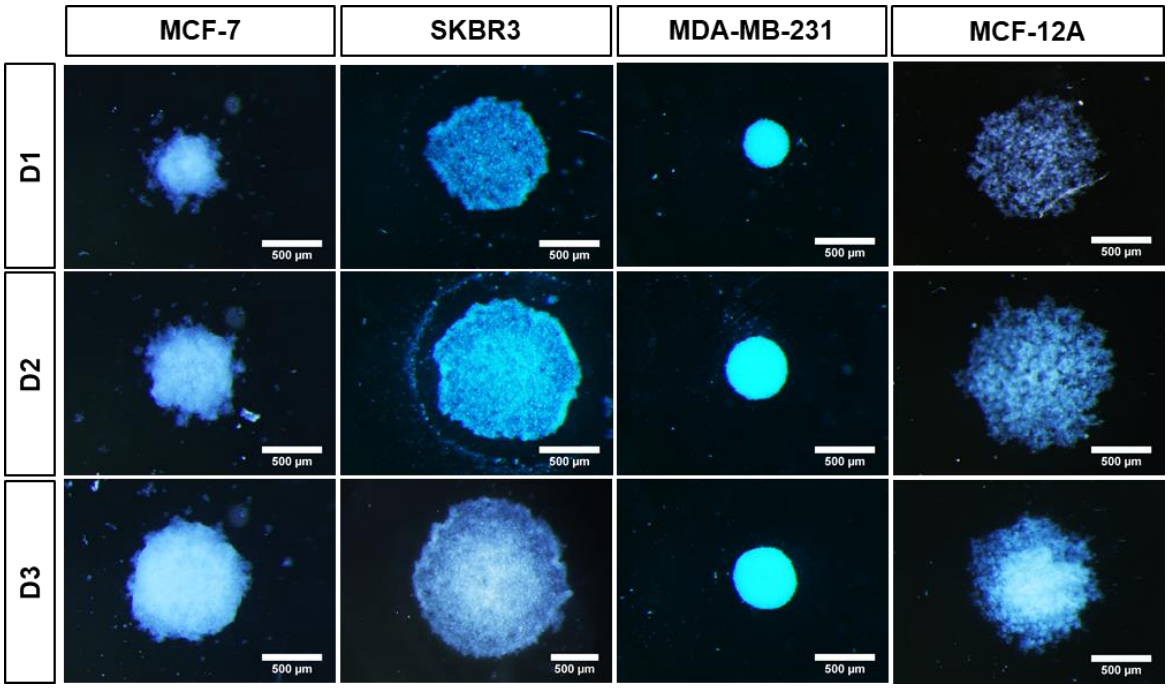



**Figure 14-** Representative morphology images, photographed in a stereomicroscope with a dark field, of the 3D MCAs at different cell densities after 3 days (72 h) of incubation in culture medium. MCF-7 and SKBR3 cells were seeded at 10 x $10^4$ cells/ml (D1), 20 x $10^4$ cells/ml (D2) and 40 x $10^4$cells/ml (D3). MDA-MB-231 cells were seeded at 20 x $10^4$ cells/ml (D1), 40 x $10^4$ cells/ml (D2) and 50 x $10^4$ cells/ml (D3). MCF-12A cells were seeded at 5 x $10^4$ cells/ml (D1), 10 x $10^4$ cells/ml (D2) and 20 x $10^4$ cells /ml (D3). Scale bar: 500µm.

Considering the results obtained after 3 days, we selected 40 x $10^4$ cells/ml as the most suitable density to generate MCAs from the MCF-7, SKBR3 and MDA-MB-231 cell lines and 20 x $10^4$ for the formation of the MCF-12A MCAs. Under those optimized conditions, MCAs were consistent in shape and reproducible in size, exhibited a homogeneous round geometry and had favourable dimensions for manipulation, and for optical and electron microscopy analysis. We decided to further investigate the behaviour of this 3D cell culture system by simulating an exposure. According to the results previously described, MCAs incubation should not overcome 7 days of cultivation, so 4 days of exposure was considered as the appropriate exposure period. Also, we wanted to increase the exposure time compared to that used in the monolayer experiments (3 days - 72 h), since cells cultured in 3D models are normally more resistant to compounds-induced anticancer effects than those cultured in 2D models (Edmondson et al., 2014). In that regard, MCAs seeded at the selected optimal densities were cultivated during a total of 7 days (168 h), correspondent to 3 days (72 h) of formation followed by total medium renewal plus 4 days (96 h) of incubation. Photographs of all the MCAs were captured daily for 7 days (168 h). Figure 15 represents the MCAs morphology at day 3 of formation and at day 7 of incubation (after 4 days of "exposure"). By the end of 7 days, MCF-7 and MCF-12A MCAs presented a more relaxed morphology, however despite the decrease in the compaction state, their structural integrity was not affected. In contrast, the morphology of SKBR3 and MDA-MB-231 aggregates remained identical from day 3 to day 7 of cultivation. All the images were analysed using the ANASP software and different morphological parameters were measured, including the MCAs' area.

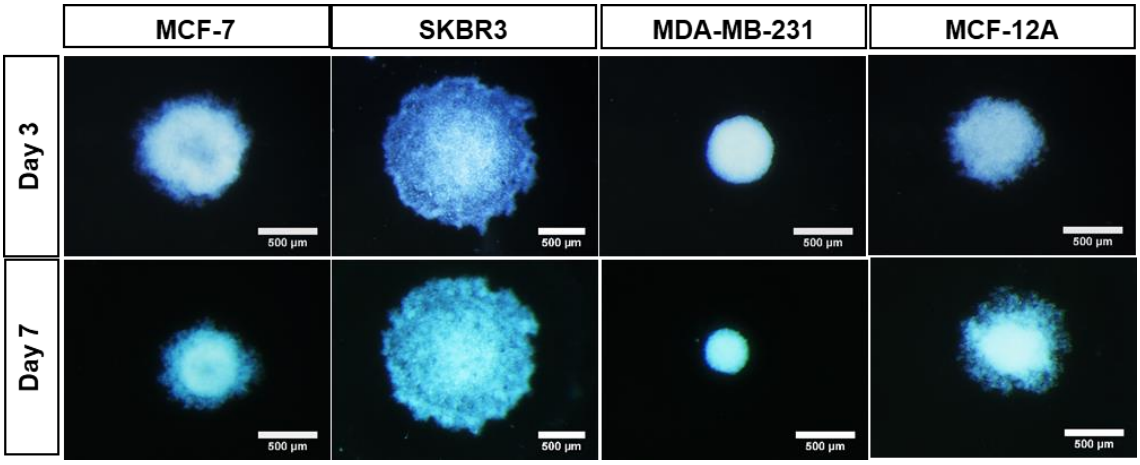



**Figure 15-** Representative morphology images, photographed in a stereomicroscope with a dark field, of the 3D MCAs at the selected cell densities at day 3 (72 h of MCAs formation) and day 7 (4 days or 96 h of MCAs incubation in culture medium, simulating the exposure period). Each two images correspond to the same MCA. MCF-7, SKBR3 and MDA-MB-231 cells were seeded at 40 x $10^4$ cells/ml. MCF-12A cells were seeded at 20 x $10^4$ cells/ml. Scale bar: 500 µm.

Area measurements showed a narrow MCAs size variation, reflected by a small standard deviation, in all the cell lines throughout the experimental period (Fig. 16). The SKBR3 cell line gave rise to the largest MCAs with approximately 1.5 x $10^6$ $\mu m^2$ of area. From day 1 to day 3 after seeding, there was a reduction of the MCAs' areas correlated to an increase in their compaction, particularly in the MDA-MB-231 and MCF-12A cell lines. During manipulation (medium changes and MCAs harvesting) we noticed that, in some cases, MCF-12A MCAs structure was markedly affected, with some MCAs destruction due to their particularly loose arrangement. Likewise, a relaxation in MCAs structure was perceived when all the medium was removed, in SKBR3, MCF-7 and MDA-MB-231 cell lines, although it was less evident in this latter one. After day 3 and until day 7 there were no major variations in the MCAs areas, except for the MDA-MB-231, where the MCAS gradually decreased in size over time. Statistical analysis was not performed since the data resulted from one single independent experiment (one replica with twelve MCAs in different wells).

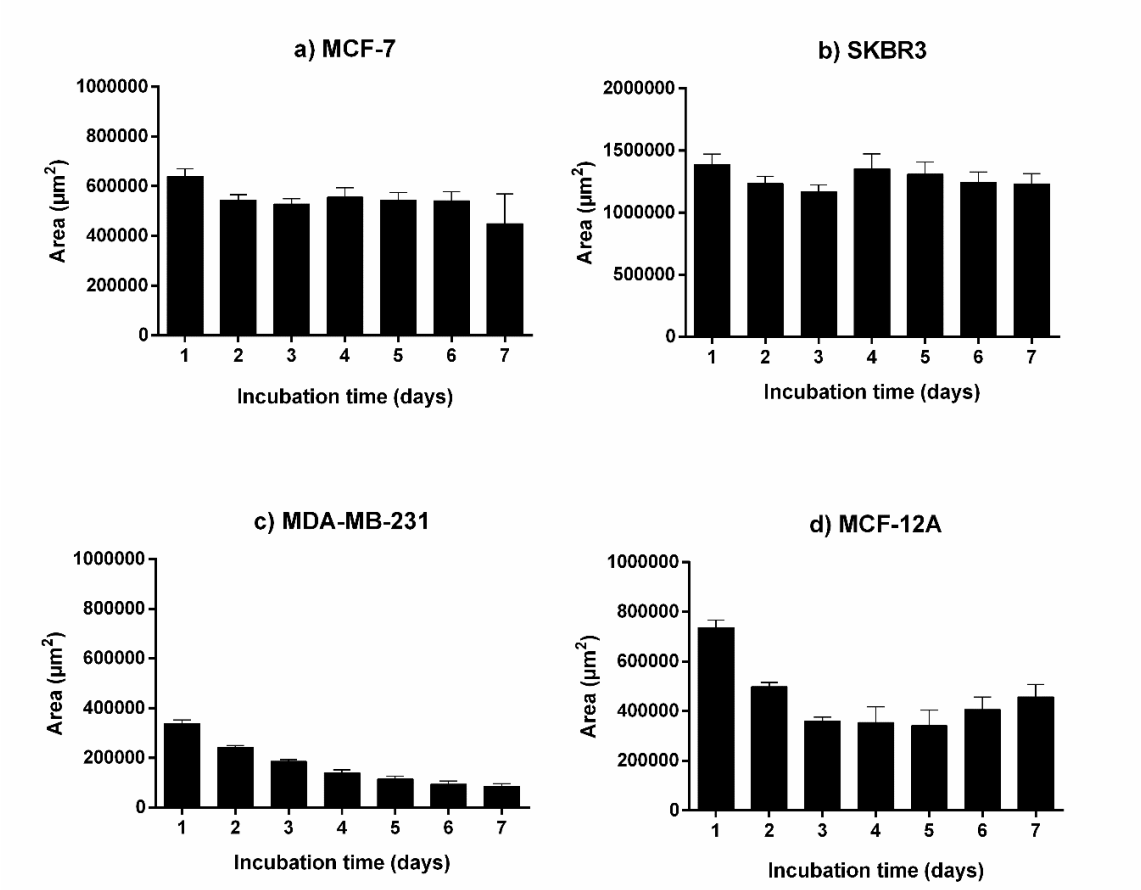



**Figure 16**- Area measurements of the 3D MCAs at day 1 (24 h), day 2 (48 h), day 3 (72 h), day 4 (96 h), day 5 (120 h), day 6 (144 h) and day 7 (168 h) of incubation. (a) SKBR3, (b) MCF-7, (c) MDA-MB-231 and (d) MCF12A cells were seeded at the previously optimized cell densities. Culture medium was completely changed after 3 days of incubation in order to simulate the exposure process. Results are presented as mean ± SD of at least twelve MCAs from one single experiment.

### 2.1.2 Histological Analysis

At the end of day 3 (before exposure simulation) and day 7 (after exposure simulation) in culture, the optimized MCAs were harvested and processed for histological sectioning and analysis. During this procedure, it was possible to asses that the MCAs from the different cell lines presented distinct levels of compactness, as previously observed. Also, concerning their 3D structure, all MCAs exhibited a disk-like shape, and those originated from the MDA-MB-231 cell line were the ones that presented higher three-dimensionality, followed by the MCF-7, MCF-12 and SKBR3 MCAs, in this order. For illustrative purposes, we selected representative images of the HE sections that displayed a wider zone of the MCAs.

Considering the MCF-7 cell line (Fig. 17), the formed MCAs revealed a compact structure with no defined borders as previously described. Comparatively to day 3, more cells scattered around the central aggregate were observed after 7 days of culturing. It was also noted the formation of many irregular shaped lumen-like structures at both time points, usually containing apoptotic cells (see the inserted images in Fig. 17).

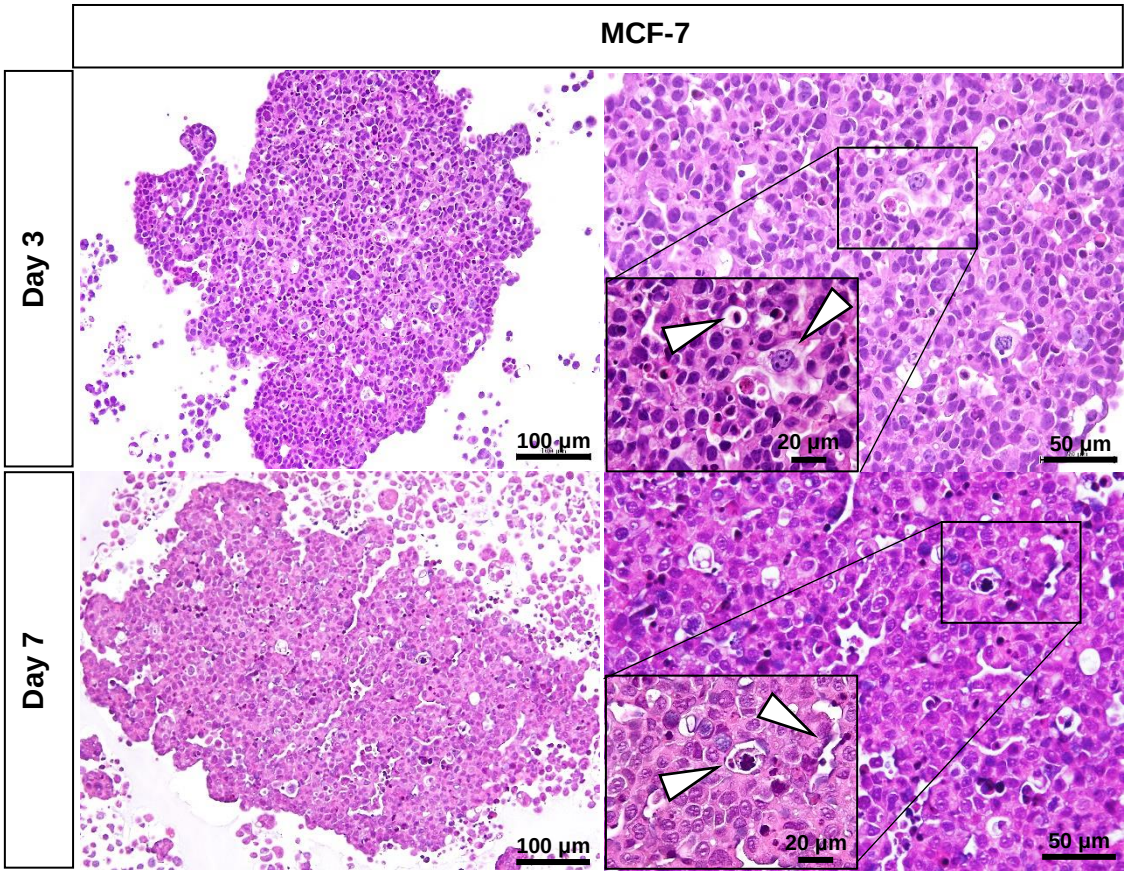



**Figure 17**- Representative images of the MCF-7 MCAs 3 µm-thick sections stained with HE after 3 days (72 h) and 7 days (168 h) in culture. Total cell culture medium changes were performed on day 3 to simulate the exposure procedure. Each pair of images of different magnifications correspond to the same MCA. The arrowheads indicate the lumen-like structures. Scale bar: 20, 50 and 100 µm.

In the SKBR3 cell line, it was evident the presence of irregular borders and large intercellular spaces reflecting their loose nature (Fig. 18). However, although the MCAs seem to have a low aggregation degree, we verified during manipulation that their structure was not easily affected. In Figure 18, the representative image from day 3 illustrates the front part of a SKBR3 MCA, while the image relative to day 7 shows the lateral part of a MCA. From the analysis of the latter image, it is clear that the SKBR3 MCAs had low three-dimensionality. No evident morphological changes were noted between MCAs harvested on day 3 and day 7.

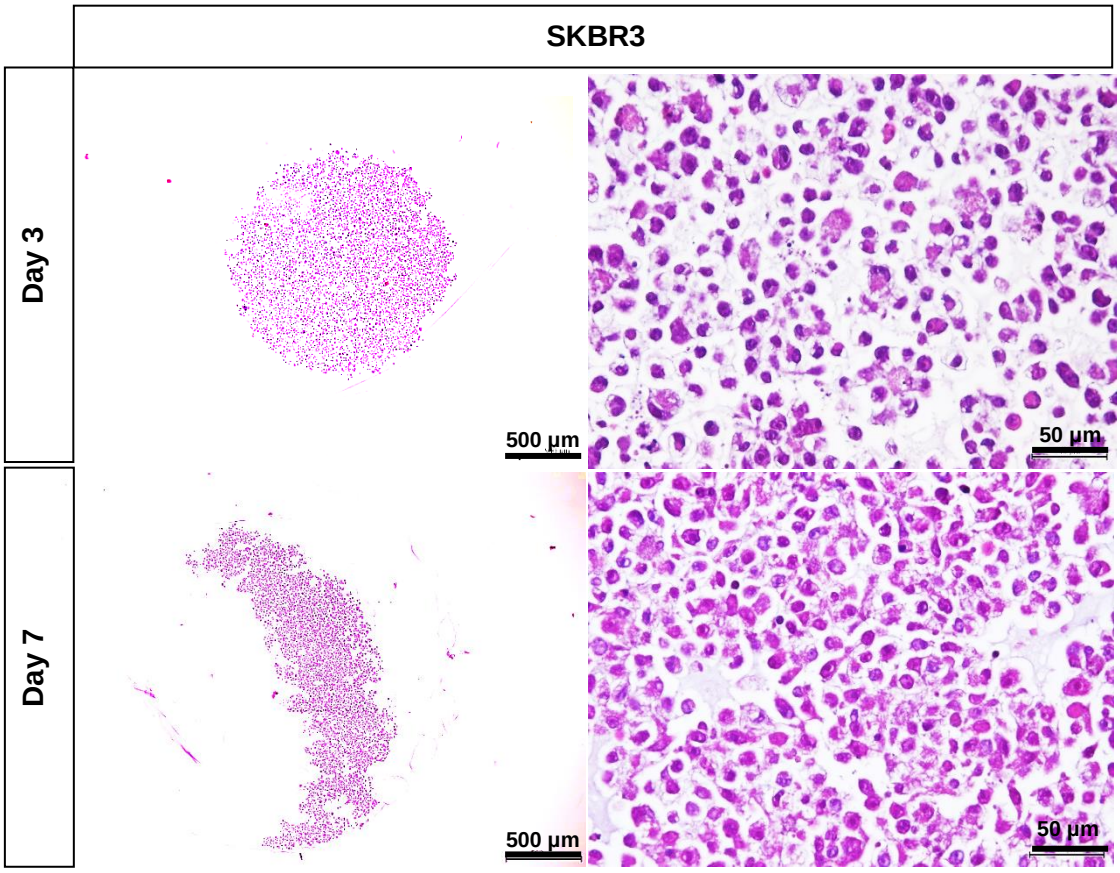



**Figure 18**- Representative images of the SKBR3 MCAs 3 µm-thick sections stained with HE after 3 days (72 h) and 7 days (168 h) in culture. Total cell culture medium changes were performed on day 3 to simulate the exposure procedure. Each pair of images of different magnifications correspond to the same MCA. Scale bar: 50 and 500 µm.

Images from the stained MDA-MB-231 sections (Fig. 19) confirm that the compaction state increased between days 3 and 7, in accordance with results from the stereomicroscope analysis and area measurements. In general, these MCAs presented a compact morphology and particularly defined borders, containing flatter peripheral cells. Certain MCAs harvested either on day 3 or day 7 displayed lower cell density in their core area along with some apoptotic cells (as shown in the representative image from day 3).

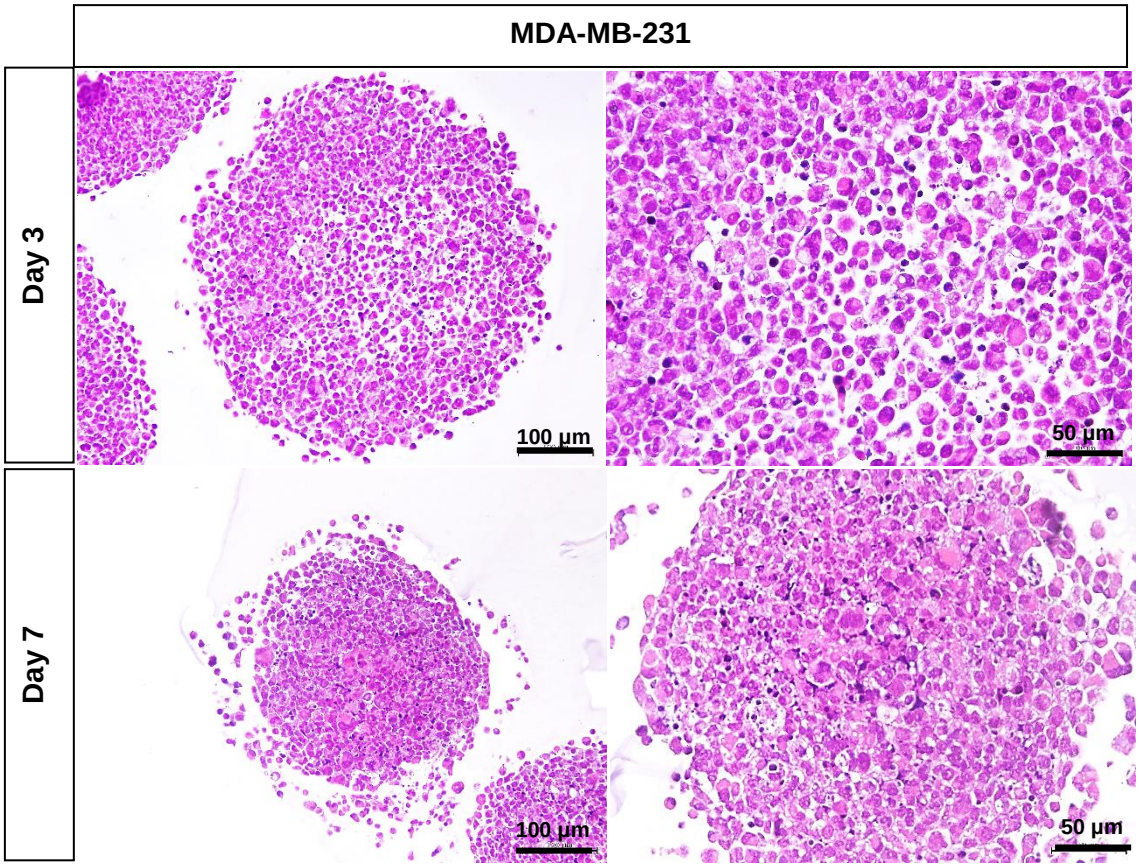



**Figure 19**- Representative images of the MDA-MB-231 MCAs 3 µm-thick sections stained with HE after 3 days (72 h) and 7 days (168 h) in culture. Total cell culture medium changes were performed on day 3 to simulate the exposure procedure. Each pair of images of different magnifications correspond to the same MCA. Scale bar: 50 and 100 µm.

The morphological analysis of the stained MCF-12A sections (Fig. 20) demonstrated that the peripheral zone of the MCAs was constituted by a cluster of unaggregated and highly dispersed cells, while the central zone displayed higher cell density and cohesion. This cell line also exhibited lumen-like structures, mainly on day 3, although not as defined as those observed in the MCF-7 MCAs. After 7 days, some MCAs presented a higher number of cells with hyperchromatic and pyknotic nuclei, common features of apoptosis, in their central zone.

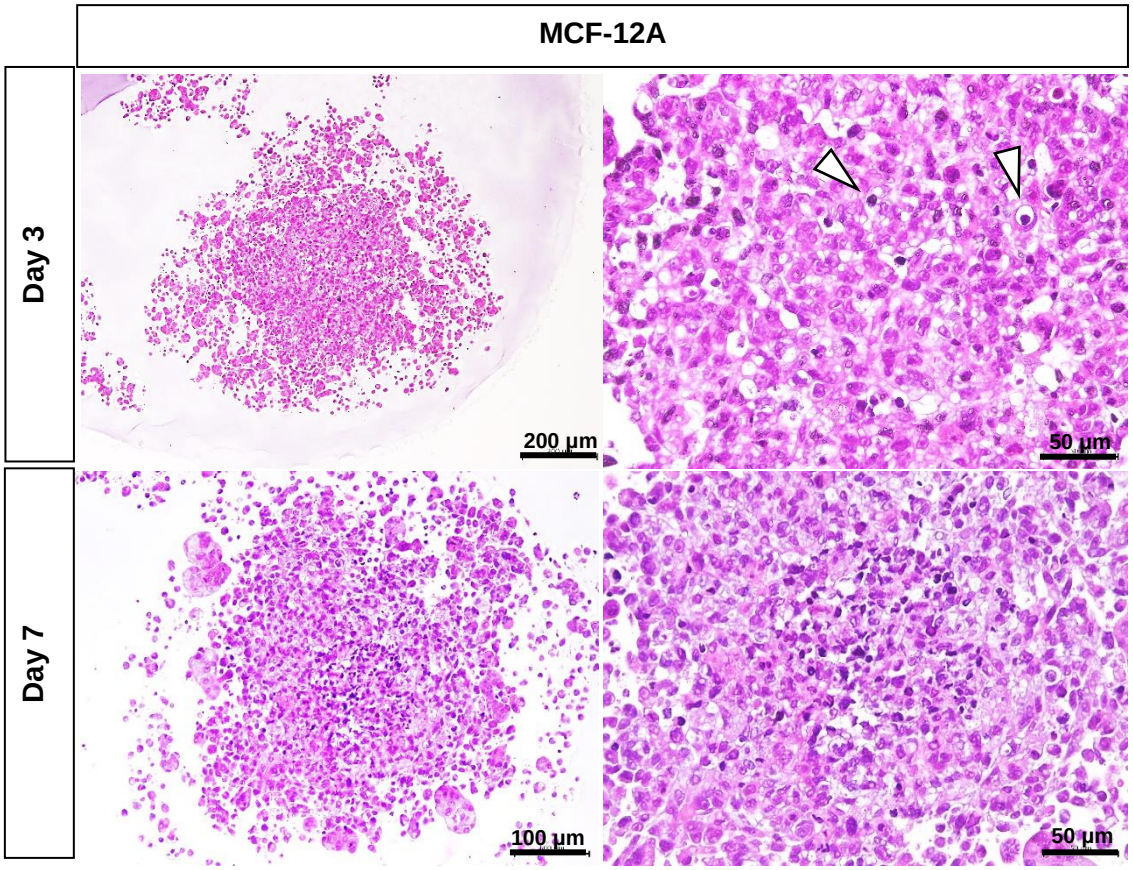



**Figure 20**- Representative images of the MCF-12A MCAs 3 µm-thick sections stained with HE after 3 days (72 h) and 7 days (168 h) in culture. Total cell culture medium changes were performed on day 3 to simulate the exposure procedure. The arrowheads indicate the lumen-like structures. Each pair of images of different magnifications correspond to the same MCA. Scale bar: 50, 100 and 200 µm.

### 2.1.3 Immunocytochemical Analysis

The immunocytochemistry technique was performed using the antibodies anti-caspase-3 and anti-Ki67 to investigate and compare the proportion of apoptotic and proliferating cells, respectively, in the MCAs harvested on days 3 and 7 (Fig. 21). The results showed that after 3 days in culture, the MCAs of all the cell lines presented a higher amount of Ki67-positive cells than caspase-3-stained cells, indicating that the proportion of proliferating cells overcame the proportion of apoptotic cells. Amongst all the cell lines, the BC MCF-7 and the normal MCF-12A cell lines were the ones that presented the highest proliferative capacity at day 3. After 7 days of cultivation, the number of apoptotic cells increased in comparison to what was observed on day 3 for all the MCAs. Remarkably, immunostaining for caspase-3 appeared to be more pronounced in the MCAs originated from the MDA-MB-231 cells. The proportion of proliferating cells also seemed to have diminished, in comparison to day 3, however high proliferative activity was still evident in all the cell lines tested. Furthermore, positively stained cells were randomly and uniformly distributed throughout the MCAs of all the cell lines at both incubation periods, except in the

MCF-12 cell line, where it was noted a slightly higher concentration of apoptotic cells in the center of the MCAs harvested on day 7.

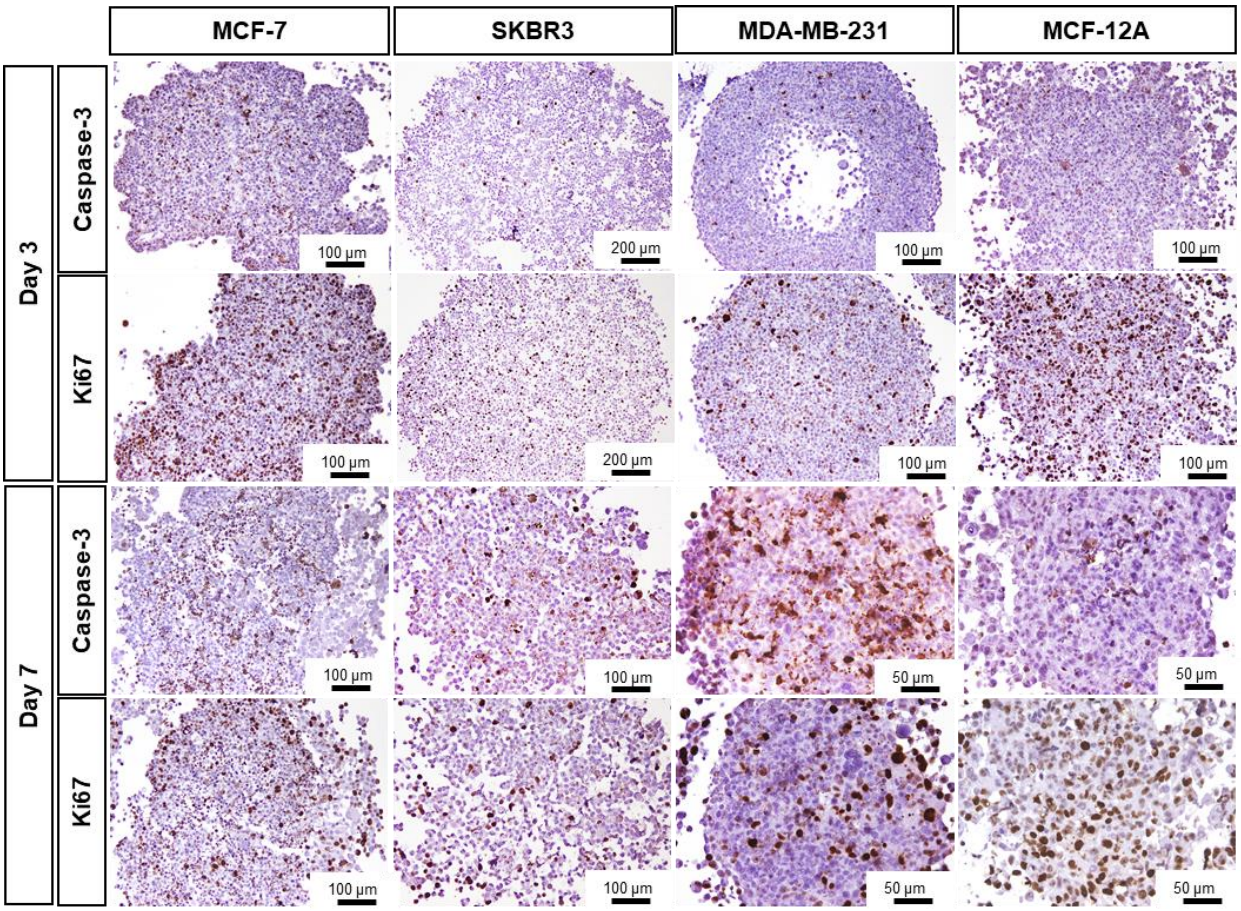



**Figure 21**- Representative images of the 3D MCAs 3 µm-thick sections immunostained against caspase-3 and Ki67 (brown staining) after 3 and 7 days of incubation. Scale bar: 50, 100 and 200 µm.

### 2.1.4 Transmission Electron Microscopy (TEM) Analysis

The ultrastructural morphology of the MCAs was analysed by TEM. All the cell lines presented some common features as euchromatic, irregular shaped nuclei with prominent nucleoli, abundant presence of mitochondria and rare occurrence of endoplasmic reticulum profiles and Golgi complexes. In MCF-7, SKBR3 and MCF-12A MCAS, several cells showed glycogen deposits and lipidic droplets, with variable amounts from cell to cell, even within the same cell the line (Fig. 22-25). No evident differences were observed between the MCAs harvested at day 3 and day 7, therefore some representative images (either from day 3 or day 7) were selected to illustrate the ultrastructural morphology of the MCAs corresponding to each cell line.

In the MCF-7 cell line, TEM images showed that MCAs displayed tight cell-cell contacts, denoting high level of cohesion. Also, MCF-7 MCAs exhibited the formation of

lumen-like structures associated with the presence of apoptotic cells with high level of vacuolization and chromatin condensation within the lumen space (Fig. 22A and B). In the cells' apical pole, it was commonly observed the presence of membrane projection towards the lumen, forming microvilli (Fig. 22A and B). These structures were also present in cellular interspaces frequently found along the MCAs and in the outer limit of the MCAs (Fig. 22C and D). Another typical aspect found in these MCAs was the presence of secretory vesicles in the cytoplasm of some cells, preferentially in the cell forming the lumina referred above. In these cells, secretory vesicle tends to align in the apical pole (Fig. 22A). Similarly, these vesicles were also accumulated around the intercellular spaces (Fig. 22C).

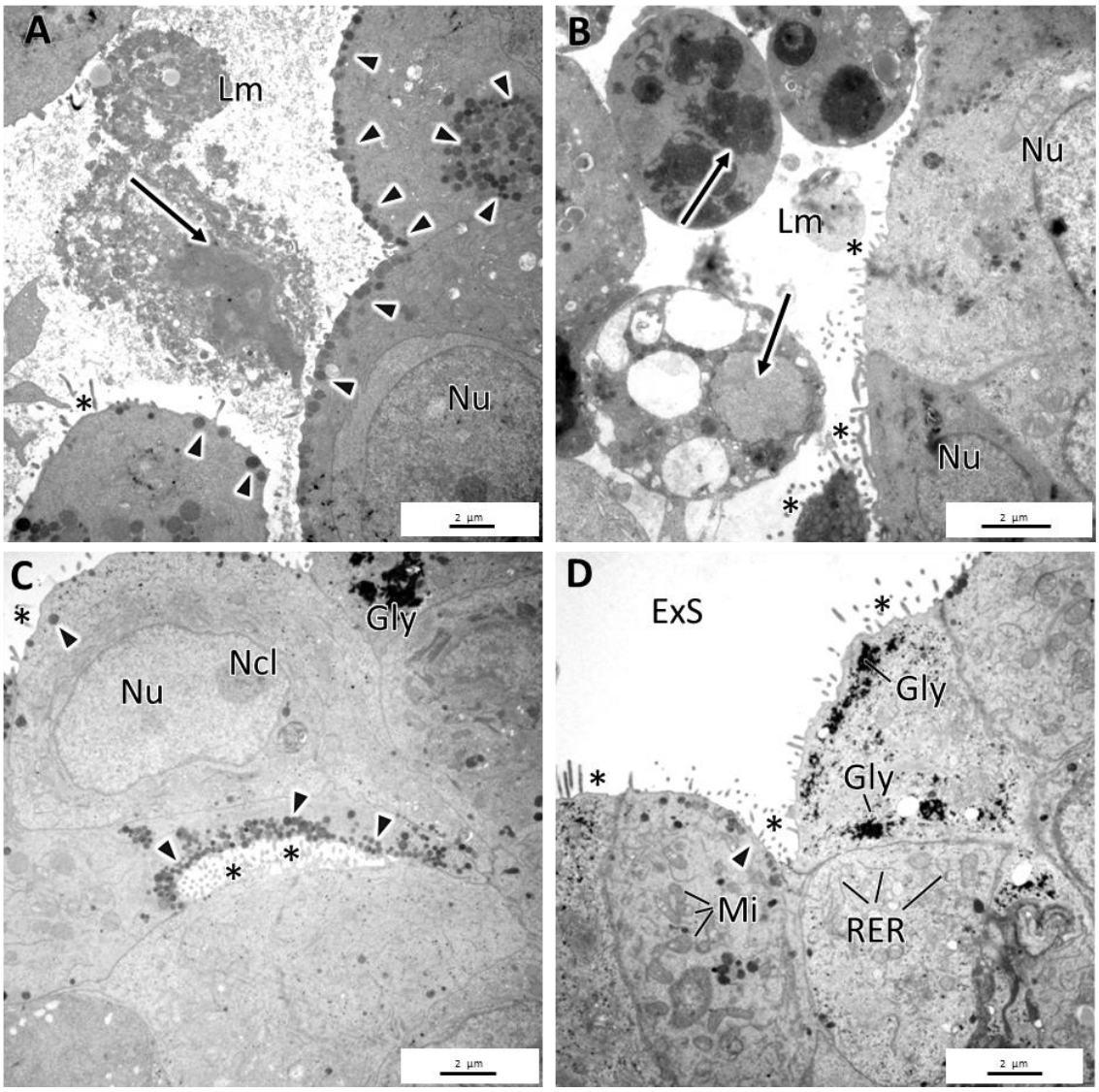



**Figure 22-** Representative images of TEM analysis of MCF-7 MCAs after 3 days of culture. Arrows: apoptotic cells; Arrowheads: secretory vesicles; Asterisks: microvilli; ExS: external surface; Gly: glycogen; Lm: lumen; Mi: Mitochondria; Nu: Nucleus; Ncl: nucleolus; RER: rough endoplasmic reticulum. Scale bar: 2 µm.

In the SKBR3 MCAs, cells were separated by large intercellular spaces, revealing a loose arrangement. High amounts of glycogen were found within the cytoplasm of these cells (Fig. 23C and D). These MCAs also exhibited high formation of plasma membrane projections varying from blebs to microvilli. (Fig. 23A, B and D).

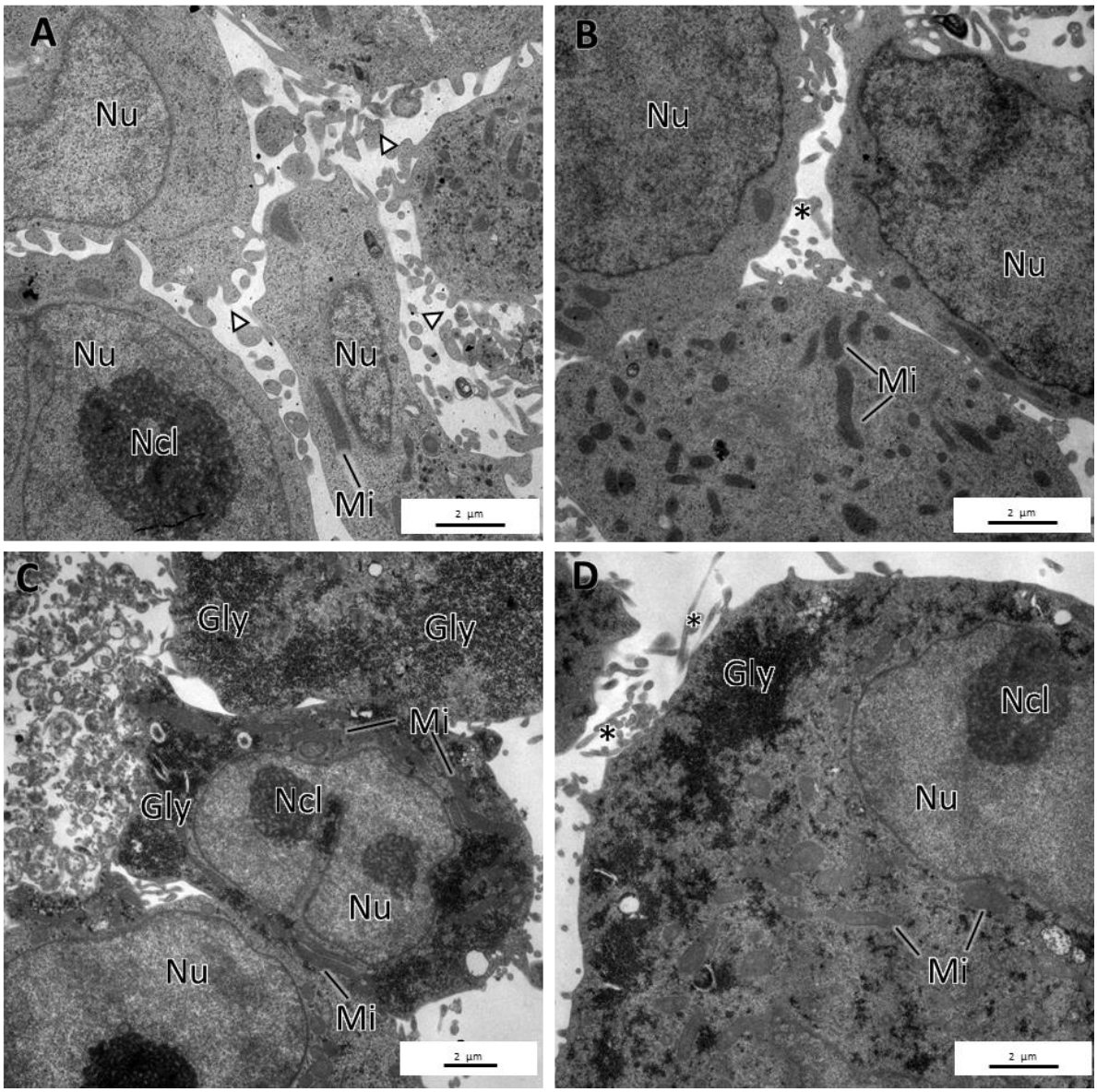



**Figure 23** - Representative images of TEM analysis of SKBR3 MCAs after 3 days of culture. Asterisks: microvilli; White arrowheads: membranes blebs; Gly: glycogen; Mi: Mitochondria; Nu: Nucleus; Ncl: nucleolus. Scale bar: 2 µm.

The ultrastructural analysis revealed that the MDA-MB-231 MCAs displayed relatively high cell-cell adhesion, with cells connecting in several regions along cellular membranes. It was also noted the presence of cells with a large number of dense bodies (Fig. 24B, C and D), small lipid droplets (Fig. 24A and B), and high levels of vacuolization (Fig. 24D). This cell line also exhibited the presence of lumina, however, these structures were smaller

and not so well defined than the ones observed in MCF-7 MCAs (Fig. 24A and B). Another evident feature was the presence of intercellular space between cells containing membrane blebs.

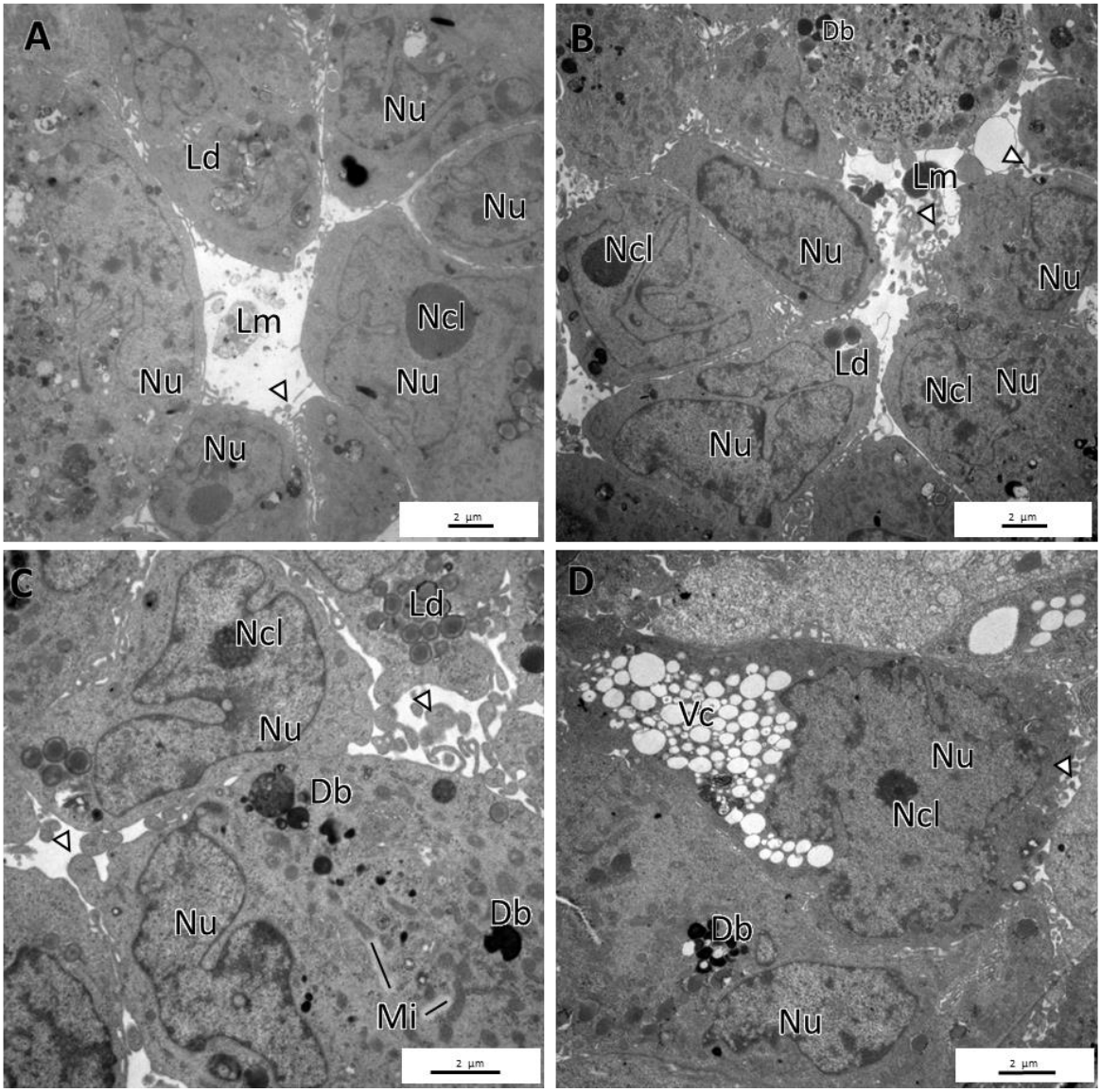



**Figure 24 -** Representative images of TEM analysis of MDA-MB-231 MCAs after 3 days of culture. White arrowheads: membranes blebs; Db: dense bodies; Ld: Lipid droplets; Lu: lumen; Mi: Mitochondria; Nu: Nucleus; Ncl: nucleolus; Vc: vacuoles. Scale bar: 2 µm.

The MCF-12A line was characterized for showing the most irregular nuclei and most abundant number of mitochondria. In the intercellular spaces, cell membranes show a great amount of membrane blebs, very evident due to the low adhesion among cells (Fig. 25A). Formation of large lipid droplets were also evident in the cytoplasm of MCF-12A cells as observed in Fig. 25B. Considering cell-cell adhesion, TEM analysis showed that cells were not totally attached to each other as in the MCF7 and MDA-MB-231 MCAs, although there were some points in which neighbor cell got in touch and were linked by junctional complexes

as desmosomes (Fig. 25C). In some cells, it was clearly observed cytoplasmic filaments arranged in bundles as seen in Figure 25D. Similarly, to MCF-7 MCAs, those originated from MCF-12A cells also presented lumen-like structures (Fig. 25A)

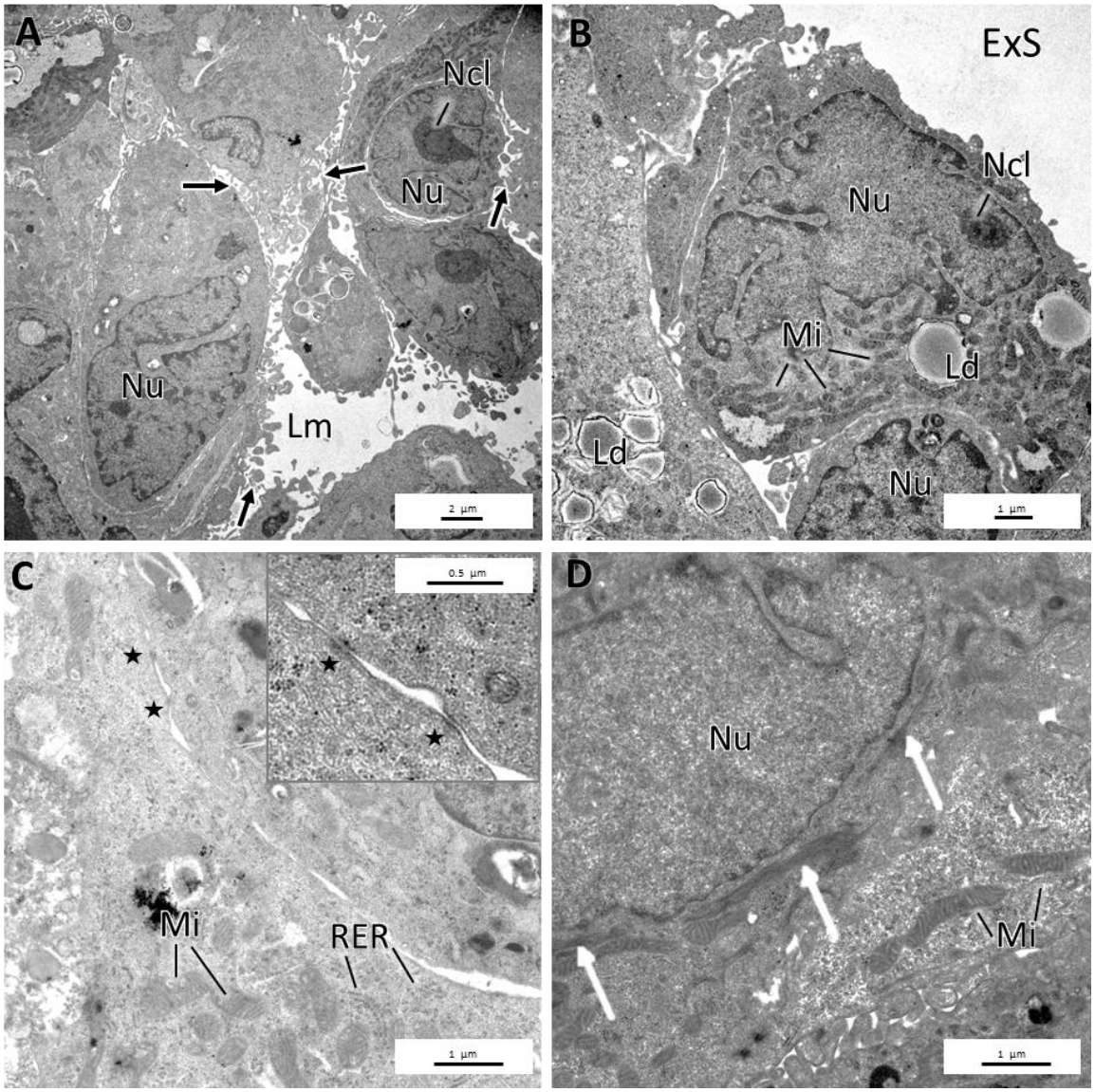



**Figure 25 -** Representative images of TEM analysis of MCF-12A MCAs after 3 days of culture. Black arrows: intercellular spaces with membrane blebs; White arrows: bundles of cytoplasmic filaments; ExS: external surface; Ld: Lipid droplets; Lm: lumen; Mi: Mitochondria; Nu: Nucleus; Ncl: nucleolus, Stars: desmosomes. Scale bar: 0.5 (C- inserted image), 1 (B, C, D) and 2 µm (A).

## 3. Effects in 3D Cultures

Following the previously described optimization, exposure experiments were performed on 3D models (MCAs). We selected two agents that exhibited evident cytotoxic effects on the 2D cultured BC cell lines to be tested in 3D cultures, correspondent to one

anticancer drug (Dox) and one seaweed-derived compound (Fx). MCAs were exposed to Dox at 1 µM and Fx at 10 µM for 4 days and effects on cell viability and proliferation were assessed. In addition, MCAs were harvested for light microscopy and immunocytochemical analysis. Although Dox at 1 µM has only been tested in MDA-MB-231 monolayer-grown cells, we decided exposure MCAs from all the cell lines to that concentration to standardize the conditions assessed in 3D cultures.

### 3.1. Assessment of Cytotoxic Effects

The MTT and LDH assays were conducted to evaluate the effects on cell viability. As presented in Figure 26, relative to the MTT, no significant cytotoxic effects were exhibited in none of the tested cell lines, when compared to the solvent control (SC, 0.1% DMSO in cell culture medium). In agreement with those results, the LDH assay also indicated that none of the compounds induced significant cytotoxicity (Fig. 27). Predictably, the positive control ($C^+$), which included cells treated with 0.1% of DMSO and posteriorly lysed for the liberation of the intracellular LDH, showed a pronounced increase of this enzyme release relative to control in all the cell lines tested.

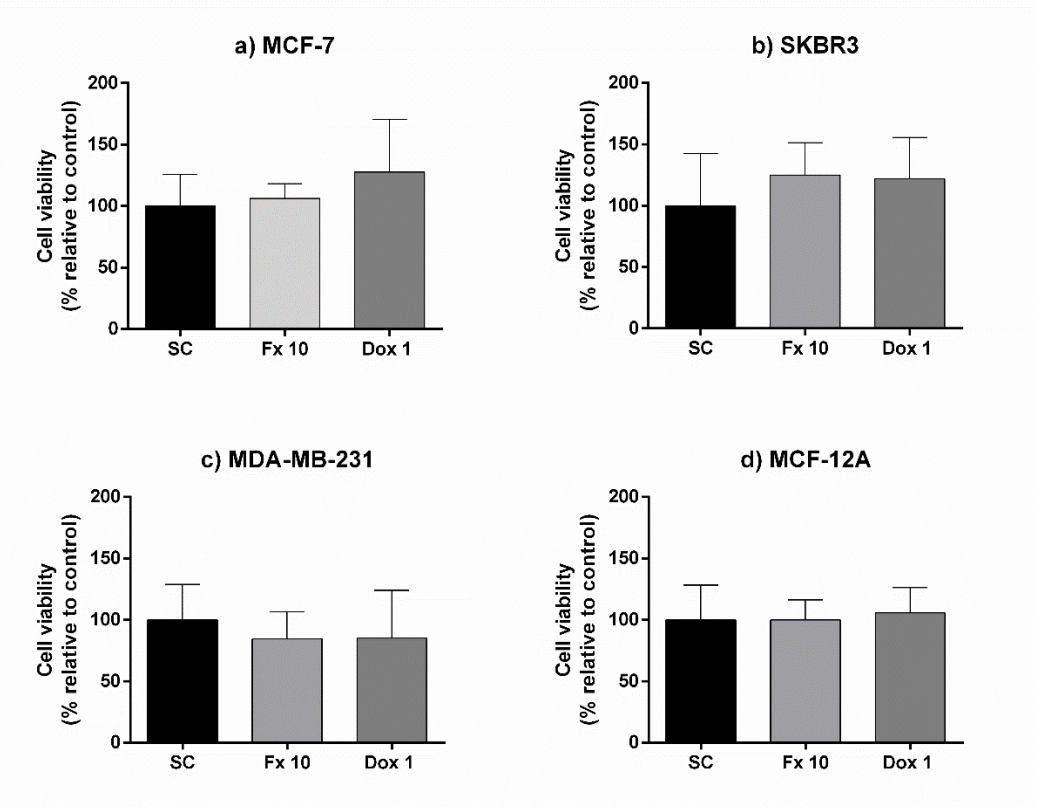



**Figure 26-** Effect of Fx at 10 µM (Fx 10) and Dox at 1 µM (Dox 1) on the viability of MCF-7 (a), SKBR3 (b), MDA-MB-231 (c) and MCF-12A (d) MCAs, assessed after 4 days of exposure by the MTT assay. Cells treated with 0.1% DMSO (SC) were included as a negative control. Results are expressed as the percentage of cell viability at 570 nm and presented as mean ± SD of four independent experiments.

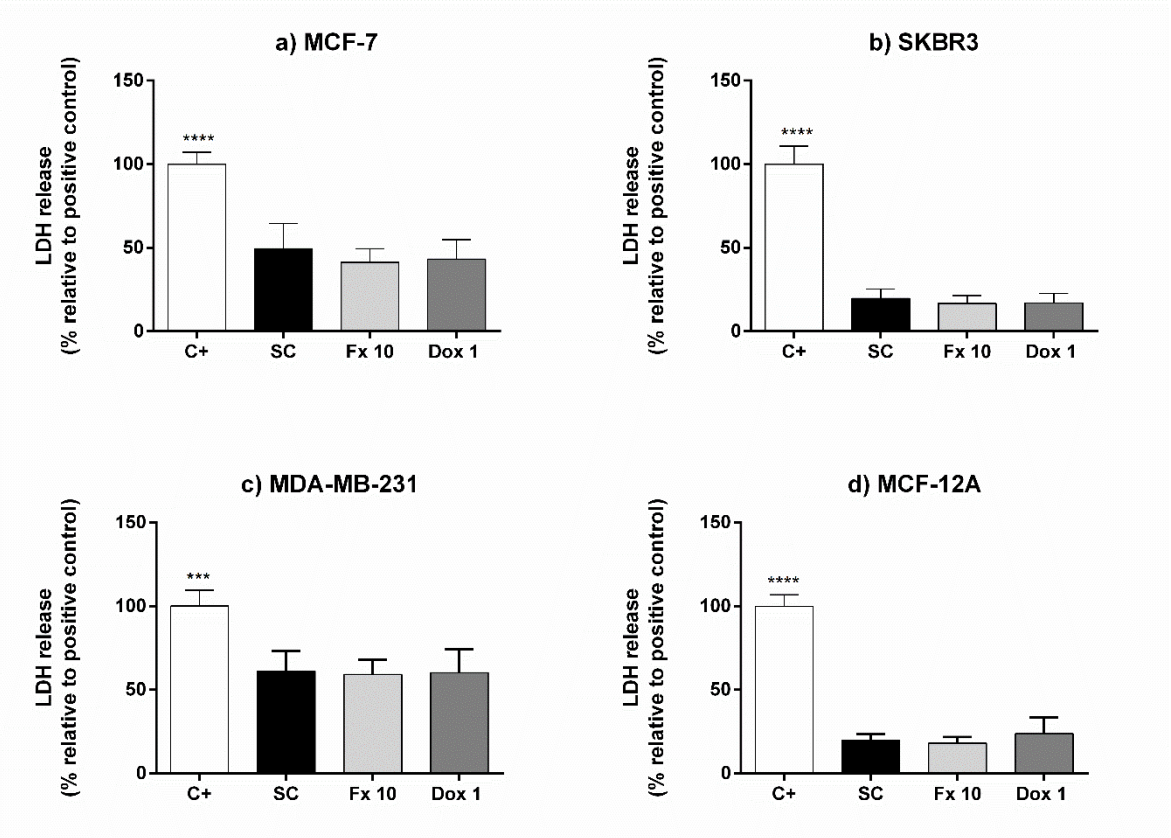



**Figure 27-** Effect of Fx at 10 µM (Fx 10) and Dox at 1 µM (Dox 1) on cell viability of MCF-7 (a), SKBR3 (b), MDA-MB-231 (c) and MCF-12A (d) MCAs, assessed after 4 days of exposure by the LDH assay. Cells treated with 0.1% DMSO (SC) and lysed with Lysis Buffer (10x) from the Pierce LDH Cytotoxicity Assay Kit (C+) were included as negative and positive controls, respectively. The percentage of LDH release was calculated in relation to the C+. Results are expressed as mean ± SD of four independent experiments. Significant differences (*** $P < 0.001$ and **** $P < 0.0001$), when compared to the negative control (SC), were determined by one-way ANOVA, followed by a Holm-Sidak's multiple comparisons test.

### 3.2. Assessment of Antiproliferative Effects

To assess the effects of Fx and Dox on cell proliferation in the MCAs, BrdU Proliferation Assay was performed. The absorbance was measured at 370 nm and 492 nm after 30 minutes of substrate incubation. As evidenced in Figure 28, Dox at 1 µM was able to remarkably reduce cell proliferation in SKBR3 (Fig. 28b) and MCF-12A (Fig. 28d) MCAs, by 43% and 57%, respectively, in comparison to the control. Noteworthy, Fx at 10 µM only inhibited SKBR3 cells' proliferation (Fig. 28b), causing a reduction of approximately 31% relative to control.

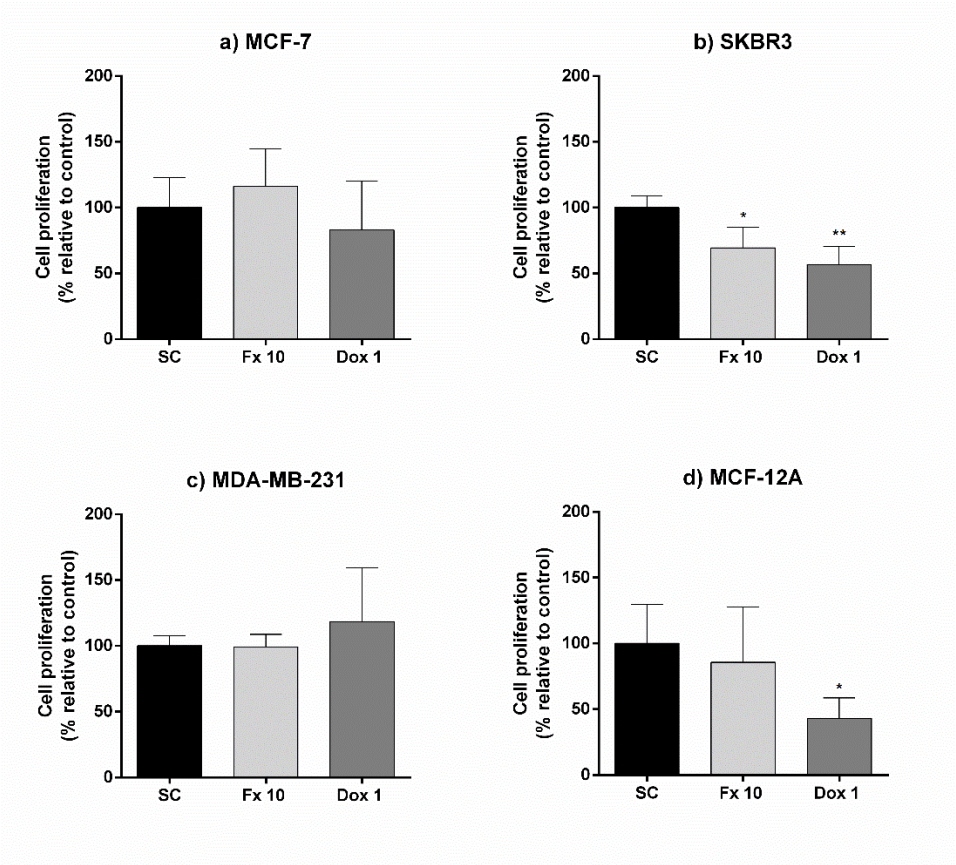



**Figure 28-** Effect of Fx at 10 µM (Fx 10) and Dox at 1 µM (Dox 1) on cell proliferation of MCF-7 (a), SKBR3 (b), MDA-MB-231 (c) and MCF-12A (d) MCAs, assessed after 4 days of exposure by the BrdU assay. Cells treated with 0.1% DMSO (SC) were included as a negative control. Results are expressed as the percentage of cell proliferation at 370 nm-492 nm and presented as mean ± SD of four independent experiments. Significant differences (* $P < 0.05$ and ** $P < 0.01$), when compared to the control, were determined by one-way ANOVA, followed by a Holm-Sidak's multiple comparisons test. An additional unpaired Student's t-test was performed to assess significant differences (* $P < 0.05$), between the condition Dox (1 µM) versus control in MCF-12A cells.

### 3.3. Image Analysis

MCAs monitoring occurred throughout the exposure period by regular observation under a stereomicroscope with a dark field, and photographs of each MCA were taken at the beginning of the exposure (t=day 0) and after 4 days of exposure (t=day 4). MCAs treated with 0.1% DMSO (SC) were used as negative control. Stereomicroscopy analysis revealed no remarkable visible differences in the MCAs' shape and size from the exposure conditions (Dox and Fx) when compared to the control (Fig 29).

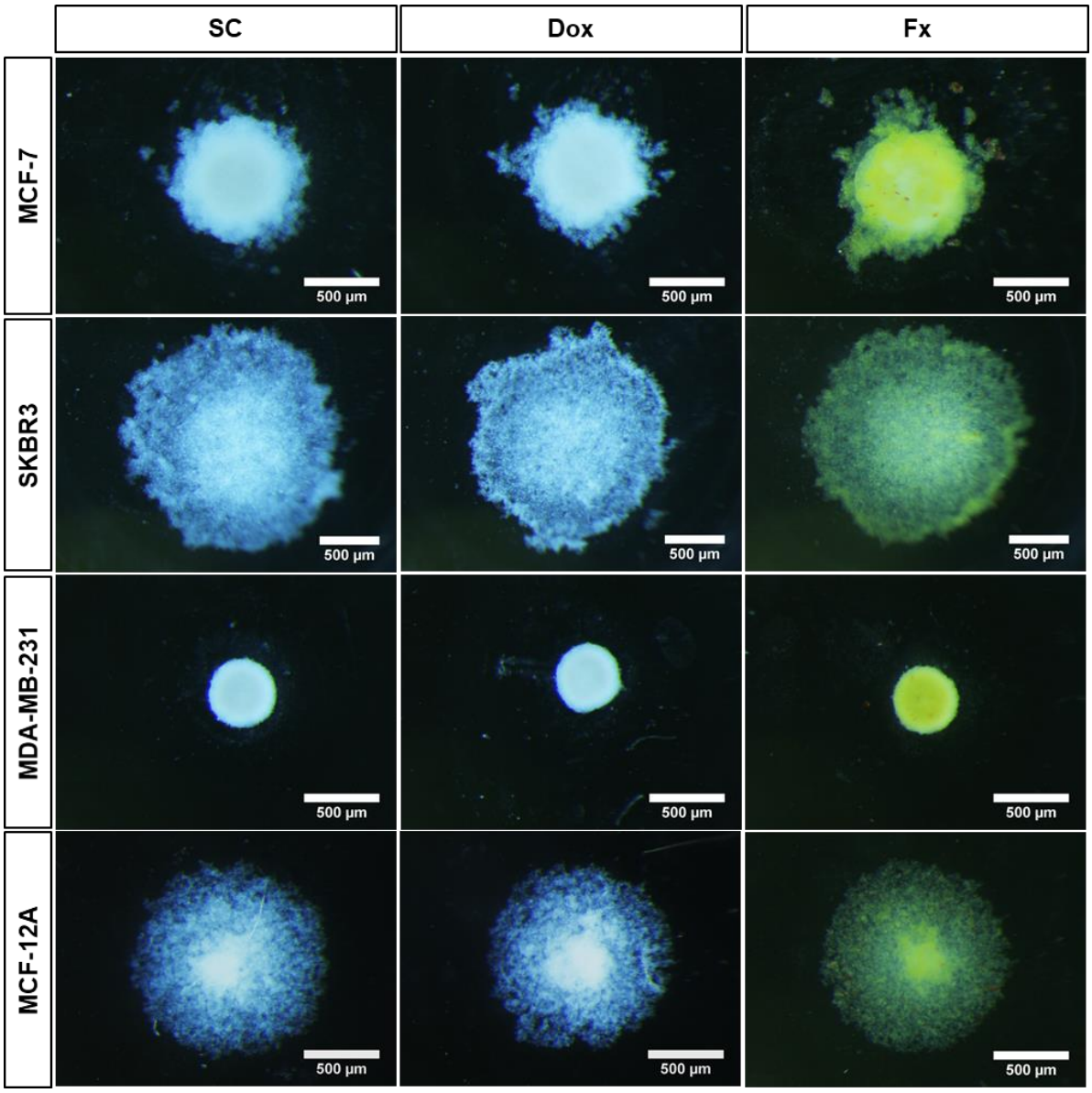



**Figure 29-** Representative morphology images, photographed in a stereomicroscope with a dark field, of the 3D multicellular aggregates (MCAs) after 4 days (96 h) of incubation with Dox at 1 µM and Fx at 10 µM. MCF-7, SKBR3 and MDA-MB-231 cells were seeded at 40 x $10^4$ cells/ml. MCF-12A cells were seeded at 20 x $10^4$ cells/ml. Cells treated with 0.1% DMSO (SC) were included as a negative control. Fx was responsible for the yellowish colour observed in the Fx-treated MCAs. Scale bar: 500 µm

To perform area measurements, MCAs were photographed with a stereomicroscope attached to a camera at two specific time points: t= day 0, before exposure and t= day 4, after 4 days of exposure. Using those pictures, the AnaSP software performed segmentation, producing binary images for subsequent estimation of MCAs areas.

Comparing MCAs' areas at day 0 (before exposure) and day 4 (after exposure), significant differences were observed in the SKBR3, MDA-MB-231 and MCF-12A cell lines (Fig. 30). There was a pronounced reduction in the SKBR3 MCAs' area on day 4 when exposed to Dox at 1 µM compared to day 0 (Fig. 30b). Furthermore, MCF-12A MCAs

exposed to Fx at 1 µM and incubated with 0.1% DMSO (negative control, SC) significantly increased their areas after 4 days of exposure in comparison with the areas measured at day 0 (Fig. 30d). All the conditions tested in the MDA-MB-231 MCAs presented significant differences after 4 days of exposure relative to day 0 (Fig. 30c).

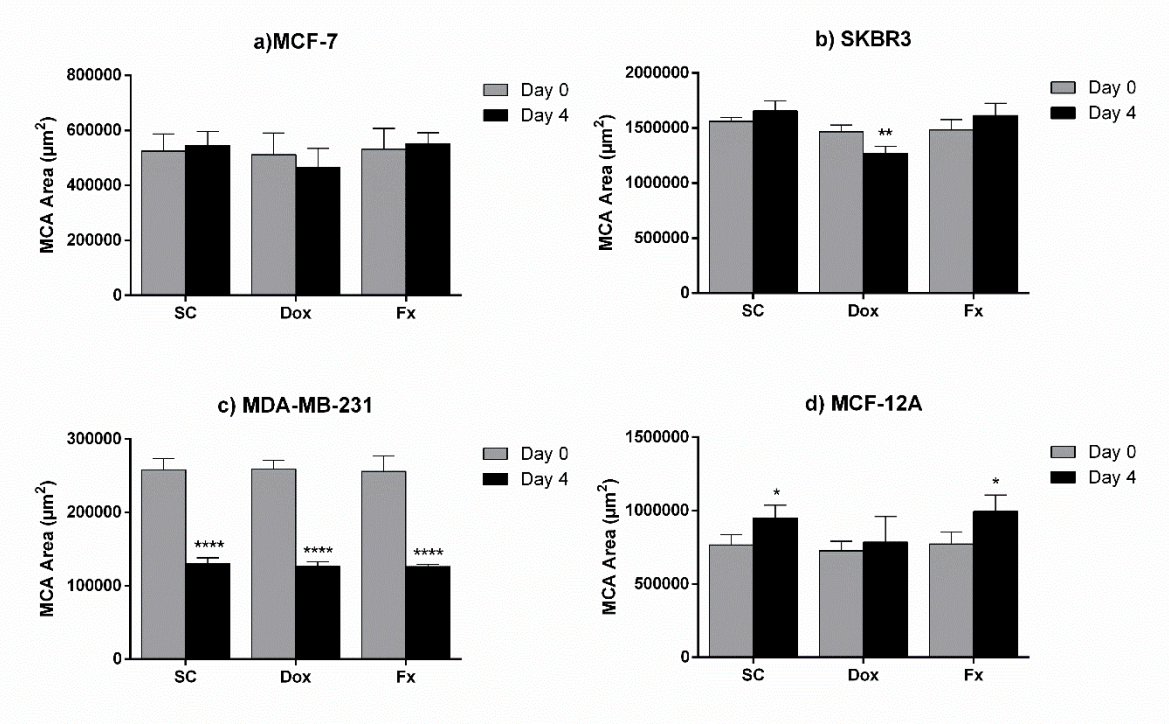



**Figure 30-** Area measurements (µm$^2$) of MCF-7 (a), SKBR3 (b), MDA-MB-231 (c) and MCF-12A (d) MCAs before exposure (day 0; grey bars) and after 4 days of exposure (day 4; black bars) at Fx at 10 µM and Dox at 1 µM. As a negative control, cells were treated with 0.1% DMSO (SC). Results are expressed as mean ± SD of four independent experiments. Significant differences (* $P < 0.05$; ** $P < 0.01$ and **** $P < 0.0001$), when compared to the MCAs area before exposure (at day 0), were determined by one-way ANOVA, followed by a Holm-Sidak's multiple comparisons test.

### 3.4. Histological Analysis

Through microscopic observation of the MCAs sections stained with HE, it was unexpectedly noticed that the MCF-7 aggregates comprised peripheral compact zones and large necrotic cores in all the conditions tested of the four independent replicas conducted (Fig.31). Besides, all the MCF-12A MCAs presented extremely loose aggregates that tended to easily disintegrate during harvesting and histological processing thus, we were only able to get sections of the MCAs from the solvent control and Dox groups representing a small central aggregate that remained intact. In Fx treatments, all the harvested MCF-12A MCAs disaggregated, as seen in Fig. 31, forming a cell suspension. Overall, no evident morphological differences were observed when comparing the MCAs from the exposure conditions (Dox and Fx) with the ones from the solvent control (cells treated with 0.1% DMSO, SC) in any of the cell lines included in this investigation (Fig. 31).

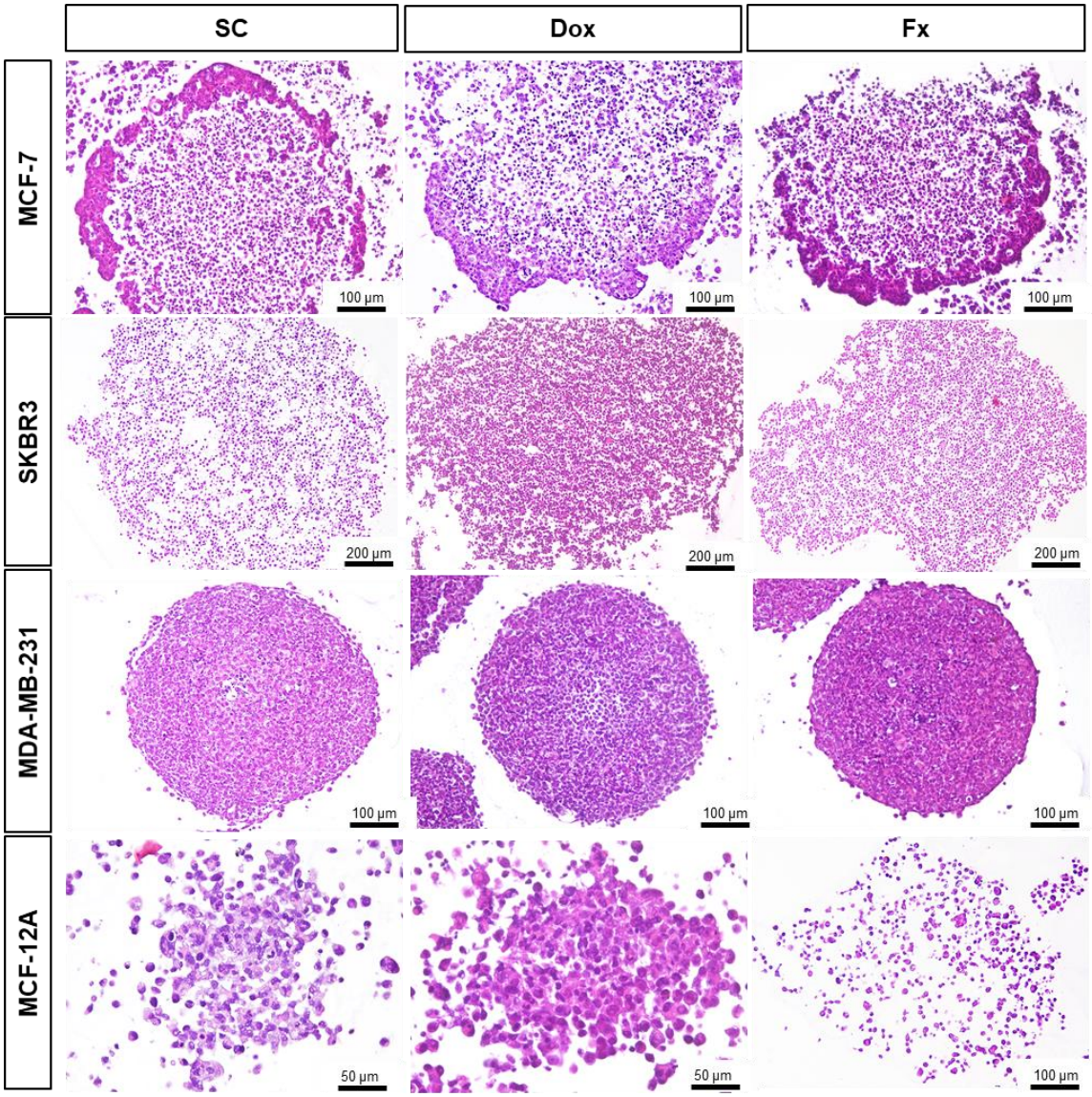



**Figure 31**- Representative images of 3 µm-thick sections of the MCAs stained with HE, after 4 days of exposure to Dox at 1 µM and Fx at 10 µM. Cells treated with 0.1% DMSO (SC) were included as a negative control. Scale bar: 50, 100 and 200 µm.

### 3.5. Immunocytochemical Analysis

Along with the morphological assessment, cell death and antiproliferative effects of Dox and Fx were evaluated through immunocytochemistry using anti-caspase-3 and anti-Ki67 antibodies, respectively. The results showed that the proportion of positive cells for caspase-3 was similar among the conditions tested and the control in all the cell lines (Fig. 32). In accordance with the results from the HE staining, the MCF-7 MCAs exhibited a higher concentration of apoptotic cells located in their inner region. The remaining MCAs from the SKBR3, MDA-MB-231 and MCF-12A cell lines showed a random distribution of caspase-3 staining. We could not evaluate the cell death induction effects of Fx in the MCF-12A MCAs, although some caspase-3 staining was observed in the cell suspensions.

Concerning their proliferative activity (Fig. 33), the MCF-7 MCAs exhibited Ki67-positive cells essentially in the external zone in all the conditions studied. Moreover, the SKBR3 MCAs exposed to the anticancer drug Dox showed a significantly lower number of Ki67-stained cells in comparison to the control and Fx groups. Additionally, it was observed that SKBR3 cells that were positive for Ki67 were homogeneously distributed all along the MCAs in all the conditions assessed. In the MDA-MB-231 MCAs of all the treatment groups, it was noted a reduced number of cells immunostained with Ki67 in the core region, while in the peripheral area this staining was more abundant. Regarding the MCF-12A MCAs of the solvent control and Dox groups, no distribution patterns or differences in the proportion of Ki67-positive cells were observed. Even though MCF-12A MCAs of Fx exposure group disaggregated, it was noted the presence of some proliferative cells in the suspension.

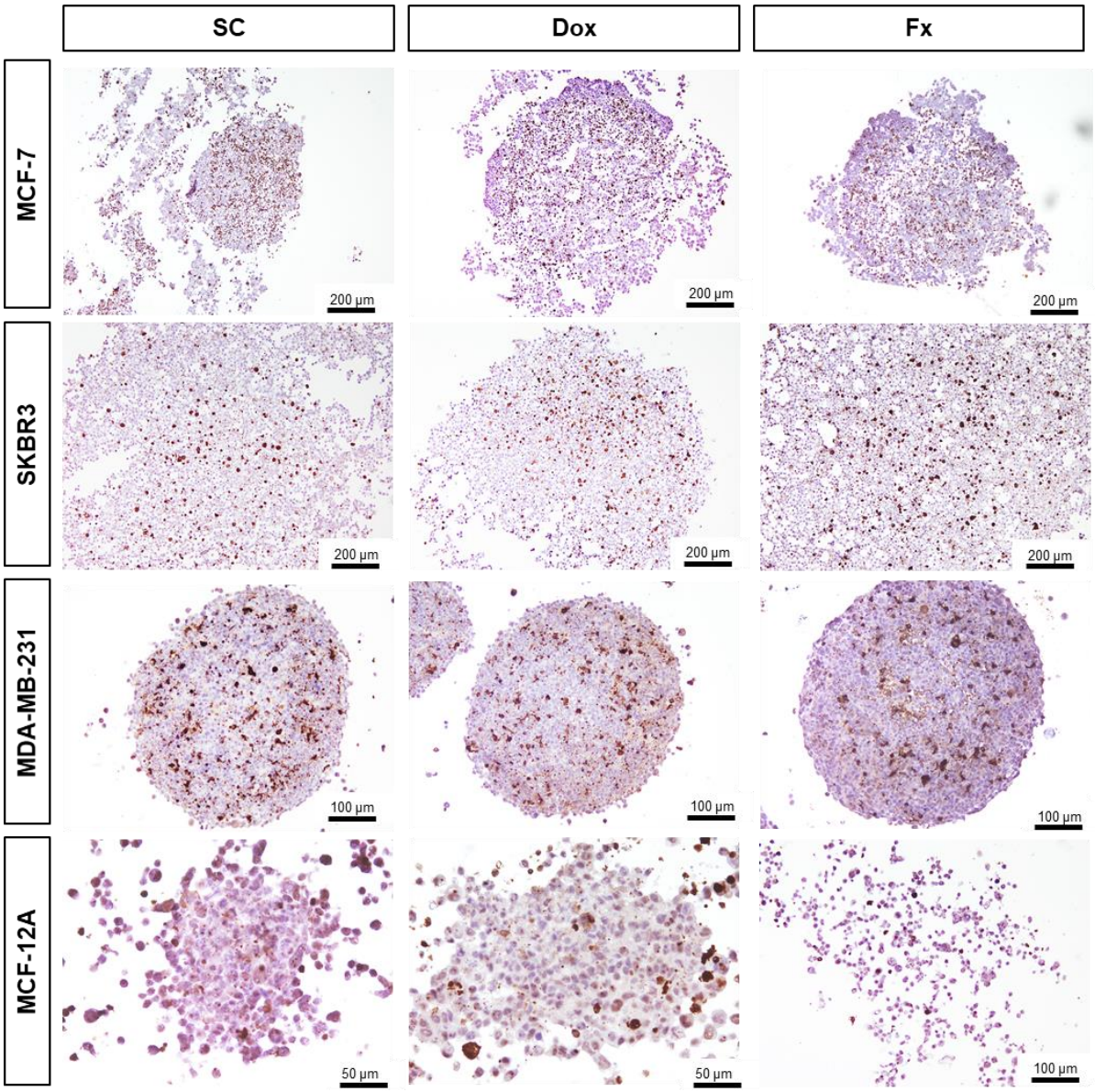



**Figure 32**- Representative images of 3 µm-thick sections of the MCAs immunostained against caspase-3, after 4 days of exposure to Dox at 1 µM and Fx at 10 µM. Cells treated with 0.1% DMSO (SC) were included as a negative control. Scale bar: 50, 100 and 200 µm.

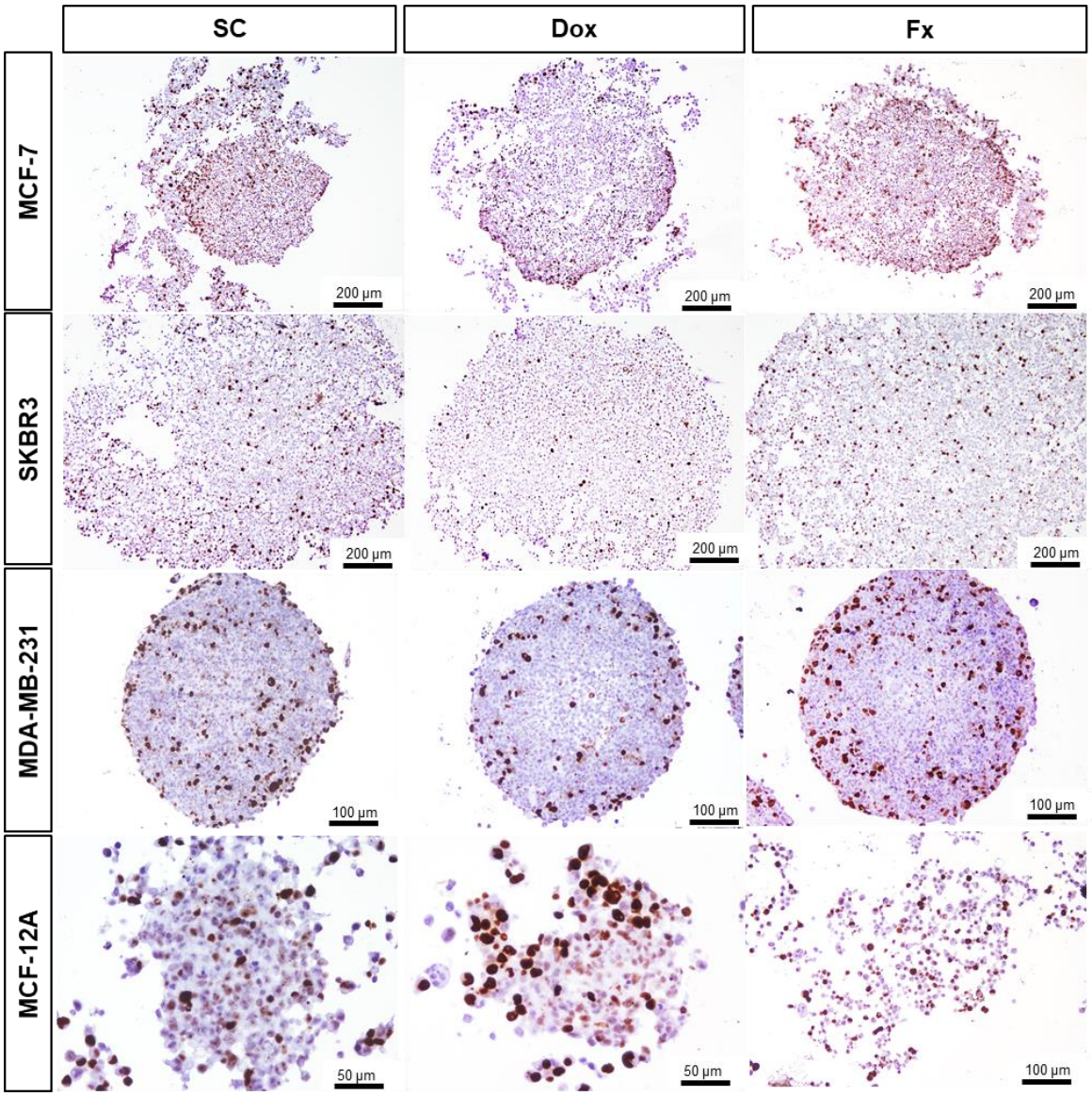



**Figure 33**- Representative images of 3 µm-thick sections of the MCAs immunostained against Ki67, after 4 days of exposure to Fx at 10 µM and Dox at 1 µM. Cells treated with 0.1% DMSO (SC) were included as a negative control. Scale bar: 50, 100 and 200 µm.

# -CHAPTER V-

Discussion

# Discussion

Finding strategies to overcome chemotherapeutic adverse effects (as drug cancer resistance and toxicity in non-tumor tissues) is a challenge that urgently requires answers for improving the treatment of BC patients. The administration of natural compounds, such as marine bioactive substances, alone but mostly in combination with anticancer drugs represents a promising strategy to increase the efficacy and reduce the side effects associated with chemotherapy (Khalifa et al., 2019). As far as we know, this is the first report on the anticancer effects of the seaweed-derived compounds Fx, Fct and Fc alone and in combination with the chemotherapy drugs Dox and Cis, using the mentioned panel of breast cell lines (MCF-7, SKBR3, MDA-MB-231 and MCF-12A) cultured under 2D and 3D conditions.

### 1. Anticancer Effects of Fx, Fct and Fc Alone and in Combination with Dox or Cis on 2D Cultures

The screening for anticancer activity of the natural compounds Fx, Fct and Fc and combinations on 2D cultured cells was performed by the evaluation of their cytotoxicity, genotoxicity and cell death induction effects using the MTT, comet and nuclear condensation assays, respectively. The non-malignant MCF-12A breast epithelial cells were included to evaluate the specificity of the anticancer effects in tumor cells. Dox and Cis, two clinical drugs widely used in the treatment of BC, were selected as reference compounds for the conducted cell-based assays. The concentrations of the drugs and natural compounds used in our study as well as the treatment periods were chosen according to the literature (Ibrahim et al., 2013; Mitchell & Engelbrecht, 2015) and results obtained from previous investigations performed in our laboratory (Almeida et al., 2018; Lopes-Costa et al., 2017; Ramos et al., 2019). Both anticancer drugs were tested at clinically relevant concentrations (Mitchell & Engelbrecht, 2015; Yamamoto et al., 2015). For instance, clinical administration of Dox is performed intravenously at doses that range between 15 and 90 mg/m$^2$, which are equivalent to plasma concentrations ranging from 0.3 to 5 μM (Mitchell & Engelbrecht, 2015).

Considering our results from the MTT assay, Dox induced cytotoxic effects on all the cell lines tested after 72 h of incubation, similarly to what was found in earlier studies (Mitchell & Engelbrecht, 2015; Pilco-Ferreto & Calaf, 2016). Several mechanisms underlying Dox's cytotoxicity activity have been identified, including DNA intercalation and formation of adducts, topoisomerase II inhibition, and induction of oxidative stress as a result of ROS production (Thorn et al., 2011; Yang et al., 2014). Thereupon, dependent on the DNA damage levels, Dox can cause cell cycle arrest, impairment of mitochondrial

function or even cell death (Kim et al., 2009). In MCF-7 and SKBR3 cells, we observed no correlation between Dox-induced decrease of cell viability and density, and the induction of DNA strand breaks nor cell death since no significant differences in DNA tail intensity, percentage of cells with condensed nuclei and no observable alterations in cell-substrate adhesion were detected. Although several articles describe the apoptotic effects of Dox on different cell models (Abdoul-Azize et al., 2018; Wang et al., 2004), our results, might suggest that other mechanisms, such as inhibition of cell proliferation through cell cycle arrest, as already reported by Bar-On et al. (2007) in MCF-7 and MDA-MB-231 cells (Bar-On et al., 2007), could be responsible for the decrease seen in the viability of MCF-7 and SKBR3 BC cell lines. In accordance, Lupertz et al. (2010) evaluated the anti-tumor effects of Dox (5 μM) on a human colon carcinoma cell line (Hct-116) and reported a decrease of viable cells and induction of cell cycle arrest in G0/G1 phase, without promoting cell death (Lüpertz et al., 2010).

Meanwhile, the cytotoxicity induced by Dox at 1 μM in MDA-MB-231 cells appeared to be related with its genotoxicity, since an increase in DNA damages was revealed by the comet assay. In agreement with our results, Antberg and collaborators showed that Dox increased DNA damage, detected by the comet assay, in MCF-7 and MDA-MB-231 cells after 1 h of exposure. However, 24 h after Dox exposure, the level of DNA damage decreased (Antberg et al., 2015). Another study performed by Apostolou et al. showed similar results, since a reduction in the percentage of DNA in tail was also reported after 24 h of Dox treatment in MCF-7 and MDA-MB-231 cells (Apostolou et al., 2014). Both studies suggest the activation of DNA repair mechanisms in these cells after longer exposure periods (24 h) to Dox that will repair the DNA damages originally induced by this drug. In the non-tumorigenic breast epithelial MCF-12A cell line, the induction of cell death might be one of the mechanisms involved in Dox's cytotoxicity, as we observed an increase in the number of cells with nuclear condensation and pyknotic nuclei. Also, Wang and collaborators showed that Dox at 0.5 μM induced apoptosis in non-tumor cells (bovine aortic endothelial cells and adult rat cardiomyocytes) after only 4 h of exposure (Wang et al., 2004).

Concluding, all of these results revealed heterogeneity in cells' response to Dox, since different cytotoxic mechanisms were activated among cell lines.

Regarding the chemotherapy drug Cis, a remarkable decrease in cell viability was observed at 24 h only in MCF-7 cells exposed to this drug (20 μM), denoting a higher potency of this anticancer agent against this cell line. At 72 h Cis decreased cell viability in all the cell lines tested. In this way, MCF-7 cells, at the tested conditions, showed higher sensitivity to Cis compared with the other cell lines, while MDA-MB-231 proved to be the most resistant cell line since its viability was not affected by Cis at 10 or 20 μM. According

to our data, Yde and Issinger also showed that MDA-MB-231 cells presented some resistance to Cis (Yde & Issinger, 2006). However, and contrarily to our results, some authors characterize MCF-7 as relatively Cis-resistant cell lines, when compared to other BC cell lines such as MDA-MB-231, MDA-MB-435, HCC-1937 and CAL-148 cells (Yde & Issinger, 2006; Zhang et al., 2013b). In our point of view, some discrepancies of data can be due to the different cell culture conditions and the preparation of Cis (namely solvent used and time in solution) (Hall et al., 2014).

Moreover, Cis induced cell death in a dose-dependent manner in MCF-7 and SKBR3 cells. Cell death induction was also noted by the nuclear condensation assay in MDA-MB-231 and MCF-12A cells treated with Cis at 50 μM and Cis at 10 μM, respectively. In agreement, Niknafs and Holiday indicated apoptosis to be one of the main mechanisms of cell death in MCF-7 and MDA-MB-231 cells exposed to Cis (Holiday et al., 2011; Niknafs, 2011). However, no effects on DNA damage were detected by comet assay.

Overall, these findings indicate that the underlying mechanisms of Cis cytotoxicity were consistent among the cell lines, and possibly associated with the activation of apoptotic pathways.

Considering the morphological changes of cells treated with Dox and Cis, we observed by contrast-phase microscopy an increase in the number of hypertrophic cells (except in SKBR3 cells) due to cytoplasmatic swelling and, in certain cell lines, higher levels of vacuolization (MCF-7, SKBR3 and MCF-12A cells exposed to Dox 0.1). These effects are postulated by some authors to be associated with cell death induction (Shubin et al., 2016). We also noted the presence of some cellular membrane extensions resembling a dendritic structure, which we named as finger-like protrusions, especially in Dox-treated conditions (except in SKBR3) and in MCF-12A cells exposed to Cis. These cellular protrusions are observed during several cellular mechanisms, as proliferation, differentiation, migration and cell death (Kohno et al., 2015). Kohno and collaborators showed that staurosporine, an apoptosis inducer, induced cellular protrusions in a panel of cancer and normal cell lines (Kohno et al., 2015). Regarding our data, the finger-like protrusions observed might be correlated to the induction of cell death by these cytostatic drugs.

In the last decades, some bioactive compounds isolated from seaweed have been showing promising anticancer effects in colon cancer, glioblastoma, leukemia and BC (Almeida et al., 2018; Ferreira et al., 2018; Lopes-Costa et al., 2017; Pádua et al., 2015). In this study, the anticancer activity of Fx, Fct and Fc was assessed individually and in combination with the anticancer drugs, Dox and Cis. Regarding their independent effects, our results indicated that Fx at 10 μM induced a decrease in the metabolic activity of all the cell lines, as well as a decrease in cell density and cell-substrate adhesion. In agreement,

other studies have also implied that Fx has considerable *in vitro* cytotoxic activities against BC cell lines, namely in MCF-7 and MDA-MB-231 cells (Ayyad et al., 2011; Rwigemera et al., 2014, 2015; Yousefi et al., 2018). Researchers reported that Fx, and its main metabolite fucoxanthinol, decreased cell viability in MCF-7 and MDA-MB-231 cells as a result of apoptosis induction by disruption of the Nuclear Factor kappa B (NF-kB) signalling pathway, which regulates apoptosis by controlling the transcription of anti-apoptotic genes (Rwigemera et al., 2014, 2015; Wang et al., 1999). However, in our study, no effects on DNA damage and cell death assessed by the comet and nuclear condensation assays, respectively, were observed. Fx is also able to inhibit cell proliferation by promoting cell cycle arrest at the G0/G1 phase (Liu et al., 2009). These antiproliferative mechanisms can explain the reduced cell density observed in all the Fx-treated cell lines tested in our study. Besides, although some authors proved that Fx did not have cytotoxic effects on normal cells (Ishikawa et al., 2008; Yousefi et al., 2018; Yamamoto et al., 2011), our results, as well as the ones obtained by Kotake-Nara et al. (2005), revealed cytotoxic activity of Fx at 10 μM against non-malignant cell lines (Kotake-Nara et al., 2005).

Regarding the effect of Fct and Fc on cell viability/death and genotoxicity, no effects were reported at none of the tested concentrations. These data are positively correlated to Jiang et al. (2018) findings, in which it was verified that the $IC_{50}$ of Fct for MCF-7 cells was 125 μM, proving that we needed to test much higher doses than those actually used in order to observe anticancer effects on BC cell lines (Jiang et al., 2018). Similarly, studies regarding the cytotoxic activity of Fc in BC cells commonly used higher concentrations, sometimes in the range of mg/ml (Abudabbus et al., 2017; Banafa et al., 2013; Zhang et al., 2013b). Also, some authors draw attention to the fact that the effective concentrations of Fc change according to the seaweed species from which it is extracted, the extraction method and its molecular weight (Van Weelden et al., 2019).

Meanwhile, the combination of seaweed-derived compounds with conventional anticancer drugs has been shown promising results (Pádua et al., 2015). However, the interaction of seaweed compounds with anticancer drugs in BC is still poorly explored. Our results showed, for the first time, that Fx in combination with Dox (1 μM) enhanced the cytotoxic effect of this anticancer drug promoting a decrease in the number of MDA-MB-231 viable cells. Nevertheless, cells co-treated with Fx and Dox showed lower amounts of DNA damages (DNA strand breaks) than cells exposed to Dox alone, evidencing a potential protective effect of Fx against Dox-induced genotoxicity. Our findings are in agreement with those reported by Ayyad et al. (2011) in MCF-7 cells. These researchers reported that Fx had a protective action against DNA damages caused by the chemotherapeutic drug bleomycin, although the mechanism was still unknown. They also evaluated the antioxidant potential of Fx, amongst other compounds extracted from *Sargassum sp*., and found that

Fx displayed the highest antioxidant activity against the MCF-7 cells (72% inhibition) (Ayyad et al., 2011). As mentioned herein, one of the principal mechanisms of action behind Dox anticancer activity is the production of ROS wich consequently leads to oxidative stress and DNA damages. Therefore, one possible explanation for Fx-promoted reduction of Dox genotoxic effects in MDA-MB-231 cells could be related to the antioxidant role of Fx, already described in the literature (Koduvayur Habeebullah et al., 2018; Sangeetha et al., 2009; Xia et al., 2013; Yan et al., 1999). The protective effect of Fx was also reported in other recent studies, where pre-treatment with Fx protected skin fibroblasts (Denis et al., 2019) and the human keratinocyte cell line HaCaT (Zheng et al., 2013) against hydrogen peroxide-induced oxidative DNA damages. Despite the genoprotective effect of Fx observed in our study, this compound increased the cytotoxic effect of Dox in MDA-MB-231 cells revealing the involvement of other mechanisms.

Although Fct alone had no cytotoxic effects, in co-incubation with Dox at 0.1 μM Fct caused a decrease in the viability of MDA-MB-231 cells. This decrease was not correlated with the induction of cell death evaluated by nuclear condensation assay. To the best of our knowledge, this is the first study assessing the effects of this combinatorial treatment in BC. According to our results, Ramos and colleagues showed that Fct in combination with 5-fluorouracil decreased cell viability in colon cancer cells, with inhibition of cell proliferation, clonogenic potential and cell migration and without effects on cell death (Ramos et al., 2019).

Hsu and Hwang in a recent review about the clinical applications of Fc, reported the results of some human clinical trials where Fc was used as an adjunct/complementary therapy with anticancer drugs and conclude that this natural compound was able to improve the activity of the conventional drugs as well as decrease their side effects (Hsu & Hwang, 2019). Regarding BC, Zhang and collaborators reported that the combinatorial treatment of a Fc extract (400 μg/ml) isolated from *Cladosiphon navae-caledoniae* with chemotherapeutic agents, such as Cis, tamoxifen and paclitaxel significantly enhanced cell viability inhibition and apoptosis in MDA-MB-231 and MCF-7 cells (Zhang et al., 2013b). In our study, although we used a similar concentration of Cis (10 μM), no significant growth inhibitory effects were observed in MDA-MB-231 cells co-exposed to Fc and Cis, which might indicate that the concentration of Fc applied was not sufficient to potentiate the cytotoxic activity of Cis.

On the other hand, the combination of Fc with Dox significantly changed the viability of MDA-MB-231 cells, however without effects on cell death and DNA damage. Interestingly, when Fc was applied at lower concentrations (10 μg/ml) we observed a potential protective effect against Dox-induced cytotoxicity in the MDA-MB-231 cell line. On the contrary, at higher concentrations (50 μg/ml), Fc potentiates the cytotoxic effect of Dox.

These findings reflect that different doses of Fc when co-exposed with the same concentration of Dox can induce opposite responses in the viability of MDA-MB-231 cells. Also, those results call attention to the possible hormetic behavior of Fc. In a recent review, Moghaddam and colleagues discuss the hormetic response of curcumin, a natural compound, showing that at low concentrations curcumin had antioxidant properties, while at high doses induced anticancer effects (Moghaddam et al., 2019). Similarly, to curcumin, Fc antioxidant activities have already been described in earlier studies (Subramanian et al., 2017; Wang et al., 2015). Hence, these findings made us believe that Fc at lower doses may have antioxidant activities against Dox oxidative damages in MDA-MB-231 cells, reducing the anticancer efficacy of this drug. In our work, we did not find a positive correlation between the cytotoxic effects, caused by the combination of Dox and Fc (50 µg/ml), and an increase in cell death, which was contrary to reported by Abudabbu et al (2017). Comparing the doses applied in both studies, this author used much higher concentrations than the ones present in our investigation, ranging between 400 to 1200 µg/m, which may justify the divergences of data (Abudabbus et al., 2017).

Overall, the three seaweed compounds (Fx, Fct and Fc) enhanced the cytotoxic activity of Dox in MDA-MB-231 cells without cytotoxic effects in non-tumor cells (MCF-12A), showing a selective effect.

**2. MCAs Generation and Characterization**

One of the specific objectives of our work was to optimize a 3D culture technique to generate homogeneous multicellular aggregates with an adequate size that would enable their visualization during manipulation and prevent their loss throughout the experimental procedures. Taking into account previous studies from our laboratory, where several 3D cell culture techniques were tested (hanging drop method, poly-HEMA coating culture plates with flat or conical bottom and ULA plates with conical bottom), the forced floating method using ULA 96-well conical-bottomed plates proved to be the most efficient and straightforward approach in obtaining 3D multicellular structures from the cell lines under investigation. Indeed, several articles have been establishing protocols based on this method (Amaral et al., 2017; Friedrich et al., 2009; Ho et al., 2012; Nagelkerke et al., 2013; Raghavan et al., 2016), as it represents a simple and reproducible approach suitable for high-throughput screening of anticancer drugs (Breslin & O'Driscoll, 2013).

According to the literature, different terms have been used to designate 3D multicellular structures, including spheroids (Ivascu & Kubbies, 2007), tumor spheroids (Nunes et al., 2019a), multicellular tumor spheroids (Nagelkerke et al., 2013), microtissues (Vantangoli et al., 2015), microtumors (Yılmaz & Sakarya, 2018), mammospheres (BC spheroids) (de la Mare et al., 2013), tumoroids (Vamvakidou et al., 2007) and multicellular

aggregates (Azadi et al., 2019). The term spheroid still lacks a concrete definition, however in the view of Nagagelkerke et al., (2013) spheroids are round or elliptic globe-like structures with high level of compactness, that can be handled without causing the disaggregation of the cells (Nagelkerke et al., 2013). By observing the morphology of our 3D models, we concluded that they did not fit into the definition described, since they displayed a flat and disk-shaped structure, and in certain cell lines (MCF-12A and SKBR3), cells adhered very weakly to each other, which made their manipulation difficult. Therefore, herein, we decided to use the term “3D multicellular aggregates (MCAs)”.

In order to achieve our aim, optimal seeding densities and formation periods were established. After testing different formation times (4, 7, 10 and 12 days), results from the stereomicroscopic analysis suggested that the application of the ULA plates method enabled the generation of round-shape and uniform sized MCAs (from all the cell lines) within 4 days. In the literature, the formation time for the generation of BC 3D models usually varies between 24 to 96 h (1 to 4 days) (Froehlich et al., 2016; Howes et al., 2014; Malhão et al., 2019; Pereira et al., 2017; Vinci et al., 2012), which is in accordance with our results. Although the morphology of the MCAs was consistent within each cell line, different degrees of compaction were observed amongst the distinct breast cell lines. Our findings were in accordance with those reported by Froehlich et al. (2016), where different BC cell lines (MCF-7, MDA-MB-231 and SKBR3) originated spheroids with divergent compactness following the application of several 3D culture methodologies (Froehlich et al., 2016). These morphologies may result from the different gene expression patterns and protein expression profiles characteristic of each cell line (Kenny et al., 2007)

Noteworthy, we also observed that culturing MCAs for more than 7 days was not beneficial as they tended to lose their cohesiveness and disaggregate. In another study, glioma cancer spheroids that were formed using emulsion-based techniques exhibited the first signs of disaggregation on day 9 of culture, however, the integrity of their structure was only remarkably compromised after 14 days (McMillan et al., 2016). Besides, an extended MCAs cultivation implies the need for culture medium changes which would affect MCAs structure, considering that some aggregates were extremely loose and easily destructed during manipulation (especially in MCF-12A MCAs).

Therefore, as increasing the formation time did not improve the generation of larger spheroids and even compromised their integrity, we decided that the best approach was to minimize the formation period and apply higher cell seeding densities. This procedure would prevent MCAs disintegration and facilitate their handling, namely during histological processing for light and electron microscopy analysis. Since no evident morphological changes were noted between MCAs cultured for 3 and 4 days, we opted to use 3 days as the optimal period for MCAs generation. Meanwhile, a positive correlation between cell

seeding densities and MCAs' size was observed, corroborating the findings of other researches (Pereira et al., 2017; Rustamov et al., 2017). This increase in MCAs' size was also associated with an increase in their cellular compaction, as observed in stereomicroscopic images correspondent to the MCF-7, SKBR3 and MCF-12A cell lines. On the other hand, MDA-MB-231 cells formed MCAs with the same compaction level regardless of the initial seeding concentrations. Thus, to standardize the 3D culture conditions for all the BC cell lines we selected the highest cell densities tested (40 x $10^4$ cells/ml and 20 x $10^4$ cells/ml for MCF-12A) as the most suitable for MCAs formation. Lower cell densities have been established for MCF-12A since the doubling time of this cell line, according to the ATCC's information, is shorter (19 h) than the other cell lines used in our study (MCF-7 and MDA-MB-231 - around 29 and 38 h, respectively), suggesting that this line would have a faster proliferation (ATCC, 2012, 2016a, 2016c). This high proliferative activity was also further confirmed by immunocytochemistry analysis for Ki67. Comparing with the literature, the cell seeding densities applied in our investigation were much higher than the ones considered optimal for the formation of BC spheroids (Benton et al., 2015; Imamura et al., 2015), leading to the formation of MCAs (MCF-7, SKBR3 and MCF-12A) with diameters exceeding 500 µm. Current evidences suggest that spheroids larger than 500 µm of diameter display a concentrically layered structure with a necrotic central region, surrounded by a rim of senescent cells and an outer layer of proliferating cells (Vinci et al., 2012; Zanoni et al., 2016). However, as we observed by histological and immunocytochemical analysis, no necrotic cores were identified in the optimized MCAs, which implies that the disk-shape of the MCAs inhibited the formation of the typical hypoxic core, similar to what was found in other studies (Nagelkerke et al., 2013). Exceptionally, in certain MCAs from the MDA-MB-231 cell line, it was detected the presence of some necrotic cells in the inner area, however, this phenomenon was not surprising, since this BC cell line presented the most compact aggregates, as seen by stereomicroscopy, light microscopy and TEM analysis. Contrary to the literature (Rifle et al., 2017), our results showed no specific pattern in the distribution of Ki67-stained cells in any of the MCAs.

In the optimization step, different parameters were measured by the AnaSP software (area, convexity, diameter, volume, sphericity and solidity), however, some of them were not the most appropriate for characterizing the MCAs formed in the present study, so we opted to solely evaluate the areas.

The MCAs generated under the optimized conditions were classified, according to the level of tightness and compactness, into compact aggregates (MDA-MB-231 and MCF-7) and loose aggregates (SKBR3 and MCF-12A). These differences in structural compactness and cohesion verified under the stereomicroscope were corroborated by morphological and ultrastructural analysis (light and electron microscopy). As described by

other authors, the MCF-7 cell line allowed the generation of compact 3D BC models. (Froehlich et al., 2016; Ivascu & Kubbies, 2007; Pereira et al., 2017). This high compactness often seen in MCF-7 3D structures is usually associated with the expression of the cell adhesion molecule E-cadherin (Ivascu & Kubbies, 2007). Results from the HE staining and TEM analysis revealed high cell-cell interactions, confirming that MCF-7 MCAs structure was very cohesive. Both histological methods also detected the presence of acinar-like structures with a lumen containing death cells. These arrangements are similar to those found in mammary glands and have already been described to occur in spheroids of the MCF-7 cell line (Amaral et al., 2011). Previous studies indicate that the luminal space morphogenesis requires the apoptotic clearance of the inner cells of the acini (Mailleux et al., 2008), which may justify the presence of dead cells inside the lumina of the MCF-7 3D models. TEM images also showed the occurrence of cytoplasmatic secretory vesicles located on the apical part of the cells and directed towards the lumina or the external surface. Some articles correlate this phenomenon with the secretion of β-casein, a protein present in human milk, into the luminal space (D'Anselmi et al., 2013). Concordantly to TEM findings of Vantangoli et al. (2015), we also observed the presence of microvilli in the apical pole, which might indicate that the cells were undergoing polarization (Vantangoli et al., 2015).

Furthermore, the MDA-MB-231 cell line formed extremely compact and cohesive MCAs with a perfect round shape and relatively high three-dimensionality. The existent data about the formation of MDA-MB-231 3D cultures using ULA or cell-repellent plates is divergent, as some authors were able to obtain compact spheroids from this cell line (Dubois et al., 2017; Scolamiero et al., 2018) while others generated compact or loose aggregates (Froehlich et al., 2016; Vinci et al., 2012; Wang et al., 2016). The use of different cell seeding densities and formation times, as well as the use of different cell culture mediums with or without additives may explain these divergences. Results from the area measurements and HE staining showed that the reduction in the MCAs size observed between day 3 to day 7 was correlated with increased compactness, which might be positively correlated to the remarkable increase in the number of apoptotic cells assessed by immunocytochemistry.

The SKBR3 cell line originated MCAs with a loose structure and remarkably poor three-dimensionality, which is in accordance with the available literature (Froehlich et al., 2016; Ivascu & Kubbies, 2007; Malhão et al., 2019). TEM images confirmed the cell-cell low adhesion, by showing the presence of large intercellular spaces. Results from scanning electron microscopy analysis, performed in another study, also showed that SKBR3 cells presented poor aggregation when cultured under 3D conditions (Colone & Kaliappan, 2016). Furthermore, we postulated that the low three-dimensionality of these MCAs probably allowed them to have similar proliferative patterns at both 3 and 7 days.

Regarding the non-tumorigenic MCF-12A line, the MCAs presented low cell-cell adhesion, which made them very delicate to manipulate. Thus, the success rate for their harvesting was lower compared to the other cell lines tested. This loose arrangement was confirmed by histological and TEM analysis and has also been described in a similar study performed by others (Malhão et al., 2019). Similarly to MCF-7, non-malignant breast cell lines are also characterized by the formation of lumina (Mailleux et al., 2008). In accordance, TEM images exhibited the presence of some lumen-like structures in the MCF-12A MCAs. These findings did not come as a surprise since MCF-7 and MCF-12A are both luminal cell lines as described on ATCC site (ATCC, 2016b) and in the literature (Holliday & Speirs, 2011; Sweeney et al., 2018). Additionally, the high number of mitochondria detected by TEM can explain the high proliferative activity observed by Ki67 staining at both 3 and 7 days (Arciuch et al., 2012).

In our view, the application of a multi-endpoint approach, including histological (light and electron microscopy) and immunocytochemistry techniques, is important for the optimization and characterization of 3D cultures, since they allow the evaluation of the structural organization, single-cell morphology and protein expression patterns of 3D models (Ivanov & Grabowska, 2018). However, the majority of the studies concerning high-throughput 3D culture techniques are still limited to microscopic analysis and conventional live/dead assays.

**3. Anticancer Effects of Fx and Dox on 3D Cultures**

According to the results obtained in 2D cultures, we selected the brown seaweed carotenoid Fx and the anticancer drug Dox, both with cytotoxic effect in 2D, to be tested on the MCAs previously optimized. To the best of our knowledge, this is the second report concerning the anticancer effects of Fx on 3D BC models. The first screening was performed by De la Mare et al. (2013) who evaluated Fx effects on mammospheres' formation using an *in vitro* tumorsphere assay (3D model). This author reported that, despite having cytotoxicity against adherent MCF-7 BC cells, Fx at 10 μM did not affect MCF-7 mammosphere formation (De la Mare et al., 2013).

In our study, the evaluation of the cytotoxicity and antiproliferative effects of Fx and Dox on MCAs was performed along with the analysis of the correspondent morphological and immunocytochemical changes. Results from the MTT and LDH assays were concordant since they showed that neither Dox at 1 μM or Fx at 10 μM exhibited a cytotoxic effect on any of the MCAs tested. The absence of activity observed in our study could be explained by the low concentration of Fx and Dox compared to that used in other studies. Data from recent investigations showed that Dox produced cytotoxic effects on MCF-7 spheroids, with an IC50 of 110.09 μM (Nunes et al., 2019b). This concentration was much

higher than the applied in our investigation. The absence of cytotoxic effects promoted by Dox, a conventional anticancer drug used herein as a reference compound, makes it impossible to draw conclusions about the effects of Fx on cell viability. In further researches, higher concentrations of Dox need to be tested in order to evaluate cytotoxic effects on these 3D models.

In addition, regarding the assessment of antiproliferative effects by the BrdU assay, it was noted a significant reduction in the proliferation of SKBR3 cells treated with Dox at 1 μM and Fx at 10 μM, and MCF-12A cells exposed to Dox at 1 μM. The decrease in the proliferation of SKBR3 cells treated with Dox was consistent with the immunocytochemical results for Ki67. We postulated that the enhanced sensitivity of the SKBR3 and MCF-12A MCAs to the antiproliferative action of the compounds tested, in comparison with the remaining cell lines, is a reflection of their loose structure and low three-dimensionality, which confer them more similar drug sensitivities to those reported in 2D cultures. These results were in accordance with the ones found by Imamura et al. (2015), in which loose spheroids from the cell lines MCF-7, HCC-1954 and MDA-MB-231 presented reduced resistance to the activity of the drugs Dox and paclitaxel when compared to compact spheroids (BT-549, BT-474 and T-47D) (Imamura et al., 2015).

No apparent morphological alterations were detected by stereomicroscopic analysis between the MCAs treated with the different conditions, however, the area measurements indicated a remarkable reduction in the size of SKBR3 (Dox), MDA-MB-231 (all conditions) and MCF-12A (SC and Fx) aggregates by the end of the exposure period (day 4). The observed decrease in size of the MDA-MB-231 MCAs did not result of the compounds' effects since the same reduction was observed in the control group. This reduction seems to be related to the gradual increase of the MDA-MB-231 MCAs' compactness, as also observed during the optimization process. Furthermore, we believe that it is unlikely that the decrease in area of the MCF-12A MCAs treated with Fx could be correlated to the anticancer effect of this carotenoid since the same phenomenon was observed in the solvent control group. Considering that this cell line presented extremely loose aggregates with poor cell-cell contact, it is postulated that probably those size variations were caused by handling procedures. On the other hand, the decrease in the area of Dox-treated SKBR3 aggregates might actually be a consequence of the lower cell proliferation confirmed by the BrdU assay. However, despite being considered as the most informative morphometric parameter by some authors (Mittler et al., 2017), we and other researchers (Malhão et al., 2019) found that studying MCAs' areas alone is not a reliable approach for assessing the compounds' effects on 3D models, especially in loose 3D aggregates, since results could present high variability and be easily influenced by external factors (e.g. manipulation).

Curiously, MCF-7 MCAs of all the treatment groups, harvested at the four independent experiments conducted, presented large necrotic central regions, contrarily to what was observed during the optimization phase. This morphology was undetectable under stereomicroscopic observation, highlighting the relevance of incorporating histological analysis in studies concerning the screening of cytotoxic compounds. In accordance, immunocytochemistry results showed a higher proportion of apoptotic cells in the inner region of the MCAs, while proliferative cells were more abundant in the peripheral areas of the aggregates. The application of inadequate cell seeding densities or cultivation periods could be a plausible explanation, however recent studies using the same conditions did not report the presence of necrotic cores (Malhão et al., 2019). Hereupon, we concluded that there is high inter-assay variability regarding the formation of the MCF-7 MCAs. To minimize this variability, we suggest optimizing some parameters such as culture medium supplementations, decrease the interval time between experiments and use cells lines at low and similar passage numbers (Melissaridou et al., 2019; Mittler et al., 2017; Shaheen et al., 2016; Vande Voorde et al., 2019).

Comparing the effects on both cell culture models, Fx and Dox were significantly more effective in 2D cultured cells than in 3D cultures, which is in accordance with the literature concerning the resistance of 3D models to cancer drugs cytotoxicity (Imamura et al., 2015; Lovitt et al., 2018; Nigjeh et al., 2018; Nunes et al., 2019b; Ramos et al., 2019). These findings are in line with the typical drug resistance profile encountered in *in vivo* solid tumors (Nunes et al., 2019b). Studies state that the components of the extracellular matrix (e.g collagen, fibronectin) have an important role in mediating the response of cells grown under 3D conditions to chemotherapeutic agents, including Dox (Langhans, 2018; Lovitt et al., 2018; Nunes et al., 2019b), possibly through the regulation of the expression of pro-survival proteins (Lovitt et al., 2018). On the other hand, Lovitt et al. (2018) correlated Dox lower efficacy with the reduced proliferation rate observed in 3D BC cell cultures, compared to cells cultured in monolayer since cells that have slower proliferation rate might be less affected by this drug's cytotoxicity than the ones with higher doubling times (Lovitt et al., 2018). Another possible explanation for the noted resistance could be related to the limited diffusion of the compounds within the MCAs. Despite 3D aggregates did not have the typical dense structure of a spheroid, their 3D architecture could reduce the penetration of Dox and Fx, therefore lowering the number of cells affected by their anticancer actions (Kim et al., 2004; Mehta et al., 2012). In order to confirm the truth of these conjectures, further testing should be conducted to evaluate and compare the proliferation and diffusion rates of the compounds throughout the experiments in 2D and 3D culture models. So far, no information was found concerning the anticancer effects of Dox on 3D models from the SKBR3 and MCF-12A cell lines.

# -CHAPTER VI-

## Conclusion and Future Perspectives

## Conclusion and Future Perspectives

The first aim of the present study was to evaluate the *in vitro* anticancer activity of the marine bioactive compounds Fx, Fct and Fc alone and combined with the anticancer drugs Dox and Cis on tumor and non-tumor breast cell lines in 2D culture. Our results, showed that Cis and Dox caused cytotoxicity in all the cells tested, involving mechanisms of cell death induction (all the cell lines treated with Cis and MCF-12A cells treated with Dox) and genotoxicity (MDA-MB-231 cells treated with Dox). The carotenoid Fx, alone, had cytotoxic effects in all the 2D cultured breast cell lines, but the observed cytotoxicity seemed to be unrelated to the induction of DNA damage or cell death, suggesting the involvement of other mechanisms. However, our data obtained until now, are not enough to conclude about the mechanisms of action of Fx in these cell lines. Under the used experimental conditions, neither Fct nor Fc exhibited anticancer activity against BC cells. Interestingly, in combination, all the natural compounds (Fx, Fct and Fc) were able to enhance Dox's cytotoxicity in the triple-negative BC MDA-MB-231 cells without effects on DNA damage and cell death. Regarding that this cell line is one of the most drug-resistant, our data look promising and should be explored. It is noteworthy to mention that Fc, when administered at lower doses, might induce cell-protective effects against the chemotherapeutic action of Dox, which might not be advantageous in a clinical scenario of BC treatment.

The second and third aims of this study were to optimize a 3D culture technique for MCAs formation from the panel of tumor and non-tumor breast cells as well as to perform their morphological, ultrastructural and immunocytochemical characterization. The optimization results showed that all the cell lines tested (at specific cell densities) were able to generate MCAs in ULA microplates after 3 days with a higher proportion of proliferative cells relative to dead cells. The MCAs in culture for more than 7 days started to have a more relaxed morphology, showing some degradation of the 3D structure with an increase of dead cells when compared to 3 days of culture. Under the selected conditions, MDA-MB-231 and MCF-7 cell lines formed compact aggregates while SKBR3 and MCF-12A cell lines originated loose aggregates. Considering the complexity of the 3D models, our results reinforce the need to use multi-endpoint approaches, including, for example, the evaluation of stereomicroscope parameters, immunocytochemistry, molecular biology techniques, histological methodologies and cell-based assays to characterize and evaluate their behaviour towards the anticancer activity of cytotoxic compounds.

The fourth aim was to evaluate the cytotoxic and antiproliferative effects of the most promising compounds tested in 2D using the optimized 3D culture system. The results showed that cells cultured under 3D conditions are more resistant to the cytotoxic activity

of Dox and Fx when compared to 2D cultures since no inhibitory effects were detected by the two viability assays performed. However, both compounds decreased cell proliferation in loose MCAs [SKBR3 (Dox and Fx) and MCF-12A (only Dox)].

Regarding the last aim of this work, our data allow us to give a positive answer about the possibility of using this panel of breast cells in 3D culture to assess the anticancer effects of natural compounds. This is important, since having a panel of different breast cell lines cultured in 3D might give us a more realistic and wider insight into the selectivity of the compounds' anticancer action, potentiating the discovery of more targeted treatments for distinct types of BC.

Overall, the main conclusions of the present work were that: 1) Fx alone and Fx, Fct and Fc in combination with Dox showed anticancer activity in BC cells in 2D culture; 2) Fx showed antiproliferative activity in MCAs. However, the precise mechanisms of action in the assessed BC cells are still unclear.

As future perspectives, other cell-based assays need to be performed to get further mechanistic insights. In our view, it would be interesting to investigate the effects on cell cycle arrest, ROS production, caspases activity, mitochondrial membrane potential, expression of genes and other proteins related to cell proliferation and death among others.

Since our data showed cytotoxic activity of Fx in tumor and non-tumor cells, we consider that the anticancer potential of this carotenoid should not be disregarded, and future studies should be aimed at devising strategies to decrease its cytotoxic effects on non-tumor cells. One suggestion could be to explore the possibility of including Fx in drug delivery systems in order to have a more selective cytotoxic effect. Regarding the genotoxicity results obtained in this work, it seems to be necessary to evaluate these effects at different time points to understand the kinetics of the DNA damages induced by the tested compounds. Evaluation of other types of DNA damages (e.g. oxidative damages) should also be assessed, for instance, by the enzyme-modified alkaline comet assay. To complement our data about the cell death induction effects on 2D cultures, evaluated by the nuclear condensation assay, other techniques (e.g. annexin/propidium iodide apoptosis assay, TUNEL, caspase activity) should be incorporated. The observed morphological changes such as loss of substrate adhesion, changes in the vacuolization levels, occurrence of cellular swelling and hypertrophy or the incidence of cell membrane protrusions should be more explored in order to understand the impact and the mechanisms of these alterations.

Taking into account the observed variability and differences in MCAs compaction, 3D culturing techniques need further optimization. So, in future researches, we suggest to evaluate the impact of different types of culture medium supplementation and the use of

lower cell passage numbers (*in vitro* age), to include other BC lines representative of the several BC subtypes, as well as to use co-culture of tumor and non-tumor cells.

Regarding the absence of cytotoxic and antiproliferative effects of Dox in MCF7 and MDA-MB-231 MCAs, we suggest in future studies to evaluate higher concentrations of Dox and Fx on 3D BC models.

Hopefully, future investigations will allow the discovery of new efficient bioactive compounds or combinations with anticancer activity that may help the establishment of new strategies for BC treatment. Also, finding suitable 3D-culturing methodologies for the application in high-throughput drug screening is the next research frontier to overcome, therefore all studies performed are an added value in this regard.

# -CHAPTER VII-

References

## References


Abdoul-Azize, S., Buquet, C., Li, H., Picquenot, J.-M., & Vannier, J.-P. (2018). Integration of Ca2+ signaling regulates the breast tumor cell response to simvastatin and doxorubicin. *Oncogene, 37*(36), 4979-4993.

Abdul, Q. A., Choi, R. J., Jung, H. A., & Choi, J. S. (2016). Health benefit of fucosterol from marine algae: a review. *J Sci Food Agric, 96*(6), 1856-1866.

Abou-El-Wafa, G. S., Shaaban, M., Shaaban, K. A., El-Naggar, M. E., Maier, A., Fiebig, H. H., & Laatsch, H. (2013). Pachydictyols B and C: new diterpenes from Dictyota dichotoma Hudson. *Mar Drugs, 11*(9), 3109-3123.

Abudabbus, A., Badmus, J. A., Shalaweh, S., Bauer, R., & Hiss, D. (2017). Effects of Fucoidan and Chemotherapeutic Agent Combinations on Malignant and Non-malignant Breast Cell Lines. *Curr Pharm Biotechnol, 18*(9), 748-757.

Ades, F., Tryfonidis, K., & Zardavas, D. (2017). The past and future of breast cancer treatment-from the papyrus to individualised treatment approaches. *Ecancermedicalscience, 11*, 746.

Airanthi, M. K. W.-A., Sasaki, N., Iwasaki, S., Baba, N., Abe, M., Hosokawa, M., & Miyashita, K. (2011). Effect of Brown Seaweed Lipids on Fatty Acid Composition and Lipid Hydroperoxide Levels of Mouse Liver. *J Agric Food Chem, 59*(8), 4156-4163.

Alluri, P., & Newman, L. A. (2014). Basal-like and triple-negative breast cancers: searching for positives among many negatives. *Surg Oncol Clin N Am, 23*(3), 567-577.

Almeida, T. P., Ferreira, J., Vettorazzi, A., Azqueta, A., Rocha, E., & Ramos, A. A. (2018). Cytotoxic activity of fucoxanthin, alone and in combination with the cancer drugs imatinib and doxorubicin, in CML cell lines. *Environ Toxicol Pharmacol, 59*, 24-33.

Amable, L. (2016). Cisplatin resistance and opportunities for precision medicine. *Pharmacol Res, 106*, 27-36.

Amaral, R. L. F., Miranda, M., Marcato, P. D., & Swiech, K. (2017). Comparative Analysis of 3D Bladder Tumor Spheroids Obtained by Forced Floating and Hanging Drop Methods for Drug Screening. *Front Physiol, 8*, 605.

Amaral, J. B., Rezende-Teixeira, P., Freitas, V. M., & Machado-Santelli, G. M. (2011). MCF-7 cells as a three-dimensional model for the study of human breast cancer. *Tissue Eng Part C Methods, 17*(11), 1097-1107.

American Cancer Society. (2015). *Breast Cancer Facts & Figures 2015-2016*. Atlanta.

Anand, P., Kunnumakkara, A. B., Sundaram, C., Harikumar, K. B., Tharakan, S. T., Lai, O. S., Sung, B., & Aggarwal, B. B. (2008). Cancer is a preventable disease that requires major lifestyle changes. *Pharm Res, 25*(9), 2097-2116.

Angsutararux, P., Luanpitpong, S., & Issaragrisil, S. (2015). Chemotherapy-Induced Cardiotoxicity: Overview of the Roles of Oxidative Stress. *Oxid Med Cell Longev, 2015*, 13.

Antberg, L., Cifani, P., Levander, F., & James, P. (2015). Pathway-centric analysis of the DNA damage response to chemotherapeutic agents in two breast cell lines. *EuPA Open Proteom, 8*, 128-136.

Apostolou, P., Toloudi, M., Kourtidou, E., Mimikakou, G., Vlachou, I., Chatziioannou, M., & Papasotiriou, I. (2014). Use of the comet assay technique for quick and reliable prediction of in vitro response to chemotherapeutics in breast and colon cancer. J *Biol Res (Thessalon), 21*(1), 14-14.

Arciuch, V. G. A., Elguero, M. E., Poderoso, J. J., & Carreras, M. C. (2012). Mitochondrial regulation of cell cycle and proliferation. *Antioxid Redox Signal, 16*(10), 1150-1180.

Asai, A., Sugawara, T., Ono, H., & Nagao, A. (2004). Biotransformation of fucoxanthinol into amarouciaxanthin A in mice and HepG2 cells: formation and cytotoxicity of fucoxanthin metabolites. *Drug Metab Dispos, 32*(2), 205-211.

Ataollahi, M. R., Sharifi, J., Paknahad, M. R., & Paknahad, A. (2015). Breast cancer and associated factors: a review. *J Med Life, 8*(Spec Iss 4), 6-11.

ATCC. (2012). *Thawing, Propagating, and Cryopreserving Protocol - NCI-PBCF-HTB26 (MDA-MB-231) Breast Adenocarcinoma (ATCC®HTB-26™)*. Retrieved from https://physics.cancer.gov/docs/bioresource/breast/NCI-PBCF-HTB26_MDA-MB-231_SOP-508.pdf

ATCC. (2016a). MCF7 (ATCC® HTB-22™). Retrieved September 2, 2019, from https://www.lgcstandards-atcc.org/products/all/HTB-22.aspx?geo_country=ro#specifications

ATCC. (2016b). MCF-12A (ATCC® CRL-10782™). Retrieved September 2, 2019, from https://www.lgcstandards-atcc.org/products/all/CRL-10782.aspx?geo_country=ro#characteristics

ATCC. (2016c). MCF-12A (ATCC® CRL-10782™). Retrieved September 2, 2019, from https://www.lgcstandards-atcc.org/products/all/CRL-10782.aspx?geo_country=ro#specifications

Aydiner, A., Igci, A., & Soran, A. (2019). *Breast Cancer A Guide to Clinical Practice: A Guide to Clinical Practice*.

Ayyad, S.-E. N., Ezmirly, S. T., Basaif, S. A., Alarif, W. M., Badria, A. F., & Badria, F. A. (2011). Antioxidant, cytotoxic, antitumor, and protective DNA damage metabolites from the red sea brown alga *Sargassum* sp. *Pharmacognosy Res, 3*(3), 160-165.

Azadi, S., Aboulkheyr Es, H., Razavi Bazaz, S., Thiery, J. P., Asadnia, M., & Ebrahimi Warkiani, M. (2019). Upregulation of PD-L1 expression in breast cancer cells

through the formation of 3D multicellular cancer aggregates under different chemical and mechanical conditions. *Biochim Biophys Acta Mol Cell Res, 1866*(12), 118526.

Badve, S., Dabbs, D. J., Schnitt, S. J., Baehner, F. L., Decker, T., Eusebi, V., Fox, S. B., Ichihara, S., Jacquemier, J., Lakhani, S. R., Palacios, J., Rakha, E. A., Richardson, A. L., Schmitt, F. C., Tan, P. H., Tse, G. M., Weigelt, B., Ellis, I. O., & Reis-Filho, J. S. (2011). Basal-like and triple-negative breast cancers: a critical review with an emphasis on the implications for pathologists and oncologists. *Mod Pathol, 24*(2), 157-167.

Bahuguna, A., Khan, I., Bajpai, V. K., & Chul, S. (2017). MTT assay to evaluate the cytotoxic potential of a drug. *Bangladesh J Pharmacol, 12*, 8.

Banafa, A. M., Roshan, S., Liu, Y. Y., Chen, H. J., Chen, M. J., Yang, G. X., & He, G. Y. (2013). Fucoidan induces G1 phase arrest and apoptosis through caspases-dependent pathway and ROS induction in human breast cancer MCF-7 cells. *J Huazhong Univ Sci Technolog Med Sci, 33*(5), 717-724.

Bancroft, J. D., & Layton, C. (2019). 10 - The hematoxylins and eosin. In S. K. Suvarna, C. Layton, & J. D. Bancroft (Eds.), *Bancroft's Theory and Practice of Histological Techniques (Eighth Edition)* (pp. 126-138).

Bar-On, O., Shapira, M., & Hershko, D. D. (2007). Differential effects of doxorubicin treatment on cell cycle arrest and Skp2 expression in breast cancer cells. *Anticancer Drugs, 18*(10), 1113-1121.

Bayat Mokhtari, R., Homayouni, T. S., Baluch, N., Morgatskaya, E., Kumar, S., Das, B., & Yeger, H. (2017). Combination therapy in combating cancer. *Oncotarget, 8*(23), 38022-38043.

Benton, G., DeGray, G., Kleinman, H. K., George, J., & Arnaoutova, I. (2015). In vitro microtumors provide a physiologically predictive tool for breast cancer therapeutic screening. *PLoS One, 10*(4), e0123312.

Beppu, F., Niwano, Y., Sato, E., Kohno, M., Tsukui, T., Hosokawa, M., & Miyashita, K. (2009). In vitro and in vivo evaluation of mutagenicity of fucoxanthin (FX) and its metabolite fucoxanthinol (FXOH). *J Toxicol Sci, 34*(6), 693-698.

Beretta, G. L., & Zunino, F. (2008). Molecular mechanisms of anthracycline activity. *Top Curr Chem, 283*, 1-19.

Bertucci, F., Finetti, P., Cervera, N., Esterni, B., Hermitte, F., Viens, P., & Birnbaum, D. (2008). How basal are triple-negative breast cancers? *Int J Cancer, 123*(1), 236-240.

Blunt, J., Copp, B., Munro, M., Northcote, P., & Prinsep, M. (2004). Marine Natural Products. *Nat Prod Rep, 21*, 1-49.

Bombardieri, E., Gianni, L., Bonadonna, G., Bombardieri, E., Gianni, L., & Bonadonna, G. (2008). *Breast cancer: Nuclear medicine in diagnosis and therapeutic options*.

Bray, F., Ferlay, J., Soerjomataram, I., Siegel, R. L., Torre, L. A., & Jemal, A. (2018). Global cancer statistics 2018: GLOBOCAN estimates of incidence and mortality worldwide for 36 cancers in 185 countries. *CA Cancer J Clin, 68*(6), 394-424.

Breslin, S., & O'Driscoll, L. (2013). Three-dimensional cell culture: the missing link in drug discovery. *Drug Discov Today, 18*(5-6), 240-249.

Breslin, S., & O'Driscoll, L. (2016). The relevance of using 3D cell cultures, in addition to 2D monolayer cultures, when evaluating breast cancer drug sensitivity and resistance. *Oncotarget, 7*(29), 45745-45756.

Burger, H., Foekens, J. A., Look, M. P., Meijer-van Gelder, M. E., Klijn, J. G., Wiemer, E. A., Stoter, G., & Nooter, K. (2003). RNA expression of breast cancer resistance protein, lung resistance-related protein, multidrug resistance-associated proteins 1 and 2, and multidrug resistance gene 1 in breast cancer: correlation with chemotherapeutic response. *Clin Cancer Res, 9*(2), 827-836.

Burney, I. (2011). Cancer Chemotherapy and Biotherapy: Principles and Practice. *Sultan Qaboos Univ Med J, 11*(3), 424-425.

Caamal-Fuentes, E., Moo-Puc, R., Freile-Pelegrin, Y., & Robledo, D. (2014). Cytotoxic and antiproliferative constituents from Dictyota ciliolata, Padina sanctae-crucis and Turbinaria tricostata. *Pharm Biol, 52*(10), 1244-1248.

Caley, A., & Jones, R. (2012). The principles of cancer treatment by chemotherapy. *Surgery (Oxford), 30*, 186-190.

Cardoso, F. (2017). *100 perguntas Chave no Cancro da Mama - 2nd Edition*.

Carey, L. A., Perou, C. M., Livasy, C. A., Dressler, L. G., Cowan, D., Conway, K., Karaca, G., Troester, M. A., Tse, C. K., Edmiston, S., Deming, S. L., Geradts, J., Cheang, M. C., Nielsen, T. O., Moorman, P. G., Earp, H. S., & Millikan, R. C. (2006). Race, breast cancer subtypes, and survival in the Carolina Breast Cancer Study. *Jama, 295*(21), 2492-2502.

Carvalho, M. R., Lima, D., Reis, R. L., Oliveira, J. M., & Correlo, V. M. (2017). Anti-Cancer Drug Validation: the Contribution of Tissue Engineered Models. *Stem Cell Rev Rep, 13*(3), 347-363.

Chakraborty, S., & Rahman, T. (2012). The difficulties in cancer treatment. *Ecancermedicalscience, 6*, ed16.

Chen, S. H., & Chang, J. Y. (2019). New Insights into Mechanisms of Cisplatin Resistance: From Tumor Cell to Microenvironment. *Int J Mol Sci, 20*(17).

Collins, A. R. (2004). The comet assay for DNA damage and repair: principles, applications, and limitations. *Mol Biotechnol, 26*(3), 249-261.

Colombo, P.-E., Milanezi, F., Weigelt, B., & Reis-Filho, J. S. (2011). Microarrays in the 2010s: the contribution of microarray-based gene expression profiling to breast cancer classification, prognostication and prediction. *Breast Cancer Res, 13*(3), 212.

Colone, M., & Kaliappan, S. (2016). Redox-active Microcapsules as Drug Delivery System in Breast Cancer Cells and Spheroids. *J Mol Genet Med, 10*.

Cortes-Funes, H., & Coronado, C. (2007). Role of anthracyclines in the era of targeted therapy. *Cardiovasc Toxicol, 7*(2), 56-60.

Costa, E. C., de Melo-Diogo, D., Moreira, A. F., Carvalho, M. P., & Correia, I. J. (2018). Spheroids Formation on Non-Adhesive Surfaces by Liquid Overlay Technique: Considerations and Practical Approaches. *Biotechnol J, 13*(1).

Costa, E. C., Moreira, A. F., de Melo-Diogo, D., Gaspar, V. M., Carvalho, M. P., & Correia, I. J. (2016). 3D tumor spheroids: an overview on the tools and techniques used for their analysis. *Biotechnol Adv, 34*(8), 1427-1441.

Cox, J., & Weinman, S. (2016). Mechanisms of doxorubicin resistance in hepatocellular carcinoma. *Hepatic oncology, 3*(1), 57-59.

Cumashi, A., Ushakova, N. A., Preobrazhenskaya, M. E., D'Incecco, A., Piccoli, A., Totani, L., Tinari, N., Morozevich, G. E., Berman, A. E., Bilan, M. I., Usov, A. I., Ustyuzhanina, N. E., Grachev, A. A., Sanderson, C. J., Kelly, M., Rabinovich, G. A., Iacobelli, S., Nifantiev, N. E., & Consorzio Interuniversitario Nazionale per la Bio-Oncologia, I. (2007). A comparative study of the anti-inflammatory, anticoagulant, antiangiogenic, and antiadhesive activities of nine different fucoidans from brown seaweeds. *Glycobiology, 17*(5), 541-552.

D'Anselmi, F., Masiello, M. G., Cucina, A., Proietti, S., Dinicola, S., Pasqualato, A., Ricci, G., Dobrowolny, G., Catizone, A., Palombo, A., & Bizzarri, M. (2013). Microenvironment promotes tumor cell reprogramming in human breast cancer cell lines. *PLoS One, 8*(12), e83770.

Dai, X., Li, T., Bai, Z., Yang, Y., Liu, X., Zhan, J., & Shi, B. (2015). Breast cancer intrinsic subtype classification, clinical use and future trends. *Am J Cancer Res, 5*(10), 2929-2943.

Dalmaso, Z. G., Ferreira, D., & Vermelho, B. A. (2015). Marine Extremophiles: A Source of Hydrolases for Biotechnological Applications. *Mar Drugs, 13*(4).

De la Mare, J.-A., Sterrenberg, J. N., Sukhthankar, M. G., Chiwakata, M. T., Beukes, D. R., Blatch, G. L., & Edkins, A. L. (2013). Assessment of potential anti-cancer stem cell activity of marine algal compounds using an in vitro mammosphere assay. *Cancer Cell Int, 13*(1), 39-39.

Denis, E., Papurina, T., Koliada, A. K., & Vaiserman, A. M. (2019). *Evaluation of the Stimulating and Protective Effects of Fucoxanthin Against Human Skin Fibroblasts : An In Vitro Study*. *Clin Dermatol (Wilmington)*, 2019; 2(1),124.

DeSantis, C. E., Bray, F., Ferlay, J., Lortet-Tieulent, J., Anderson, B. O., & Jemal, A. (2015). International Variation in Female Breast Cancer Incidence and Mortality Rates. *Cancer Epidemiol Biomarkers Prev, 24*(10), 1495-1506.

Dubois, C., Daumar, P., Aubel, C., Gauthier, J., Vidalinc, B., Mounetou, E., Penault-Llorca, F., & Bamdad, M. (2019). The New Synthetic Serum-Free Medium OptiPASS Promotes High Proliferation and Drug Efficacy Prediction on Spheroids from MDA-MB-231 and SUM1315 Triple-Negative Breast Cancer Cell Lines. *J Clin Med, 8*(3), 397.

Dubois, C., Dufour, R., Daumar, P., Aubel, C., Szczepaniak, C., Blavignac, C., Mounetou, E., Penault-Llorca, F., & Bamdad, M. (2017). Development and cytotoxic response of two proliferative MDA-MB-231 and non-proliferative SUM1315 three-dimensional cell culture models of triple-negative basal-like breast cancer cell lines. *Oncotarget, 8*(56), 95316-95331.

Dyshlovoy, A. S., & Honecker, F. (2018). Marine Compounds and Cancer: 2017 Updates. *Mar Drugs, 16*(2).

Eastman, A. (2006). The Mechanism of Action of Cisplatin: From Adducts to Apoptosis. In Cisplatin, B. Lippert (Ed.).

Edmondson, R., Broglie, J. J., Adcock, A. F., & Yang, L. (2014). Three-dimensional cell culture systems and their applications in drug discovery and cell-based biosensors. *Assay Drug Dev Technol, 12*(4), 207-218.

Fang, Y., & Eglen, R. M. (2017). Three-Dimensional Cell Cultures in Drug Discovery and Development. *SLAS Discov, 22*(5), 456-472.

Ferreira, J., Ramos, A. A., Almeida, T., Azqueta, A., & Rocha, E. (2018). Drug resistance in glioblastoma and cytotoxicity of seaweed compounds, alone and in combination with anticancer drugs: A mini review. *Phytomedicine, 48*, 84-93.

Florea, A.-M., & Büsselberg, D. (2013). Breast cancer and possible mechanisms of therapy resistance. *Journal of Local and Global Health Science*(2013).

Forjaz de Lacerda, G., Kelly, S. P., Bastos, J., Castro, C., Mayer, A., Mariotto, A. B., & Anderson, W. F. (2018). Breast cancer in Portugal: Temporal trends and age-specific incidence by geographic regions. *Cancer Epidemiol, 54*, 12-18.

Friedrich, J., Seidel, C., Ebner, R., & Kunz-Schughart, L. A. (2009). Spheroid-based drug screen: considerations and practical approach. *Nat Protoc, 4*(3), 309-324.

Froehlich, K., Haeger, J. D., Heger, J., Pastuschek, J., Photini, S. M., Yan, Y., Lupp, A., Pfarrer, C., Mrowka, R., Schleussner, E., Markert, U. R., & Schmidt, A. (2016).

Generation of Multicellular Breast Cancer Tumor Spheroids: Comparison of Different Protocols. *J Mammary Gland Biol Neoplasia, 21*(3-4), 89-98.

Garrido-Castro, A. C., Lin, N. U., & Polyak, K. (2019). Insights into Molecular Classifications of Triple-Negative Breast Cancer: Improving Patient Selection for Treatment. *Cancer Discov, 9*(2), 176-198.

Gauthier, D. T., Cartwright, D. D., Densmore, C. L., Blazer, V. S., & Ottinger, C. A. (2003). Measurement of in vitro leucocyte mitogenesis in fish: ELISA based detection of the thymidine analogue 5′-bromo-2′-deoxyuridine. *Fish Shellfish Immunol, 14*(4), 279-288.

Gencoglu, M. F., Barney, L. E., Hall, C. L., Brooks, E. A., Schwartz, A. D., Corbett, D. C., Stevens, K. R., & Peyton, S. R. (2018). Comparative Study of Multicellular Tumor Spheroid Formation Methods and Implications for Drug Screening. *ACS Biomater Sci Eng, 4*(2), 410-420.

Gianni, L., Ravaioli, A., & Arcangeli, V. (2011). Adjuvant Chemoendocrine Therapy. In M. Schwab (Ed.), *Encyclopedia of Cancer* (pp. 75-78). Berlin, Heidelberg: Springer Berlin Heidelberg.

GLOBOCAN 2018. (2018a). Cancer Today – IARC: Estimated age-standardized incidence rates (World) in 2018, breast, females, all ages. Retrieved January 19, 2019, from http://gco.iarc.fr/today/online-analysis-map?v=2018&mode=population&mode_population=continents&population=900&populations=900&key=asr&sex=2&cancer=20&type=0&statistic=5&prevalence=0&population_group=0&ages_group%5B%5D=0&ages_group%5B%5D=17&nb_items=5&group_cancer=1&include_nmsc=1&include_nmsc_other=1&projection=natural-earth&color_palette=default&map_scale=quantile&map_nb_colors=5&continent=0&rotate=%255B10%252C0%255D

GLOBOCAN 2018. (2018b). Cancer Today – Global Cancer Observatory: Estimated number of new cases in 2018, worldwide, all cancers, both sexes all ages. Retrieved January 19, 2019, from http://gco.iarc.fr/today/online-analysis-pie?v=2018&mode=cancer&mode_population=continents&population=900&populations=900&key=total&sex=0&cancer=39&type=0&statistic=5&prevalence=0&population_group=0&ages_group%5B%5D=0&ages_group%5B%5D=17&nb_items=7&group_cancer=1&include_nmsc=1&include_nmsc_other=1&half_pie=0&donut=0&population_group_globocan_id=

GLOBOCAN 2018. (2018c). Cancer Today – Global Cancer Observatory: Estimated number of deaths in 2018, worldwide, all cancers, both sexes all ages. Retrieved January 19, 2019, from http://gco.iarc.fr/today/online-analysis-

pie?v=2018&mode=cancer&mode_population=continents&population=900&populations=900&key=total&sex=0&cancer=39&type=1&statistic=5&prevalence=0&population_group=0&ages_group%5B%5D=0&ages_group%5B%5D=17&nb_items=7&group_cancer=1&include_nmsc=1&include_nmsc_other=1&half_pie=0&donut=0&population_group_globocan_id=

Gruber, B. M., Anuszewska, E. L., Bubko, I., Gozdzik, A., Fokt, I., & Priebe, W. (2007). Effect of structural modification at the 4, 3', and 2' positions of doxorubicin on topoisomerase II poisoning, apoptosis, and cytotoxicity in human melanoma cells. *Arch Immunol Ther Exp (Warsz), 55*(3), 193-198.

Guedes, A. C., Amaro, H. M., Sousa-Pinto, I., & Malcata, F. X. (2019). Chapter 16 - Algal spent biomass—A pool of applications. In A. Pandey, J.-S. Chang, C. R. Soccol, D.-J. Lee, & Y. Chisti (Eds.), *Biofuels from Algae (Second Edition)* (pp. 397-433): Elsevier.

Gupta, S., & Abu-Ghannam, N. (2011). Bioactive potential and possible health effects of edible brown seaweeds. *Trends Food Sci Technol, 22*(6), 315-326.

Hall, M. D., Telma, K. A., Chang, K. E., Lee, T. D., Madigan, J. P., Lloyd, J. R., Goldlust, I. S., Hoeschele, J. D., & Gottesman, M. M. (2014). Say no to DMSO: dimethylsulfoxide inactivates cisplatin, carboplatin, and other platinum complexes. *Cancer Res, 74*(14), 3913-3922.

Ham, S. L., Joshi, R., Luker, G. D., & Tavana, H. (2016). Engineered Breast Cancer Cell Spheroids Reproduce Biologic Properties of Solid Tumors. *Adv Healthc Mater, 5*(21), 2788-2798.

Han, Y. S., Lee, J. H., & Lee, S. H. (2015). Antitumor Effects of Fucoidan on Human Colon Cancer Cells via Activation of Akt Signaling. *Biomol Ther (Seoul), 23*(3), 225-232.

Haroun, F., Lindenmeyer, F., Lu, H., Soria, C., Jozefonvicz, J., & Boisson-vidal, C. (2002). In Vitro effects of fucans on MDA-MB231 tumor cell adhesion and invasion. *Anticancer Res, 22*, 2285-2292.

Harvey, A. L. (2008). Natural products in drug discovery. *Drug Discov Today, 13*(19-20), 894-901.

Hashimoto, T., Ozaki, Y., Taminato, M., Das, S. K., Mizuno, M., Yoshimura, K., Maoka, T., & Kanazawa, K. (2009). The distribution and accumulation of fucoxanthin and its metabolites after oral administration in mice. *Br J Nutr, 102*(2), 242-248.

Heo, S. J., & Jeon, Y. J. (2009). Protective effect of fucoxanthin isolated from Sargassum siliquastrum on UV-B induced cell damage. *J Photochem Photobiol B, 95*(2), 101-107.

Ho-Yen, C., Bowen, R. L., & Jones, J. L. (2012). Characterization of basal-like breast cancer: an update. *Diagn Histopathol, 18*(3), 104-111.

Ho, W. Y., Yeap, S. K., Ho, C. L., Rahim, R. A., & Alitheen, N. B. (2012). Development of multicellular tumor spheroid (MCTS) culture from breast cancer cell and a high throughput screening method using the MTT assay. *PLoS One, 7*(9), e44640.

Holiday, C., Singh, R., Johnson, E., Grizzle, W., & Lillard, J. (2011). CCR9-CCL25 interactions promote cisplatin resistance in breast cancer cell through Akt activation in a PI3K-dependent and FAK-independent fashion. *World J Surg Oncol, 9*, 46.

Holliday, D. L., & Speirs, V. (2011). Choosing the right cell line for breast cancer research. *Breast Cancer Res, 13*(4), 215.

Hon, J. D. C., Singh, B., Sahin, A., Du, G., Wang, J., Wang, V. Y., Deng, F.-M., Zhang, D. Y., Monaco, M. E., & Lee, P. (2016). Breast cancer molecular subtypes: from TNBC to QNBC. *Am J Cancer Res, 6*(9), 1864-1872.

Hosokawa, M., Kudo, M., Maeda, H., Kohno, H., Tanaka, T., & Miyashita, K. (2004). Fucoxanthin induces apoptosis and enhances the antiproliferative effect of the PPARgamma ligand, troglitazone, on colon cancer cells. *Biochim Biophys Acta, 1675*(1-3), 113-119.

Howes, A. L., Richardson, R. D., Finlay, D., & Vuori, K. (2014). 3-Dimensional Culture Systems for Anti-Cancer Compound Profiling and High-Throughput Screening Reveal Increases in EGFR Inhibitor-Mediated Cytotoxicity Compared to Monolayer Culture Systems. *PLoS One, 9*(9), e108283.

Hsu, H. Y., & Hwang, P. A. (2019). Clinical applications of fucoidan in translational medicine for adjuvant cancer therapy. *Clin Transl Med, 8*(1), 15.

Hsu, H. Y., Lin, T. Y., Hwang, P. A., Tseng, L. M., Chen, R. H., Tsao, S. M., & Hsu, J. (2013). Fucoidan induces changes in the epithelial to mesenchymal transition and decreases metastasis by enhancing ubiquitin-dependent TGFbeta receptor degradation in breast cancer. *Carcinogenesis, 34*(4), 874-884.

Hu, G.-P., Yuan, J., Sun, L., She, Z.-G., Wu, J.-H., Lan, X.-J., Zhu, X., Lin, Y.-C., & Chen, S.-P. (2011). Statistical Research on Marine Natural Products Based on Data Obtained between 1985 and 2008. *Mar Drugs, 9*(4).

Ibrahim, T., Liverani, C., Mercatali, L., Sacanna, E., Zanoni, M., Fabbri, F., Zoli, W., & Amadori, D. (2013). Cisplatin in combination with zoledronic acid: a synergistic effect in triple-negative breast cancer cell lines. *Int J Oncol, 42*(4), 1263-1270.

Ignatiadis, M., & Sotiriou, C. (2013). Luminal breast cancer: from biology to treatment. *Nat Rev Clin Oncol, 10*(9), 494-506.

Imamura, Y., Mukohara, T., Shimono, Y., Funakoshi, Y., Chayahara, N., Toyoda, M., Kiyota, N., Takao, S., Kono, S., Nakatsura, T., & Minami, H. (2015). Comparison of 2D- and 3D-culture models as drug-testing platforms in breast cancer. *Oncol Rep, 33*(4), 1837-1843.

Ishikawa, C., Tafuku, S., Kadekaru, T., Sawada, S., Tomita, M., Okudaira, T., Nakazato, T., Toda, T., Uchihara, J.-N., Taira, N., Ohshiro, K., Yasumoto, T., Ohta, T., & Mori, N. (2008). Antiadult T-cell leukemia effects of brown algae fucoxanthin and its deacetylated product, fucoxanthinol. *Int J Cancer, 123*(11), 2702-2712.

Ivanov, D. P., & Grabowska, A. M. (2018). In Vitro Tissue Microarrays for Quick and Efficient Spheroid Characterization. *SLAS Discov, 23*(2), 211-217.

Ivascu, A., & Kubbies, M. (2007). Diversity of cell-mediated adhesions in breast cancer spheroids. *Int J Oncol, 31*(6), 1403-1413.

Jiang, H., Li, J., Chen, A., Li, Y., Xia, M., Guo, P., Yao, S., & Chen, S. (2018). Fucosterol exhibits selective antitumor anticancer activity against HeLa human cervical cell line by inducing mitochondrial mediated apoptosis, cell cycle migration inhibition and downregulation of m-TOR/PI3K/Akt signalling pathway. *Oncol Lett, 15*(3), 3458-3463.

Joseph, J. S., Malindisa, S. T., & Ntwasa, M. (2018). *Two-Dimensional (2D) and Three-Dimensional (3D) Cell Culturing in Drug Discovery*.

Kaja, S., Payne, A. J., Naumchuk, Y., & Koulen, P. (2017). Quantification of Lactate Dehydrogenase for Cell Viability Testing Using Cell Lines and Primary Cultured Astrocytes. *Curr Protoc Toxicol, 72*, 2 26 21-22 26 10.

Kapalczynska, M., Kolenda, T., Przybyla, W., Zajaczkowska, M., Teresiak, A., Filas, V., Ibbs, M., Blizniak, R., Luczewski, L., & Lamperska, K. (2018). 2D and 3D cell cultures - a comparison of different types of cancer cell cultures. *Arch Med Sci, 14*(4), 910-919.

Kelland, L. (2007). The resurgence of platinum-based cancer chemotherapy. *Nat Rev Cancer, 7*(8), 573-584.

Kenny, P. A., Lee, G. Y., Myers, C. A., Neve, R. M., Semeiks, J. R., Spellman, P. T., Lorenz, K., Lee, E. H., Barcellos-Hoff, M. H., Petersen, O. W., Gray, J. W., & Bissell, M. J. (2007). The morphologies of breast cancer cell lines in three-dimensional assays correlate with their profiles of gene expression. *Mol Oncol, 1*(1), 84-96.

Khalid, S., Abbas, M., Saeed, F., Bader Ul Ain, H., & Suleria, H. A. R. (2018). Therapeutic Potential of Seaweed Bioactive Compounds.

Khalifa, S. A. M., Elias, N., Farag, M. A., Chen, L., Saeed, A., Hegazy, M. F., Moustafa, M. S., Abd El-Wahed, A., Al-Mousawi, S. M., Musharraf, S. G., Chang, F. R., Iwasaki, A., Suenaga, K., Alajlani, M., Goransson, U., & El-Seedi, H. R. (2019). Marine Natural Products: A Source of Novel Anticancer Drugs. *Mar Drugs, 17*(9).

Khanavi, M., Gheidarloo, R., Sadati, N., Ardekani, M. R., Nabavi, S. M., Tavajohi, S., & Ostad, S. N. (2012). Cytotoxicity of fucosterol containing fraction of marine algae against breast and colon carcinoma cell line. *Pharmacogn Mag, 8*(29), 60-64.

Khanavi, M., Nabavi, M., Sadati, N., Shams Ardekani, M., Sohrabipour, J., Nabavi, S. M., Ghaeli, P., & Ostad, S. N. (2010). Cytotoxic activity of some marine brown algae against cancer cell lines. *Biol Res, 43*(1), 31-37.

Kim, H.-S., Lee, Y.-S., & Kim, D.-K. (2009). Doxorubicin Exerts Cytotoxic Effects through Cell Cycle Arrest and Fas-Mediated Cell Death. *Pharmacology, 84*, 300-309.

Kim, J. B., Stein, R., & O'Hare, M. J. (2004). Three-dimensional in vitro tissue culture models of breast cancer-- a review. *Breast Cancer Res Treat, 85*(3), 281-291.

Kim, K. N., Heo, S. J., Kang, S. M., Ahn, G., & Jeon, Y. J. (2010). Fucoxanthin induces apoptosis in human leukemia HL-60 cells through a ROS-mediated Bcl-xL pathway. *Toxicol In Vitro, 24*(6), 1648-1654.

Kim, S.-K. (2012). Marine pharmacognosy : trends and applications. CRC Press Inc.

Kim, S. K., & Ta, Q. V. (2011). Potential beneficial effects of marine algal sterols on human health. *Adv Food Nutr Res, 64*, 191-198.

Kim, S. W., Roh, J., & Park, C. S. (2016). Immunohistochemistry for Pathologists: Protocols, Pitfalls, and Tips. *J Pathol Transl Med, 50*(6), 411-418.

Koduvayur Habeebullah, S. F., Surendraraj, A., & Jacobsen, C. (2018). Isolation of Fucoxanthin from Brown Algae and Its Antioxidant Activity: In Vitro and 5% Fish Oil-In-Water Emulsion. *J A O C S, 95*(7), 835-843.

Kohno, T., Ninomiya, T., Kikuchi, S., Konno, T., & Kojima, T. (2015). Staurosporine induces formation of two types of extra-long cell protrusions: actin-based filaments and microtubule-based shafts. *Mol Pharmacol, 87*(5), 815-824.

Kondo, N., Takahashi, A., Ono, K., & Ohnishi, T. (2010). DNA damage induced by alkylating agents and repair pathways. *J Nucleic Acids, 2010*, 543531.

Konishi, I., Hosokawa, M., Sashima, T., Kobayashi, H., & Miyashita, K. (2006). Halocynthiaxanthin and fucoxanthinol isolated from Halocynthia roretzi induce apoptosis in human leukemia, breast and colon cancer cells. *Comp Biochem Physiol C Toxicol Pharmacol, 142*(1-2), 53-59.

Koparde, A., Doijad, R., & Magdum, C. (2019). Natural Products in Drug Discovery. *Intech Open.*

Kotake-Nara, E., Sugawara, T., & Nagao, A. (2005). Antiproliferative effect of neoxanthin and fucoxanthin on cultured cells. *Fish. Sci., 71*, 459-461.

Kroemer, G., Galluzzi, L., Vandenabeele, P., Abrams, J., Alnemri, E. S., Baehrecke, E. H., Blagosklonny, M. V., El-Deiry, W. S., Golstein, P., Green, D. R., Hengartner, M., Knight, R. A., Kumar, S., Lipton, S. A., Malorni, W., Nunez, G., Peter, M. E., Tschopp, J., Yuan, J., Piacentini, M., Zhivotovsky, B., & Melino, G. (2009). Classification of cell death: recommendations of the Nomenclature Committee on Cell Death 2009. *Cell Death Differ, 16*(1), 3-11.

Kumar, S. R., Hosokawa, M., & Miyashita, K. (2013). Fucoxanthin: a marine carotenoid exerting anti-cancer effects by affecting multiple mechanisms. *Mar Drugs, 11*(12), 5130-5147.

Kurian, A. W., Fish, K., Shema, S. J., & Clarke, C. A. (2010). Lifetime risks of specific breast cancer subtypes among women in four racial/ethnic groups. *Breast Cancer Res, 12*(6), R99.

Langhans, S. A. (2018). Three-Dimensional in Vitro Cell Culture Models in Drug Discovery and Drug Repositioning. *Front Pharmacol, 9*, 6.

Lanz, H. L., Saleh, A., Kramer, B., Cairns, J., Ng, C. P., Yu, J., Trietsch, S. J., Hankemeier, T., Joore, J., Vulto, P., Weinshilboum, R., & Wang, L. (2017). Therapy response testing of breast cancer in a 3D high-throughput perfused microfluidic platform. *BMC cancer, 17*(1), 709.

Lee, H., Kim, J. S., & Kim, E. (2012). Fucoidan from seaweed Fucus vesiculosus inhibits migration and invasion of human lung cancer cell via PI3K-Akt-mTOR pathways. *PLoS One, 7*(11), e50624.

Li, B., Lu, F., Wei, X., & Zhao, R. (2008). Fucoidan: structure and bioactivity. *Molecules, 13*(8), 1671-1695.

Li, X. J., Zha, Q. B., Ren, Z. J., Tang, J. H., & Yao, Y. F. (2015). Mechanisms of breast cancer resistance to anthracyclines or taxanes: an overview of the proposed roles of noncoding RNA. *Curr Opin Oncol, 27*(6), 457-465.

Lim, S. W., Loh, H. S., Ting, K. N., Bradshaw, T. D., & Allaudin, Z. N. (2015). Reduction of MTT to Purple Formazan by Vitamin E Isomers in the Absence of Cells. *Trop Life Sci Res, 26*(1), 111-120.

Lin, R., & Tripuraneni, P. (2011). Radiation therapy in early-stage invasive breast cancer. *Indian J Surg Oncol, 2*(2), 101-111.

Liu, C. L., Chiu, Y. T., & Hu, M. L. (2011). Fucoxanthin enhances HO-1 and NQO1 expression in murine hepatic BNL CL.2 cells through activation of the Nrf2/ARE system partially by its pro-oxidant activity. *J Agric Food Chem, 59*(20), 11344-11351.

Liu, C. L., Huang, Y. S., Hosokawa, M., Miyashita, K., & Hu, M. L. (2009). Inhibition of proliferation of a hepatoma cell line by fucoxanthin in relation to cell cycle arrest and enhanced gap junctional intercellular communication. *Chem Biol Interact, 182*(2-3), 165-172.

Lopes-Costa, E., Abreu, M., Gargiulo, D., Rocha, E., & Ramos, A. A. (2017). Anticancer effects of seaweed compounds fucoxanthin and phloroglucinol, alone and in combination with 5-fluorouracil in colon cells. *J Toxicol Environ Health, Part A, 80*(13-15), 776-787.

Lopes, G. (2013). Sterols in Algae and Health. In Bioactive Compounds from Marine Foods (eds B. Hernández-Ledesma and M. Herrero).

Lovitt, C. J., Shelper, T. B., & Avery, V. M. (2018). Doxorubicin resistance in breast cancer cells is mediated by extracellular matrix proteins. *BMC cancer, 18*(1), 41.

Lu, J., Shi, K. K., Chen, S., Wang, J., Hassouna, A., White, L. N., Merien, F., Xie, M., Kong, Q., Li, J., Ying, T., White, W. L., & Nie, S. (2018). Fucoidan Extracted from the New Zealand Undaria pinnatifida-Physicochemical Comparison against Five Other Fucoidans: Unique Low Molecular Weight Fraction Bioactivity in Breast Cancer Cell Lines. *Mar Drugs, 16*(12).

Lüpertz, R., Wätjen, W., Kahl, R., & Chovolou, Y. (2010). Dose- and time-dependent effects of doxorubicin on cytotoxicity, cell cycle and apoptotic cell death in human colon cancer cells. *Toxicology, 271*(3), 115-121.

Mailleux, A. A., Overholtzer, M., & Brugge, J. S. (2008). Lumen formation during mammary epithelial morphogenesis: insights from in vitro and in vivo models. *Cell Cycle, 7*(1), 57-62.

Malhão, F., Ramos, A. A., Buttachon, S., Dethoup, T., Kijjoa, A., & Rocha, E. (2019). Cytotoxic and Antiproliferative Effects of Preussin, a Hydroxypyrrolidine Derivative from the Marine Sponge-Associated Fungus Aspergillus candidus KUFA 0062, in a Panel of Breast Cancer Cell Lines and Using 2D and 3D Cultures. *Mar Drugs, 17*(8), 448.

Martin, L. J. (2015). Fucoxanthin and Its Metabolite Fucoxanthinol in Cancer Prevention and Treatment. *Mar Drugs, 13*(8), 4784-4798.

Masood, S. (2016). Neoadjuvant chemotherapy in breast cancers. *Womens Health (Lond), 12*(5), 480-491.

McArthur, H. L., & Hudis, C. A. (2007). Breast cancer chemotherapy. *Cancer J, 13*(3), 141-147.

McMillan, K. S., McCluskey, A. G., Sorensen, A., Boyd, M., & Zagnoni, M. (2016). Emulsion technologies for multicellular tumour spheroid radiation assays. *Analyst, 141*(1), 100-110.

Mebrahtu, L., Magoha, P., Asgedom, G., & Kasimala, M. (2015). A Review on biochemical composition and nutritional aspects of Seaweeds. *Carib.j.SciTech*, 3, 789-797.

Mehta, G., Hsiao, A. Y., Ingram, M., Luker, G. D., & Takayama, S. (2012). Opportunities and challenges for use of tumor spheroids as models to test drug delivery and efficacy. *J Control Release, 164*(2), 192-204.

Mei, C., Zhou, S., Zhu, L., Ming, J., Zeng, F., & Xu, R. (2017). Antitumor Effects of Laminaria Extract Fucoxanthin on Lung Cancer. *Mar Drugs, 15*(2).

Melissaridou, S., Wiechec, E., Magan, M., Jain, M. V., Chung, M. K., Farnebo, L., & Roberg, K. (2019). The effect of 2D and 3D cell cultures on treatment response, EMT profile and stem cell features in head and neck cancer. *Cancer Cell Int, 19*, 16-16.

Metzger, W., Sossong, D., Bachle, A., Putz, N., Wennemuth, G., Pohlemann, T., & Oberringer, M. (2011). The liquid overlay technique is the key to formation of co-culture spheroids consisting of primary osteoblasts, fibroblasts and endothelial cells. *Cytotherapy, 13*(8), 1000-1012.

Mikami, K., & Hosokawa, M. (2013). Biosynthetic pathway and health benefits of fucoxanthin, an algae-specific xanthophyll in brown seaweeds. *Int J Mol Sci, 14*(7), 13763-13781.

Minotti, G., Menna, P., Salvatorelli, E., Cairo, G., & Gianni, L. (2004). Anthracyclines: molecular advances and pharmacologic developments in antitumor activity and cardiotoxicity. *Pharmacol Rev, 56*(2), 185-229.

Miranda-Delgado, A., Montoya, M., Paz, M., Mellado, M., Villena, J., Arancibia, P., Madrid, A., & Jara, C. (2018). Antioxidant and anti-cancer activities of brown and red seaweed extracts from Chilean coasts. *Lat Am J Aquat Res, 46*.

Mitchell, M. I., & Engelbrecht, A.-M. (2015). Circadian Rhythms and Breast Cancer: The Role of Per2 in Doxorubicin-Induced Cell Death. *J Toxicol, 2015*, 392360-392360.

Mittler, F., Obeïd, P., Rulina, A. V., Haguet, V., Gidrol, X., & Balakirev, M. Y. (2017). High-Content Monitoring of Drug Effects in a 3D Spheroid Model. *Front Oncol, 7*(293).

Moghadamtousi, S. Z., Karimian, H., Khanabdali, R., Razavi, M., Firoozinia, M., Zandi, K., & Abdul Kadir, H. (2014). Anticancer and antitumor potential of fucoidan and fucoxanthin, two main metabolites isolated from brown algae. *ScientificWorldJournal, 2014*, 768323.

Moghaddam, N. S. A., Oskouie, M. N., Butler, A. E., Petit, P. X., Barreto, G. E., & Sahebkar, A. (2019). Hormetic effects of curcumin: What is the evidence? *J Cell Physiol, 234*(7), 10060-10071.

Nagai, H., & Kim, Y. H. (2017). Cancer prevention from the perspective of global cancer burden patterns. *J Thorac Dis, 9*(3), 448-451.

Nagelkerke, A., Bussink, J., Sweep, F. C., & Span, P. N. (2013). Generation of multicellular tumor spheroids of breast cancer cells: how to go three-dimensional. *Anal Biochem, 437*(1), 17-19.

Newman, D. J., & Cragg, G. M. (2016). Natural Products as Sources of New Drugs from 1981 to 2014. *J Nat Prod, 79*(3), 629-661.

Nguyen, H. T.-L., Nguyen, S. T., & Van Pham, P. (2016). Concise Review: 3D cell culture systems for anticancer drug screening. *Biomedical Research and Therapy, 3*(5).

Nigjeh, S. E., Yeap, S. K., Nordin, N., Kamalideghan, B., Ky, H., & Rosli, R. (2018). Citral induced apoptosis in MDA-MB-231 spheroid cells. *BMC complementary and alternative medicine, 18*(1), 56-56.

Niknafs, B. (2011). Induction of apoptosis and non-apoptosis in human breast cancer cell line (MCF-7) by cisplatin and caffeine. *Iranian biomedical journal, 15*(4), 130-133.

Nounou, M. I., ElAmrawy, F., Ahmed, N., Abdelraouf, K., Goda, S., & Syed-Sha-Qhattal, H. (2015). Breast Cancer: Conventional Diagnosis and Treatment Modalities and Recent Patents and Technologies. *Breast Cancer (Auckl), 9*(Suppl 2), 17-34.

Nunes, A. S., Barros, A. S., Costa, E. C., Moreira, A. F., & Correia, I. J. (2019a). 3D tumor spheroids as in vitro models to mimic in vivo human solid tumors resistance to therapeutic drugs. *Biotechnology and Bioengineering, 116*(1), 206-226.

Nunes, A. S., Costa, E. C., Barros, A. S., de Melo-Diogo, D., & Correia, I. J. (2019b). Establishment of 2D Cell Cultures Derived From 3D MCF-7 Spheroids Displaying a Doxorubicin Resistant Profile. *Biotechnol J, 14*(4), e1800268.

Oronsky, B. T., Reid, T., Knox, S. J., & Scicinski, J. J. (2012). The scarlet letter of alkylation: a mini review of selective alkylating agents. *Transl Oncol, 5*(4), 226-229.

Pacheco, B. S., dos Santos, M. A. Z., Schultze, E., Martins, R. M., Lund, R. G., Seixas, F. K., Colepicolo, P., Collares, T., Paula, F. R., & De Pereira, C. M. P. (2018). Cytotoxic Activity of Fatty Acids From Antarctic Macroalgae on the Growth of Human Breast Cancer Cells. *Frontiers in Bioengineering and Biotechnology, 6*(185).

Pádua, D., Rocha, E., Gargiulo, D., & Ramos, A. A. (2015). Bioactive compounds from brown seaweeds: Phloroglucinol, fucoxanthin and fucoidan as promising therapeutic agents against breast cancer. *Phytochemistry Letters, 14*, 91-98.

Park, H. Y., Kim, G. Y., Moon, S. K., Kim, W. J., Yoo, Y. H., & Choi, Y. H. (2014). Fucoidan inhibits the proliferation of human urinary bladder cancer T24 cells by blocking cell cycle progression and inducing apoptosis. *Molecules, 19*(5), 5981-5998.

Peng, J., Yuan, J. P., Wu, C. F., & Wang, J. H. (2011). Fucoxanthin, a marine carotenoid present in brown seaweeds and diatoms: metabolism and bioactivities relevant to human health. *Mar Drugs, 9*(10), 1806-1828.

Pereira, P. M. R., Berisha, N., Bhupathiraju, N., Fernandes, R., Tome, J. P. C., & Drain, C. M. (2017). Cancer cell spheroids are a better screen for the photodynamic efficiency of glycosylated photosensitizers. *PLoS One, 12*(5), e0177737.

Petrovic, M., & Todorović, D. V. (2016). Biochemical and molecular mechanisms of action of cisplatin in cancer cells. *Medicine and Biology*, 18(1), 12-18.

Piccinini, F. (2015). AnaSP: a software suite for automatic image analysis of multicellular spheroids. *Comput Methods Programs Biomed, 119*(1), 43-52.

Pilco-Ferreto, N., & Calaf, G. M. (2016). Influence of doxorubicin on apoptosis and oxidative stress in breast cancer cell lines. *Int J Oncol, 49*(2), 753-762.

Prabhakaran, P., Hassiotou, F., Blancafort, P., & Filgueira, L. (2013). Cisplatin induces differentiation of breast cancer cells. *Front Oncol, 3*, 134.

Prat, A., Pineda, E., Adamo, B., Galvan, P., Fernandez, A., Gaba, L., Diez, M., Viladot, M., Arance, A., & Munoz, M. (2015). Clinical implications of the intrinsic molecular subtypes of breast cancer. *Breast, 24 Suppl 2*, S26-35.

Pusztai, L., Mazouni, C., Anderson, K., Wu, Y., & Symmans, W. F. (2006). Molecular classification of breast cancer: limitations and potential. *Oncologist, 11*(8), 868-877.

Raghavan, S., Mehta, P., Horst, E. N., Ward, M. R., Rowley, K. R., & Mehta, G. (2016). Comparative analysis of tumor spheroid generation techniques for differential in vitro drug toxicity. *Oncotarget, 7*(13), 16948-16961.

Rakha, E. A., Reis-Filho, J. S., & Ellis, I. O. (2008). Basal-like breast cancer: a critical review. *J Clin Oncol, 26*(15), 2568-2581.

Ramos, A. A., Almeida, T., Lima, B., & Rocha, E. (2019). Cytotoxic activity of the seaweed compound fucosterol, alone and in combination with 5-fluorouracil, in colon cells using 2D and 3D culturing. *J Toxicol Environ Health A, 82*(9), 537-549.

Rastogi, S., Aggarwal, A., Tiwari, A., & Sharma, V. (2018). Chemotherapy in Nonmetastatic Osteosarcoma: Recent Advances and Implications for Developing Countries. *Journal of Global Oncology*(4), 1-5.

Ribeiro, D. A., Marques, M. E. A., & Salvadori, D. M. F. (2006). Study of DNA damage induced by dental bleaching agents in vitro. *Brazilian Oral Research, 20*, 47-51.

Rivankar, S. (2014). An overview of doxorubicin formulations in cancer therapy. *J Cancer Res Ther, 10*(4), 853-858.

Rosenberg, B., Vancamp, L., & Krigas, T. (1965). INHIBITION OF CELL DIVISION IN ESCHERICHIA COLI BY ELECTROLYSIS PRODUCTS FROM A PLATINUM ELECTRODE. *Nature, 205*, 698-699.

Rustamov, V., Rudolf, R., Yagublu, V., Kuhn, H.-M., Vitacolonna, M., & Hafner, M. (2017). Long-term 3D culture of the SCC4 cell line using three different culture methods and initial seeding densities. *Journal of Cellular Biotechnology, 3*, 41-50.

Rwigemera, A., Mamelona, J., & Martin, L. J. (2014). Inhibitory effects of fucoxanthinol on the viability of human breast cancer cell lines MCF-7 and MDA-MB-231 are correlated with modulation of the NF-kappaB pathway. *Cell Biol Toxicol, 30*(3), 157-167.

Rwigemera, A., Mamelona, J., & Martin, L. J. (2015). Comparative effects between fucoxanthinol and its precursor fucoxanthin on viability and apoptosis of breast cancer cell lines MCF-7 and MDA-MB-231. *Anticancer Res, 35*(1), 207-219.

Saad, S. Y., Najjar, T. A., & Alashari, M. (2004). Role of non-selective adenosine receptor blockade and phosphodiesterase inhibition in cisplatin-induced nephrogonadal toxicity in rats. *Clin Exp Pharmacol Physiol, 31*(12), 862-867.

Sachindra, N. M., Sato, E., Maeda, H., Hosokawa, M., Niwano, Y., Kohno, M., & Miyashita, K. (2007). Radical scavenging and singlet oxygen quenching activity of marine carotenoid fucoxanthin and its metabolites. *J Agric Food Chem, 55*(21), 8516-8522.

Saepudin, E., Qosthalani, F. A., & Sinurat, E. (2018). Fucoidan cytotoxicity against human breast cancer T47D cell line increases with higher level of sulfate ester group. *IOP Conference Series: Materials Science and Engineering, 299*.

Sanchez-Machado, D. I., Lopez-Hernandez, J., Paseiro-Losada, P., & Lopez-Cervantes, J. (2004). An HPLC method for the quantification of sterols in edible seaweeds. *Biomed Chromatogr, 18*(3), 183-190.

Sangeetha, R. K., Bhaskar, N., & Baskaran, V. (2009). Comparative effects of beta-carotene and fucoxanthin on retinol deficiency induced oxidative stress in rats. *Mol Cell Biochem, 331*(1-2), 59-67.

Sanguinetti, A., Polistena, A., Lucchini, R., Monacelli, M., Galasse, S., Avenia, S., Triola, R., Bugiantella, W., Cirocchi, R., Rondelli, F., & Avenia, N. (2016). Male breast cancer, clinical presentation, diagnosis and treatment: Twenty years of experience in our Breast Unit. *International journal of surgery case reports, 20S*(Suppl), 8-11.

Santilli, G., Binda, M., Zaffaroni, N., & Daidone, M. G. (2011). Breast cancer-initiating cells: insights into novel treatment strategies. *Cancers (Basel), 3*(1), 1405-1425.

Santo, V. E., Rebelo, S. P., Estrada, M. F., Alves, P. M., Boghaert, E., & Brito, C. (2017). Drug screening in 3D in vitro tumor models: overcoming current pitfalls of efficacy read-outs. *Biotechnol J, 12*(1).

Sarfaraj, M., Sheeba, F., Saba, A., & Khan, M. S. (2012). Marine natural products: A lead for Anti-cancer. *Indian Journal of Geo-Marine Sciences, 41*, 27-39.

Satomi, Y. (2012). Fucoxanthin induces GADD45A expression and G1 arrest with SAPK/JNK activation in LNCap human prostate cancer cells. *Anticancer Res, 32*(3), 807-813.

Satomi, Y. (2017). Antitumor and Cancer-preventative Function of Fucoxanthin: A Marine Carotenoid. *Anticancer Res, 37*(4), 1557-1562.

Sawadogo, R. W., Boly, R., Cerella, C., Teiten, H. M., Dicato, M., & Diederich, M. (2015). A Survey of Marine Natural Compounds and Their Derivatives with Anti-Cancer Activity Reported in 2012. *Molecules, 20*(4).

Schnitt, S. J. (2010). Classification and prognosis of invasive breast cancer: from morphology to molecular taxonomy. *Mod Pathol, 23 Suppl 2*, S60-64.

Schumacher, M., Kelkel, M., Dicato, M., & Diederich, M. (2011). Gold from the sea: marine compounds as inhibitors of the hallmarks of cancer. *Biotechnol Adv, 29*(5), 531-547.

Scolamiero, G., Pazzini, C., Bonafe, F., Guarnieri, C., & Muscari, C. (2018). Effects of alpha-Mangostin on Viability, Growth and Cohesion of Multicellular Spheroids Derived from Human Breast Cancer Cell Lines. *International journal of medical sciences, 15*(1), 23-30.

Senthilkumar, K., Jayachandran, V., & Se-Kwon, K. (2014). Marine Derived Bioactive Compounds for Breast and Prostate Cancer Treatment: A Review. *Current Bioactive Compounds, 10*(1), 62-74.

Shah, R., Rosso, K., & Nathanson, S. D. (2014). Pathogenesis, prevention, diagnosis and treatment of breast cancer. *World J Clin Oncol, 5*(3), 283-298.

Shaheen, S., Ahmed, M., Lorenzi, F., & Nateri, A. S. (2016). Spheroid-Formation (Colonosphere) Assay for in Vitro Assessment and Expansion of Stem Cells in Colon Cancer. *Stem Cell Reviews and Reports, 12*(4), 492-499.

Sherman, E. J., Lim, S. H., Ho, A. L., Ghossein, R. A., Fury, M. G., Shaha, A. R., Rivera, M., Lin, O., Wolden, S., Lee, N. Y., & Pfister, D. G. (2011). Concurrent doxorubicin and radiotherapy for anaplastic thyroid cancer: a critical re-evaluation including uniform pathologic review. *Radiother Oncol, 101*(3), 425-430.

Shevchuk, O., Posokhova, E., Sakhno, L., & Nikolaev, V. (2012). Theoretical ground for adsorptive therapy of anthracyclines cardiotoxicity. *Experimental oncology, 34*, 314-322.

Shim, H. J., Kim, S. H., Kang, B. J., Choi, B. G., Kim, H. S., Cha, E. S., & Song, B. J. (2014). Breast cancer recurrence according to molecular subtype. *Asian Pac J Cancer Prev, 15*(14), 5539-5544.

Shubin, A. V., Demidyuk, I. V., Komissarov, A. A., Rafieva, L. M., & Kostrov, S. V. (2016). Cytoplasmic vacuolization in cell death and survival. *Oncotarget, 7*(34), 55863-55889.

Siegel, R. L., Miller, K. D., & Jemal, A. (2019). Cancer statistics, 2019. *CA: A Cancer Journal for Clinicians, 69*(1), 7-34.

Sliwka, L., Wiktorska, K., Suchocki, P., Milczarek, M., Mielczarek, S., Lubelska, K., Cierpial, T., Lyzwa, P., Kielbasinski, P., Jaromin, A., Flis, A., & Chilmonczyk, Z. (2016). The Comparison of MTT and CVS Assays for the Assessment of Anticancer Agent Interactions. *PLoS One, 11*(5), e0155772.

Smith, L., Welham, K. J., Watson, M. B., Drew, P. J., Lind, M. J., & Cawkwell, L. (2007). The proteomic analysis of cisplatin resistance in breast cancer cells. *Oncol Res, 16*(11), 497-506.

Strother, R., & Matei, D. (2009). Pegylated liposomal doxorubicin in ovarian cancer. *Ther Clin Risk Manag, 5*(3), 639-650.

Subik, K., Lee, J. F., Baxter, L., Strzepek, T., Costello, D., Crowley, P., Xing, L., Hung, M. C., Bonfiglio, T., Hicks, D. G., & Tang, P. (2010). The Expression Patterns of ER, PR, HER2, CK5/6, EGFR, Ki-67 and AR by Immunohistochemical Analysis in Breast Cancer Cell Lines. *Breast Cancer (Auckl), 4*, 35-41.

Subramanian, P., Vinosha, M., Thangapandi, M., Rajasekar, P., & Prabhu, N. m. (2017). Isolation of fucoidan from Sargassum polycystum brown algae: Structural characterization, in vitro antioxidant and anticancer activity. *International Journal of Biological Macromolecules, 102*.

Sweeney, M. F., Sonnenschein, C., & Soto, A. M. (2018). Characterization of MCF-12A cell phenotype, response to estrogens, and growth in 3D. *Cancer cell international, 18*, 43.

Tang, P., & Tse, G. M. (2016). Immunohistochemical Surrogates for Molecular Classification of Breast Carcinoma: A 2015 Update. *Arch Pathol Lab Med, 140*(8), 806-814.

Taymaz-Nikerel, H., Karabekmez, M. E., Eraslan, S., & Kırdar, B. (2018). Doxorubicin induces an extensive transcriptional and metabolic rewiring in yeast cells. *Scientific Reports, 8*(1), 13672.

Teas, J., Vena, S., Cone, D. L., & Irhimeh, M. (2013). The consumption of seaweed as a protective factor in the etiology of breast cancer: proof of principle. *J Appl Phycol, 25*(3), 771-779.

Thirumaran, R., Prendergast, G. C., & Gilman, P. B. (2007). Chapter 7 - Cytotoxic Chemotherapy in Clinical Treatment of Cancer. In G. C. Prendergast & E. M. Jaffee (Eds.), *Cancer Immunotherapy* (pp. 101-116). Burlington: Academic Press.

Thorn, C. F., Oshiro, C., Marsh, S., Hernandez-Boussard, T., McLeod, H., Klein, T. E., & Altman, R. B. (2011). Doxorubicin pathways: pharmacodynamics and adverse effects. *Pharmacogenetics and genomics, 21*(7), 440-446.

Tice, R. R., Agurell, E., Anderson, D., Burlinson, B., Hartmann, A., Kobayashi, H., Miyamae, Y., Rojas, E., Ryu, J. C., & Sasaki, Y. F. (2000). Single cell gel/comet assay: guidelines for in vitro and in vivo genetic toxicology testing. *Environ Mol Mutagen, 35*(3), 206-221.

Tocaciu, S., Oliver, L. J., Lowenthal, R. M., Peterson, G. M., Patel, R., Shastri, M., McGuinness, G., Olesen, I., & Fitton, J. H. (2018). The Effect of Undaria pinnatifida Fucoidan on the Pharmacokinetics of Letrozole and Tamoxifen in Patients With Breast Cancer. *Integr Cancer Ther, 17*(1), 99-105.

Torre, L. A., Siegel, R. L., Ward, E. M., & Jemal, A. (2016). Global Cancer Incidence and Mortality Rates and Trends—An Update. *Cancer Epidemiol Biomarkers Prev, 25*(1), 16-27.

Trendowski, M. (2015). Recent Advances in the Development of Antineoplastic Agents Derived from Natural Products. *Drugs, 75*(17), 1993-2016.

Vamvakidou, A. P., Mondrinos, M. J., Petushi, S. P., Garcia, F. U., Lelkes, P. I., & Tozeren, A. (2007). Heterogeneous breast tumoroids: An in vitro assay for investigating cellular heterogeneity and drug delivery. *J Biomol Screen, 12*(1), 13-20.

Van Weelden, G., Bobinski, M., Okla, K., van Weelden, W. J., Romano, A., & Pijnenborg, J. M. A. (2019). Fucoidan Structure and Activity in Relation to Anti-Cancer Mechanisms. *Mar Drugs, 17*(1).

Vande Voorde, J., Ackermann, T., Pfetzer, N., Sumpton, D., Mackay, G., Kalna, G., Nixon, C., Blyth, K., Gottlieb, E., & Tardito, S. (2019). Improving the metabolic fidelity of cancer models with a physiological cell culture medium. *Sci Adv, 5*(1), eaau7314.

Vantangoli, M. M., Madnick, S. J., Huse, S. M., Weston, P., & Boekelheide, K. (2015). MCF-7 Human Breast Cancer Cells Form Differentiated Microtissues in Scaffold-Free Hydrogels. *PLoS One, 10*(8), e0135426.

Verjans, E. T., Doijen, J., Luyten, W., Landuyt, B., & Schoofs, L. (2018). Three-dimensional cell culture models for anticancer drug screening: Worth the effort? *J Cell Physiol, 233*(4), 2993-3003.

Verrill, M. (2001). Anthracyclines in breast cancer: therapy and issues of toxicity. *The Breast, 10*, 8-15.

Vinci, M., Gowan, S., Boxall, F., Patterson, L., Zimmermann, M., Court, W., Lomas, C., Mendiola, M., Hardisson, D., & Eccles, S. A. (2012). Advances in establishment and analysis of three-dimensional tumor spheroid-based functional assays for target validation and drug evaluation. *BMC biology, 10*, 29-29.

Vishchuk, O. S., Ermakova, S. P., & Zvyagintseva, T. N. (2011). Sulfated polysaccharides from brown seaweeds Saccharina japonica and Undaria pinnatifida: isolation, structural characteristics, and antitumor activity. *Carbohydr Res, 346*(17), 2769-2776.

Wali, A. F., Majid, S., Rasool, S., Shehada, S. B., Abdulkareem, S. K., Firdous, A., Beigh, S., Shakeel, S., Mushtaq, S., Akbar, I., Madhkali, H., & Rehman, M. U. (2019). Natural products against cancer: Review on phytochemicals from marine sources in preventing cancer. *Saudi Pharm J, 27*(6), 767-777.

Wang, C.-Y., Wu, T.-C., Hsieh, S.-L., Tsai, Y.-H., Yeh, C.-W., & Huang, C.-Y. (2015). Antioxidant activity and growth inhibition of human colon cancer cells by crude and

purified fucoidan preparations extracted from Sargassum cristaefolium. *J Food Drug Anal, 23*(4), 766-777.

Wang, C. Y., Cusack, J. C., Jr., Liu, R., & Baldwin, A. S., Jr. (1999). Control of inducible chemoresistance: enhanced anti-tumor therapy through increased apoptosis by inhibition of NF-kappaB. *Nat Med, 5*(4), 412-417.

Wang, J., Ma, Y., Yang, J., Jin, L., Gao, Z., Xue, L., Hou, L., Sui, L., Liu, J., & Zou, X. (2019). Fucoxanthin inhibits tumour-related lymphangiogenesis and growth of breast cancer. *J Cell Mol Med, 23*(3), 2219-2229.

Wang, J., Zhang, X., Li, X., Zhang, Y., Hou, T., Wei, L., Qu, L., Shi, L., Liu, Y., Zou, L., & Liang, X. (2016). Anti-gastric cancer activity in three-dimensional tumor spheroids of bufadienolides. *Scientific Reports, 6*, 24772.

Wang, S., Konorev, E. A., Kotamraju, S., Joseph, J., Kalivendi, S., & Kalyanaraman, B. (2004). Doxorubicin induces apoptosis in normal and tumor cells via distinctly different mechanisms. intermediacy of H(2)O(2)- and p53-dependent pathways. *J Biol Chem, 279*(24), 25535-25543.

Weigelt, B., Mackay, A., A'Hern, R., Natrajan, R., Tan, D. S., Dowsett, M., Ashworth, A., & Reis-Filho, J. S. (2010). Breast cancer molecular profiling with single sample predictors: a retrospective analysis. *Lancet Oncol, 11*(4), 339-349.

WHO. (2015). 19th WHO Model List of Essential Medicines (April 2015). http://www.who.int/medicines/publications/essentialmedicines/EML2015_8-May-15.pdf.

Wright, G. D. (2019). Unlocking the potential of natural products in drug discovery. *Microbial biotechnology, 12*(1), 55-57.

Wu, S. Y., Wu, A. T., Yuan, K. S., & Liu, S. H. (2016). Brown Seaweed Fucoidan Inhibits Cancer Progression by Dual Regulation of mir-29c/ADAM12 and miR-17-5p/PTEN Axes in Human Breast Cancer Cells. *J Cancer, 7*(15), 2408-2419.

Xia, S., Wang, K., Wan, L., Li, A., Hu, Q., & Zhang, C. (2013). Production, Characterization, and Antioxidant Activity of Fucoxanthin from the Marine Diatom Odontella aurita. *Marine Drugs, 11*(7), 2667-2681.

Xue, M., Ge, Y., Zhang, J., Wang, Q., Hou, L., Liu, Y., Sun, L., & Li, Q. (2012). Anticancer Properties and Mechanisms of Fucoidan on Mouse Breast Cancer In Vitro and In Vivo. *PLoS One, 7*(8), e43483.

Yamamoto, K., Ishikawa, C., Katano, H., Yasumoto, T., & Mori, N. (2011). Fucoxanthin and its deacetylated product, fucoxanthinol, induce apoptosis of primary effusion lymphomas. *Cancer Lett, 300*(2), 225-234.

Yamamoto, T., Tsigelny, I. F., Götz, A. W., & Howell, S. B. (2015). Cisplatin inhibits MEK1/2. *Oncotarget, 6*(27), 23510-23522.

Yamasaki-Miyamoto, Y., Yamasaki, M., Tachibana, H., & Yamada, K. (2009). Fucoidan induces apoptosis through activation of caspase-8 on human breast cancer MCF-7 cells. *J Agric Food Chem, 57*(18), 8677-8682.

Yan, X., Chuda, Y., Suzuki, M., & Nagata, T. (1999). Fucoxanthin as the major antioxidant in Hijikia fusiformis, a common edible seaweed. *Biosci Biotechnol Biochem, 63*(3), 605-607.

Yang, F., Teves, S. S., Kemp, C. J., & Henikoff, S. (2014). Doxorubicin, DNA torsion, and chromatin dynamics. *Biochimica et biophysica acta, 1845*(1), 84-89.

Yde, C. W., & Issinger, O. G. (2006). Enhancing cisplatin sensitivity in MCF-7 human breast cancer cells by down-regulation of Bcl-2 and cyclin D1. *Int J Oncol, 29*(6), 1397-1404.

Yersal, O., & Barutca, S. (2014). Biological subtypes of breast cancer: Prognostic and therapeutic implications. *World J Clin Oncol, 5*(3), 412-424.

Yılmaz, Ö., & Sakarya, S. (2018). Is 'Hanging Drop' a Useful Method to Form Spheroids of Jimt, Mcf-7, T-47d, Bt-474 That are Breast Cancer Cell Lines. *Single Cell Biology, 07*.

Yousefi, M. K., Hashtroudi, M. S., Moradi, A. M., & Ghasempour, A. R. (2018). In vitro investigating of anticancer activity of focuxanthin from marine brown seaweed species. *Global Journal of Environmental Science and Management, 4*(1), 81-90.

Yu, M.-H. (2005). *Environmental toxicology : biological and health effects of pollutants* (2nd ed. ed.): Boca Raton : CRC Press.

Zanoni, M., Piccinini, F., Arienti, C., Zamagni, A., Santi, S., Polico, R., Bevilacqua, A., & Tesei, A. (2016). 3D tumor spheroid models for in vitro therapeutic screening: a systematic approach to enhance the biological relevance of data obtained. *Sci Rep, 6*, 19103.

Zarifi, F., Etebari, M., & Jafarian- Dehkordi, A. (2018). Modulatory Effects of Dexrazoxane Against Genotoxicity and Lipid Peroxidation Induced by Idarubicin in HepG2 Cells. *International Journal of Cancer Management, 11*(1).

Zhan, Q.-H., Fu, J.-Q., Fu, F.-M., Zhang, J., & Wang, C. (2017). Survival and time to initiation of adjuvant chemotherapy among breast cancer patients: a systematic review and meta-analysis. *Oncotarget, 9*(2), 2739-2751.

Zhang, H., Tang, Y., Zhang, Y., Zhang, S., Qu, J., Wang, X., Kong, R., Han, C., & Liu, Z. (2015). Fucoxanthin: A Promising Medicinal and Nutritional Ingredient. *Evid Based Complement Alternat Med, 2015*, 723515.

Zhang, Z., Teruya, K., Eto, H., & Shirahata, S. (2011). Fucoidan Extract Induces Apoptosis in MCF-7 Cells via a Mechanism Involving the ROS-Dependent JNK Activation and Mitochondria-Mediated Pathways. *PLoS One, 6*(11), e27441.

Zhang, Z., Teruya, K., Eto, H., & Shirahata, S. (2013a). Induction of apoptosis by low-molecular-weight fucoidan through calcium- and caspase-dependent mitochondrial pathways in MDA-MB-231 breast cancer cells. *Biosci Biotechnol Biochem, 77*(2), 235-242.

Zhang, Z., Teruya, K., Yoshida, T., Eto, H., & Shirahata, S. (2013b). Fucoidan extract enhances the anti-cancer activity of chemotherapeutic agents in MDA-MB-231 and MCF-7 breast cancer cells. *Mar Drugs, 11*(1), 81-98.

Zhao, D., Kim, S. M., Pan, C. H., & Chung, D. (2014a). Effects of heating, aerial exposure and illumination on stability of fucoxanthin in canola oil. *Food Chem, 145*, 505-513.

Zhao, Y., Yang, C., Haslam, SZ., Schwartz, RC. (2014b). Breast Cancer Agents: Treatment & Prevention. *J Cancer Biol Res*, 2(1), 1033.

Zheng, J., Piao, M. J., Keum, Y. S., Kim, H. S., & Hyun, J. W. (2013). Fucoxanthin Protects Cultured Human Keratinocytes against Oxidative Stress by Blocking Free Radicals and Inhibiting Apoptosis. *Biomol Ther (Seoul), 21*(4), 270-276.

Zhou, W., Tan, W., Huang, X., & Yu, H. G. (2018). Doxorubicin combined with Notch1-targeting siRNA for the treatment of gastric cancer. *Oncology letters, 16*(3), 2805-2812.